POLYMERIC BONDED PHASES FOR PROTEIN EXTRACTION AND INTACT GLYCOPROTEIN ANALYSIS

by

Edwin Jhovany Alzate Rodríguez

A Dissertation

Submitted to the Faculty of Purdue University

In Partial Fulfillment of the Requirements for the degree of

Doctor of Philosophy

Department of Chemistry

West Lafayette, Indiana

August 2019

THE PURDUE UNIVERSITY GRADUATE SCHOOL
STATEMENT OF COMMITTEE APPROVAL

Dr. Mary Wirth, Chair
Department of Chemistry
Dr. Garth Simpson
Department of Chemistry
Dr. Chittaranjan Das
Department of Chemistry
Dr. Jonathan Wilker
Department of Chemistry

Approved by:

Dr. Christine Hyrcyna
Head of the Graduate Program

A mi familia

ACKNOWLEDGMENTS

My genuine gratitude goes to all people who supported me during this challenging process in graduate school. I am infinitely thankful for all the experiences that made me grow not only as an academic, but also as a person. My sincerest thanks to my research advisor, Dr Mary Wirth, for keeping me motivated, and for her guidance that allowed me to stay focused on my goals.

Special mention also to my thesis committee members, Prof. Garth Simpson, Prof. Chitta Das, and Prof. Jonathan Wilker, for their collaboration and time assisting my research.

I would like to acknowledge all excellent Wirth's lab members for their advices, intense discussions and invaluable contributions to my success: Charlie, Aaron, Tyler, Cameron, Yun, Tamika, Jonathan, John, Yiyang, and Alexis. Sincere thanks to Nick and Rachel for the training, patience, and setting the paths for my research.

My deepest gratefulness to my family and friends. My mother for all the wise guides, prays and emotional support. My father's memory, I know I did not become the kind of "doctor" he wanted, but he would be the proudest. My colombian friends at Purdue, who always made me feel at home. Endless gratitude to those deep inside my heart, who made me go slower, but further away.

Finally, I would like to thank Universidad Tecnologica de Pereira and COLCIENCIAS-COLFUTURO for their financial support, and the opportunity to begin this journey.

TABLE OF CONTENTS

LIST OF TABLES

LIST OF FIGURES

LIST OF ABBREVIATIONS

AAM	Acrylamide
ACN	Acetonitrile
AGET	Activators Generated by Electron Transfer
ATRP	Atom Transfer Radical Polymerization
BSA	Bovine Serum Albumin
DFA	Difluoroacetic acid
DMSO	Dimethyl Sulfoxide
ESI	Electrospray ionization
FA	Formic acid
FWHM	Full width at half maximum
GMA	Glycidyl methacrylate
HEAA	N-Hydroxyethyl Acrylamide
HMAA	N-Hydroxymethyl Acrylamide
HILIC	Hydrophilic interaction liquid chromatography
HPLC	High performance liquid chromatography
IPA	Isopropyl alcohol
k	Retention factor
LBSA	Fluorescent Labeled Bovine Serum Albumin
LCMS	Liquid chromatography – mass spectrometry
mAb	Monoclonal antibody
MALDI	Matrix assisted laser desorption/ionization
mC1	Trimethylchlorosilane
mBC	((Chloromethyl) phenylethyl) dimethylchlorosilane
Me_6TREN	Tris[2-(dimethylamino)ethyl]amine
MS	Mass Spectrometry
N	Number of theoretical plates
PAAM	Polyacrylamide
PBS	Phosphate-buffered saline
PDE2	phosphodiesterase 2

PEI	Polyethylenimine
PHEAA	poly N-Hydroxyethyl Acrylamide
PHMAA	poly N-Hydroxymethyl Acrylamide
PTBAA	poly Tert-butyl Acrylamide
PSA	Prostate specific antigen
RPLC	Reversed phase liquid chromatography
SDS	Sodium dodecyl sulfate
SEM	Scanning electron microscope
SI	Surface initiated
TEM	Transmission electron microscope
TEOS	Tetraethyl orthosilicate
TFA	Trifluoroacetic acid
TIC	Total Ion Count
t_R	Retention time
TRIS	Tris(hydroxymethyl)aminomethane
t_0	Dead time
UHPLC	Ultra high-performance liquid chromatography
W	Peak width

ABSTRACT

Author: Alzate, Edwin, J. PhD
Institution: Purdue University
Degree Received: August 2019
Title: Polymeric Bonded Phases for Protein Extraction and Intact Glycoprotein Analysis
Committee Chair: Dr. Mary Wirth

Polymer brushes are extremely versatile materials, as monomer choice allows the user to design a material with the desired physiochemical properties. Given the wide variety in monomer functionality, polymers can be fine-tuned for a specific application. In this work, polymer brushes bound to a silica support are designed and utilized to enhance performance of protein extraction and chromatographic separations.

The effectiveness of an analytical method is strongly affected by matrix composition, however, the presence of species other than the target analyte is usually unavoidable. An excellent technique will be able to identify and/or quantify the analyte even when its concentration is low compared with interfering molecules. Protein analysis is particularly challenging, since many proteins of clinical and scientific significance are present in complicated matrices such as plasma or cell lysates.

A common method to specifically separate a protein from a complicated matrix is solid phase extraction. In this method, a species (such as an antibody) with high specificity towards the target is immobilized onto a solid substrate (commonly beads or small particles for greater surface area). Next, the target is collected onto the surface, bound by the species. The solid substrate is rinsed of the liquid matrix, before elution of the target. Only the active species should interact with the analyte, and the surface should be otherwise inactive. However, nonspecific interactions lead to binding/adsorption of undesirable compounds. Therefore, an optimal substrate for protein extraction must be 1) easily and completely removable from the liquid phase, 2) have a high concentration of active sites for specific binding, and 3) exhibit low nonspecific binding. As part of this work, commercial magnetic particles were coated with a nonporous silica layer that tolerates the acid bath and silane coating necessary to attach a polymer layer. On the silane coating, a polymer layer was covalently bound; this layer contains epoxide active groups for immobilizing

antibodies. These antibodies bind to the target molecule with high specificity, and low nonspecific binding. Obtained particles were evaluated for protein extraction, where antibodies as well as specifically engineered drug compounds were successfully bound to the particle surface.

Glycosylation influences several physiopathological processes in proteins. Glycans can act as receptors, modify protein solubility, and participate in folding conformation. Altered glycosylation is a common feature in tumorous cells. As such, many modifications in glycoproteins have been related to cancer, including increased branching of N-glycans or augmented units of sialic acid. Therefore, characterization of glycoproteins is important not only as a diagnostic tool, but also to monitor patients' response to treatment. Furthermore, it is important in the growing field of monoclonal antibodies as drug carriers.

Among different methods used for glycosylation analysis, Hydrophilic Interaction Liquid Chromatography (HILIC) has showed important advantages over time-consuming digestion-MS based techniques. An adequate HILIC stationary phase can be used to rapidly differentiate glycoforms present in a sample. In the second part of this work, a polymer brush based bonded phase was developed as a HILIC stationary phase. The new polymer improved the separation of a model glycoprotein compared with a commercial HILIC column, while also exhibiting enhanced stability over a previous bonded phase synthetized in our group.

CHAPTER 1. INTRODUCTION

1.1 Polymer Brushes

Polymer brushes are thin films of polymeric molecules bound to a substrate in a high graft density to obtain chains oriented perpendicularly to the surface.[1] As depicted in Figure 1.1, the bottom of the polymer chains are immobilized on the surface by physical adsorption or covalent bonds, while the end of the chains are extended away from the surface. Polymer brush architecture, such as surface formation and density, is controlled by the choice in polymerization technique. Solvent also plays an important role in polymer conformation. In some solvents, brushes undergo swelling, extending chain lengths, in some cases up to three times longer.[2] By choosing the polymer brush architecture, one can select the functionality and/or configuration necessary for a given application.

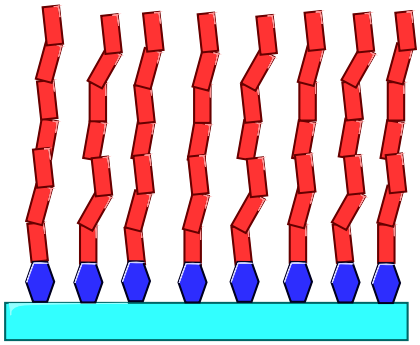

Figure 1.1. General scheme of polymer brushes.

1.1.1 Techniques for obtention of polymer brushes

An early method for polymer brushes synthesis was physisorption of block polymers.[3] One polymeric block with high affinity for the surface was initially attached, followed by the other block which had improved compatibility with the solvent. Mechanical instability of such configurations limited their applicability, leading to advances in polymerization techniques for obtaining brushes covalently bound to surfaces. Synthesis of covalent attached brushes can be carried out by either "grafting to"[4] or "grafting from"[5] methods. In the "grafting to" approach, polymer chains with end reactive groups are bound to reactive groups pre-functionalized on the

surface (Figure 1.2A). Graft densities of brushes obtained by this method are usually low, because steric hindrance, caused by initially attached chains, blocks reactive sites for incoming chains. In the "grafting from" method, polymer chains are extended directly from surface initiators by addition of monomer units. (Figure 1.2A). This methodology produces high grafting densities, since small monomer units can easily reach the initiator on the surface and growing chains.

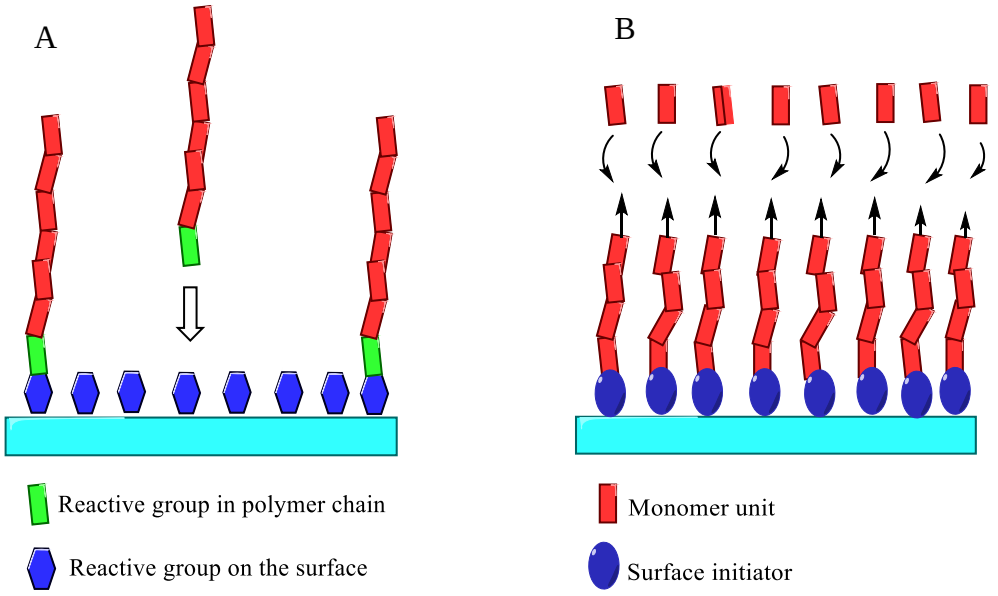

Figure 1.2. Scheme of polymer brush synthesis. A) "Grafting to" method. B) "Grafting from" approach.

Appropriate surface initiator selection plays a fundamental role in the "grafting from" method, allowing control over polymer conformation and brush density.[6-7] Common surface initiation techniques include reaction of superficial amino or hydroxyl groups with acidic halides,[8] reaction of silanes with silica or iron oxide,[9-10] functionalization of gold using disulfides or thiol groups,[11] and reactions with adsorbed carboxylic acid.[12]

Almost all polymerization methods have been used with the "grafting from" technique, including radical,[13] ring opening,[14] electrochemical,[15] photochemical,[16] cationic,[17] and anionic polymerization.[18] Controlled radical polymerization techniques such as atom transfer radical polymerization (ATRP)[19], nitroxide-mediated polymerization (NMP)[20], and reversible addition−fragmentation chain transfer (RAFT)[21] have arisen as the most dominant techniques for polymer brushes synthesis, since they provide control over reaction rate, density and polymer

polydispersity. Furthermore, the "grafting from" approach combined with these techniques permits complex polymer architectures and minimizes free polymer formation in solution. ATRP is an especially user-friendly polymerization technique due to its moderate reaction conditions such as relative lower temperature, and the availability of initiators, catalysts, and monomers with a wide variety of functional groups.[22-24] A more detailed discussion of ATRP can be found in section 1.2.

1.1.2 Complex polymer brush architectures

The elimination of transfer and termination reactions of a growing polymer chain allowed development of the so-called "controlled/living radical polymerization (CRP)"[25]. In this type of polymerization, the rate of initiation is much larger than the propagation rate. This results in a constant rate of chain growth, producing polymers with lower polydispersity (i.e. chains have very similar lengths). Due to the inherent predictability of this method, it is possible to calculate the molecular weight of the final polymer from reaction conditions and have control over end-groups. Since polymerization can occur in stages, CRP permits variations of polymer brush architecture, such as synthesis of block copolymers using different monomers in each stage.[26] Other architectures include random, cross-linked, hyperbranched, highly branched, and y-shaped binary mixed. A brief overview of polymer architectures of relevance for this thesis is described below for convenience.

1.1.2.1 Block copolymer brushes

A first polymer layer is attached to the surface, then, the active end-chains are used as initiators for subsequent layers (Figure 1.3A). Polystyrene and polymethyl methacrylate diblock polymer (PS-b-PMMA) has been successfully prepared from silicon wafers via surface initiated ATRP (SI-ATRP).[27] SI-CRP has also been used to obtain triblock polymer brushes (PS-PMMA-PS).[28]

1.1.2.2 Random copolymer brushes

A mixture of two or more monomers react simultaneously to obtain random copolymers (Figure 1.3B). This type of polymerization is mainly used to adjust properties such as hydrophilicity and responsiveness, or to exploit features of mixed functional groups.[29] Composition of a copolymer can be different from the one of monomer feed, due to differences in monomer reactivity. For instance, with SI-ATRP copolymerization of equimolar mixtures of 2-

(tert-butylamino) ethyl methacrylate (tBAEMA) with styrene (S) or acrylic acid (AA), were obtained poly(tBAEMA-co-PS) and poly(tBAEMA-co-AA) with molar compositions of 47:53 and 40:60, respectively.[30]

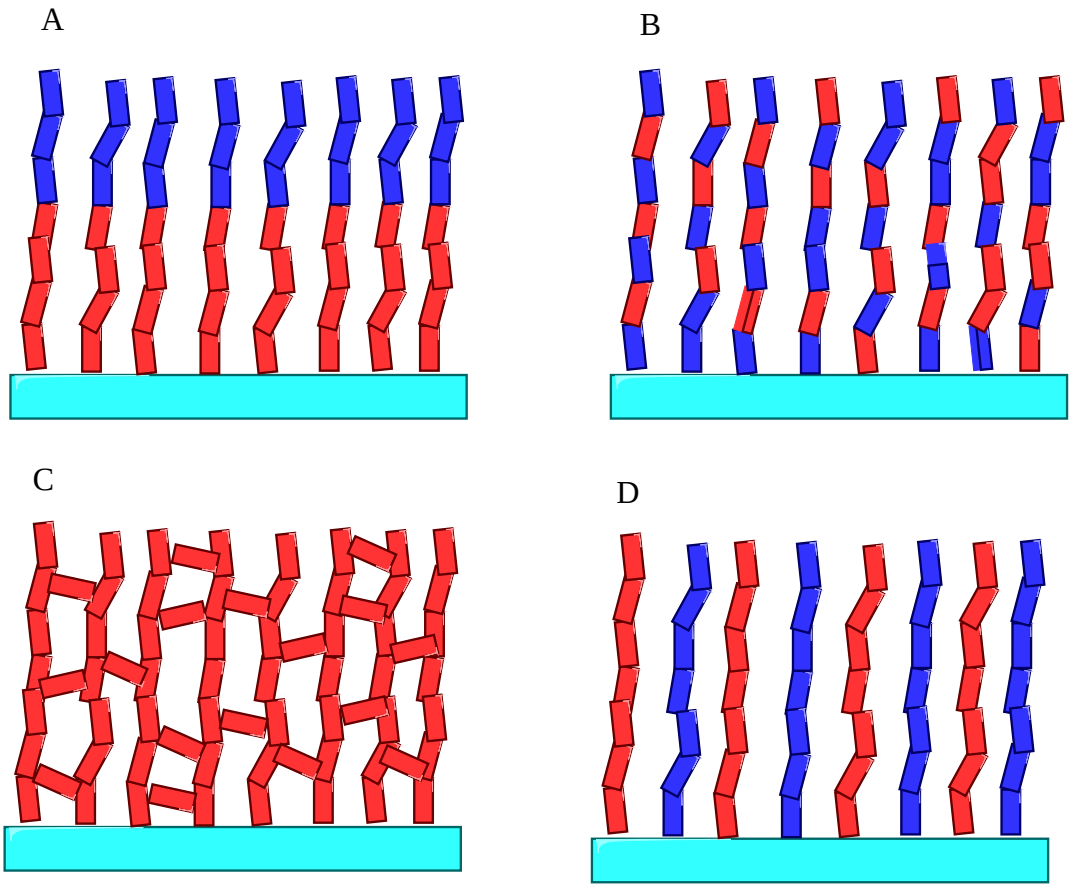

Figure 1.3. Scheme of some common polymer brush architectures. A) Block copolymer brushes. B) Random copolymer brushes. C) Cross-linked polymer brushes. D) Binary mixed brushes

1.1.2.3 Cross-linked brushes

Synthesis of cross-linked brushes (Figure 1.3C) can be accomplished using two different approaches: homo- or copolymerization of bifunctional monomers and post-polymerization modification of polymer brushes with cross-linking agents. Monomers such as ethylene glycol methacrylate and N,N'-methylenebisacrylamide have been added to the polymerization mixture to prepare cross-linked brushes.[31-32] Linear polyglycidyl methacrylate (PGMA) brushes can be post-

modified to yield cross-linked brushes, using reaction of the epoxide groups with diamines such as ethylendiamine.[33]

1.1.2.4 Binary brushes

This type of mixed brushes is formed by two different polymer chains attached to a solid support (Figure 1.3D). Multiple configurations can be achieved depending on the initiator employed. For example, simultaneous surface functionalization with ATRP and NMP initiators produce binary brushes.[34] Similarly, synthetic asymmetric difunctional silanes (Y-silane) have been used to prepare binary PMMA/PS and PtBA/PS brushes.[35-36]

1.1.3 Important applications of polymer brushes

Polymer brushes have been extensively employed in many fields due to their versatility as surface modifiers. Obtention of multiple architectures has been exploited in applications as antifouling and antibacterial surfaces, membrane design, biosensors and biomedical materials.[37] Polymer brushes are attractive materials due to their stability in harsh environments and the ability to adjust their physicochemical properties such as hydrophilicity, adsorption and adhesion features. In this section are presented advances with emphasis in biomedical and analytical applications with specific importance for the present work.

1.1.3.1 Antifouling and low nonspecific binding surfaces

A common goal in producing an antifouling surface is to reduce intermolecular interactions between biomolecules and the interface. Thus, adsorbed material can be released without difficulty using mild conditions. Hydrophobic surfaces present high protein adsorption, while hydrophilic interfaces exhibit low protein adhesion. Neutral and zwitterionic polymers are the two main types of hydrophilic brushes that can be employed as antifouling materials.[38] In both cases, low fouling capability is related with a hydration layer formed above the surface. This water layer becomes a physical and energetic barrier that blocks protein adhesion. In addition to this hydration layer, polymer chains produce steric hindrance, avoiding interaction of the protein with the surface due to unfavorable entropic changes. A combination of these two mechanisms produces ideal conditions for resistance to protein adsorption, thereby obtaining an antifouling surface.[39]

1.1.3.1.1 Neutral hydrophilic brush polymers

A representative example for this group of hydrophilic polymers is the widely used poly (ethylene glycol) (PEG), valued for its high biocompatibility.[40] Other neutral polymers prepared from monomers such as hydroxyethyl methacrylate (HEMA) or poly (ethylene glycol) methacrylate (PEGMA) have shown antifouling properties as well. In Figure 1.4, chemical structures of common hydrophilic monomers used to obtain antifouling polymer brushes are displayed.

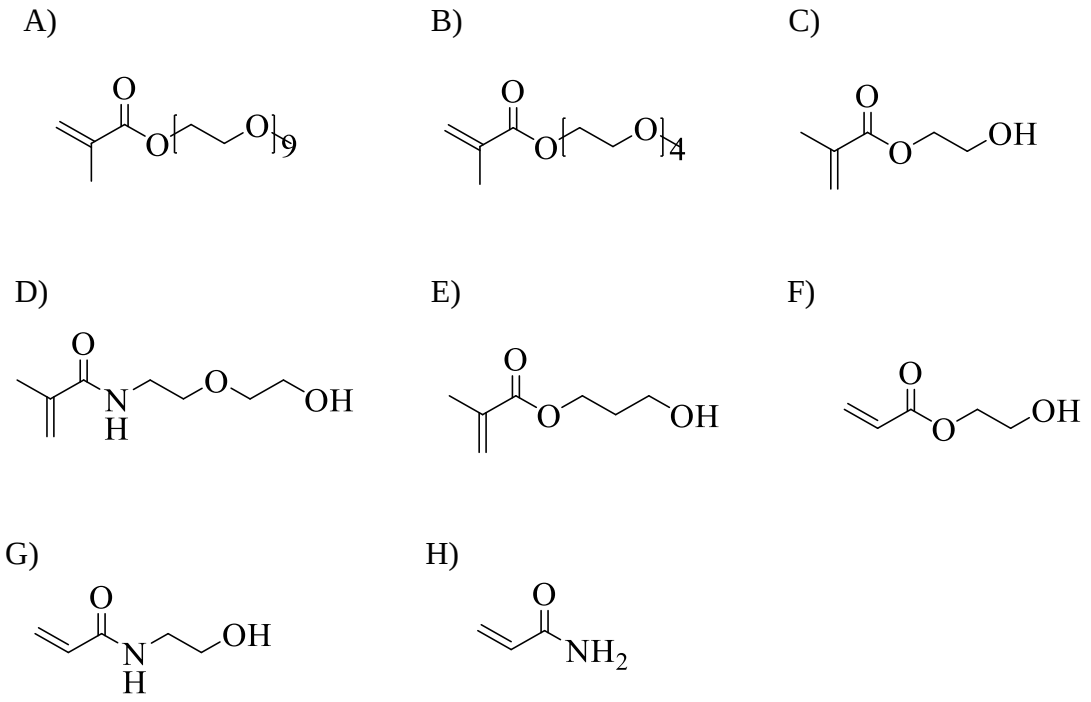

Figure 1.4. Chemical structures of common monomers used to obtain neutral antifouling polymer brushes. A) Oligo (ethylene glycol) methyl methacrylate.[41] B) Poly (ethylene glycol) methyl ether methacrylate.[42] C) 2-hydroxyethyl methacrylate.[43] D) N-acryloylaminoethoxyethanol.[43] E) hydroxypropyl methacrylate.[43] F) 2-hydroxyethyl acrylate.[44] G) N-Hydroxyethyl acrylamide.[45] H) Acrylamide.[46]

Besides hydrophilicity and chemical composition, grafting density has a vital contribution to nonspecific adsorption in polymer brushes. Studies with poly (N, N-dimethylacrylamide) revealed that at low densities, adsorption of proteins is increased due to the "mushroom" configuration of the polymer brushes (Figure 1.5).[47] However, at high densities, polymer chains are greatly stretched which provides the steric hindrance necessary for minimizing protein

adsorption to the surface (Figure 1.6). Furthermore, some studies with PHEMA and PHPMA (poly (hydroxypropyl methacrylate) showed that polymer thickness varies the amount of proteins absorbed during exposure to blood plasma.[48] These studies concluded that an augment in brush length produces more resistance nonspecific absorption due to an enhanced hydration layer that makes energetically unfavorable protein adsorption (Figure 1.7). Different studies demonstrated that there is a minimum polymer thickness, that varies with every polymer, in which a grafted surface exhibits enhanced antifouling performance.[49-50] Below that optimal range, the hydration layer is not enough to prevent protein adsorption (Figure 1.8).

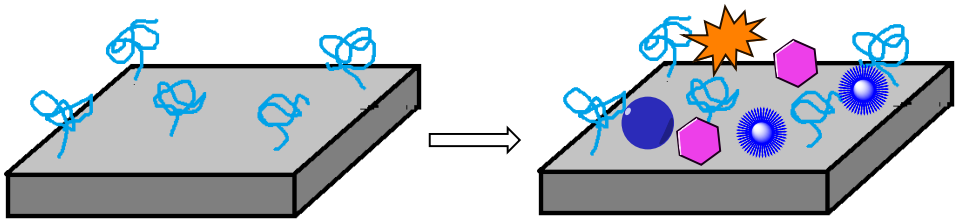

Low density polymer Nonspecific binding

Figure 1.5. Schematic of low-density polymer brush in "mushroom" configuration, allowing nonspecific binding of biomolecules to the surface.

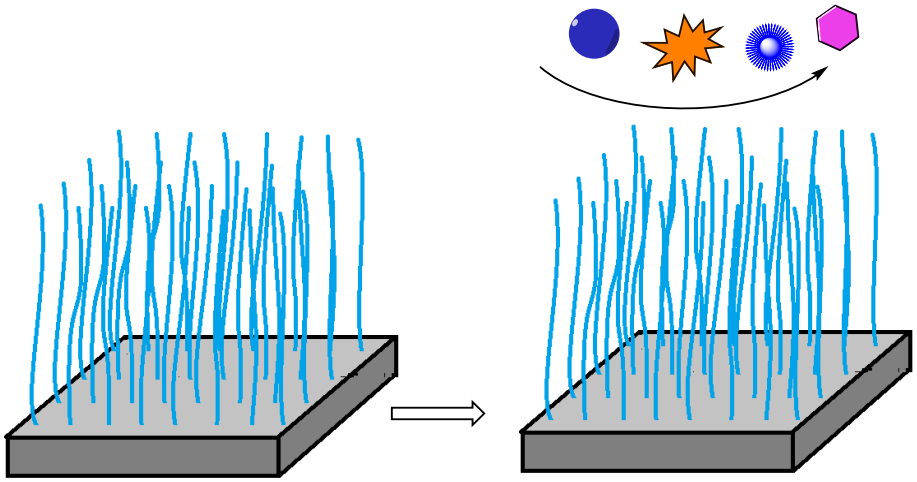

High density extended polymer brushes Adsorption resistance

Figure 1.6. Schematic of high-density polymer brushes. Stretched polymer chains avoid adsorption of proteins to the surface.

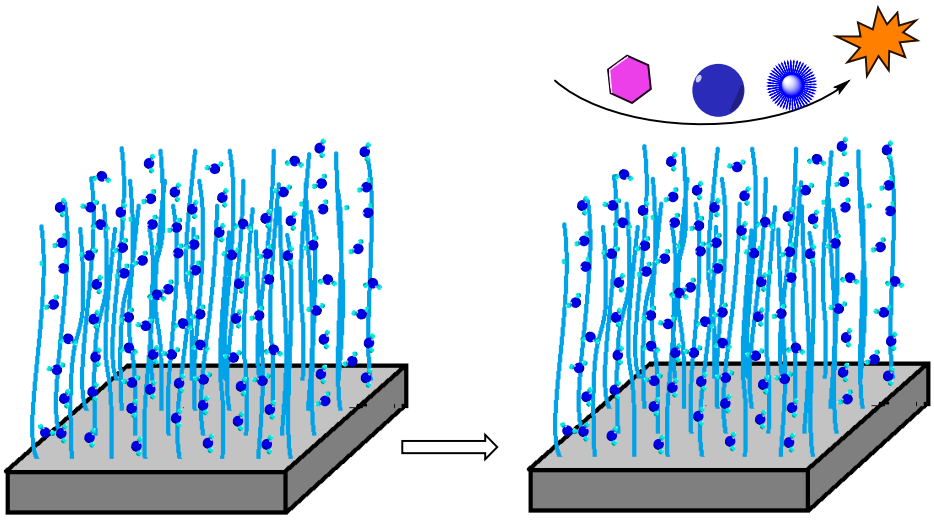

Hydration layer in long polymer brushes Nonspecific binding Resistance

Figure 1.7. Schematic of hydration layer in long polymer brushes. The water layer makes protein adsorption energetically unfavorable.

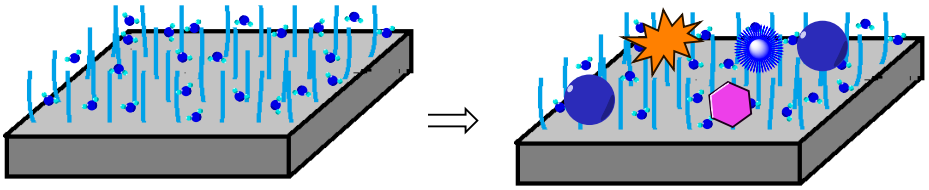

Hydration layer in short polymer brushes Nonspecific Adsorption

Figure 1.8. Schematic of the hydration layer in short polymer brushes.

1.1.3.1.2 Zwitterionic brush polymers

Charged polymers can be divided into betaines, which have a positive and a negative charge on the same monomer unit (Figure 1.9), and polyampholytes, which are block copolymers containing the same amount of positive and negative charges on two different monomer units (Figure 1.10). Electrostatic forces in zwitterionic polymers induce a strongly bound water layer, more stable than in neutral hydrophilic polymers. [51] Two key requirements for the antifouling behavior of zwitterionic polymer brushes are 1) a homogeneous distribution of charge and 2) an

overall neutral charge on the substrate. If these two requirements are met, a more efficient hydration layer is produced. The hydration layer in turn diminishes electrostatic interactions with proteins, minimizing nonspecific binding.

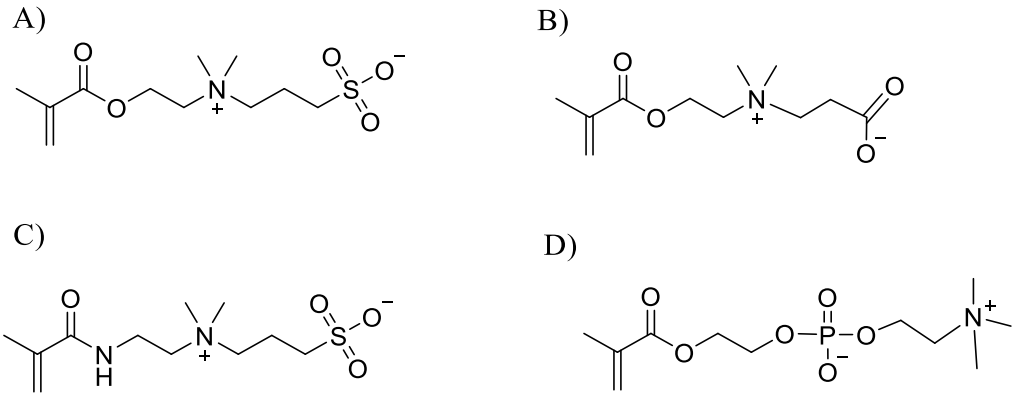

Figure 1.9. Chemical structures of common betaine monomers used for obtaining antibiofouling surfaces. A) Sulfobetaine methacrylate.[42] B) Carboxybetaine methacrylate.[42] C) Sulfobetaineacrylamide.[44] D) Methacryloyloxylethyl phosphorylcholine.[51]

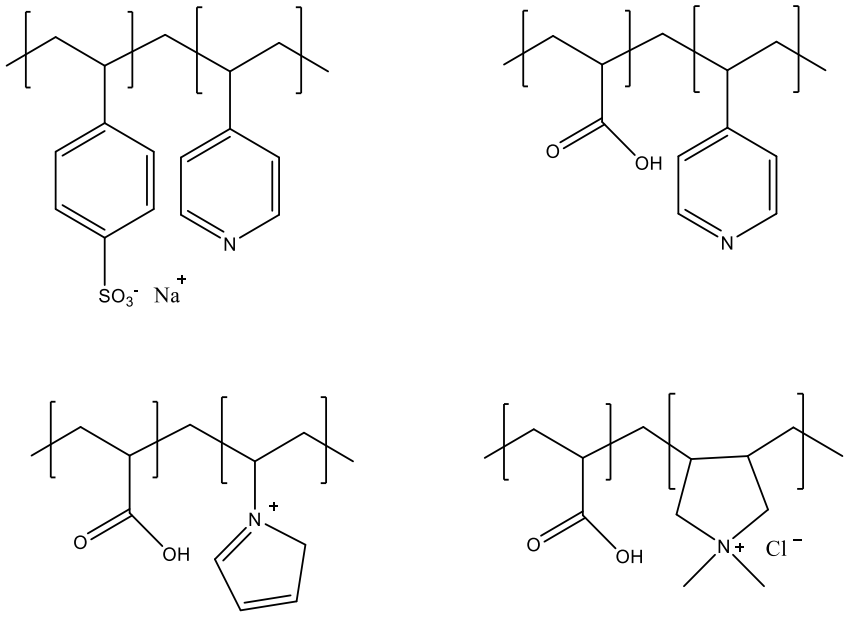

Figure 1.10. Chemical structures of common polyampholytes. A) Poly(Sodium styrene sulfonate-co-4-Vinylpyridine).[52] B) Poly(4-Vinylpyridine-co-Acrylic acid).[53] C) Poly(Acrylic acid-co-N-Vinylimidazole).[54] D) Poly(Acrylic acid-co-N,N'-dimethyl-N,N'-diallylammonium chloride).[54]

Polybetaines have been used in several applications to improve a surface's resistance to biomolecule adsorption from undiluted plasma.[55] As in the case of neutral polymer brushes, grafting density and thickness play a critical role in antibiofouling performance. Polyampholytes are considered artificial equivalents of natural biomolecules as proteins, containing positive and negative charges in different units. Like for polybetaines, uniform charge distribution and overall charge neutrality determine antibiofouling behavior of polyampholytes. This is normally accomplished by copolymerizing equimolar mixtures of monomers with similar reactivity. In a random copolymerization, it could be expected to obtain two or more consecutive units with the same charge, however, some studies in ion-pairing demonstrated that these defects have minor consequences for protein adsorption.[56-57]

1.1.3.2 Covalent immobilization of proteins

Water-swollen polymer brushes have adequate available volume to attach monolayers of proteins. This property makes them extremely useful for protein immobilization and purification. Methods for protein immobilization include electrostatic interactions,[58] covalent binding,[59] and formation of metal-ion complexes.[60] Covalent binding exhibits the highest mechanical stability among binding methods. This section describes the most important functional groups used in polymer brushes for protein covalent immobilization: carboxylic acids, hydroxyl, epoxides, and active esters.

1.1.3.2.1 Polymer brushes containing carboxylic acid groups

Carboxylic acids can react directly with primary and secondary amines in proteins to form amides, however, activation with intermediates as carbodiimide or NHS ester provides a faster reaction.[61] Figure 1.11 shows activation of carboxylic groups with 1-ethyl-3-(3-dimethylaminopropyl)carbodiimide hydrochloride (EDC). Acrylic acid and methacrylic acid are the most used monomers to obtain polymer brushes containing carboxylic acids, Figure 1.12 displays chemical structures of some polymers used to immobilize proteins via covalent bonds.

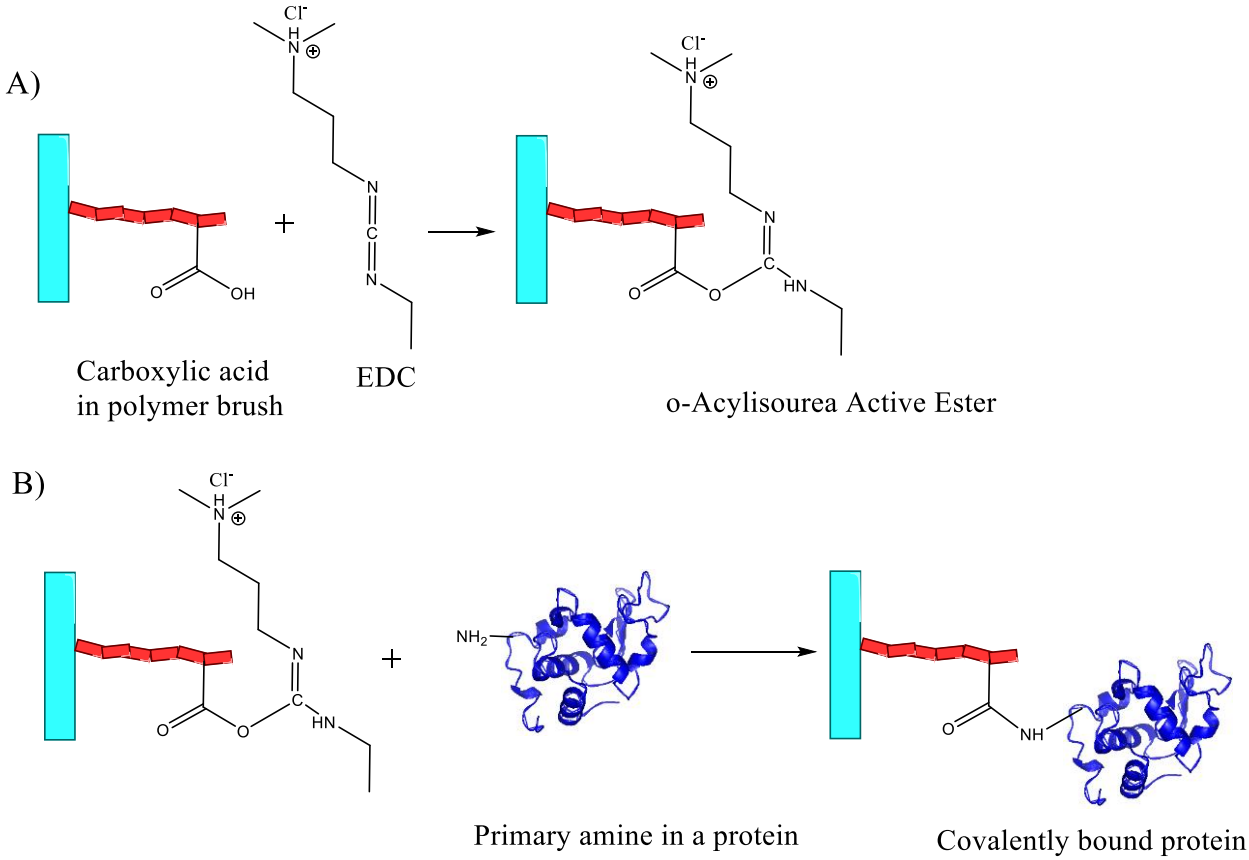

Figure 1.11. Protein binding using carboxylic groups in polymer brushes via carbodiimide activation with EDC. A) Activation with EDC produces a more reactive o-Acylisourea ester. B) Protein is covalently immobilized via reaction with a primary amine.

1.1.3.2.2 Polymer brushes containing hydroxyl groups

In order to covalently bind proteins to polymer brushes with hydroxyl groups, it is necessary to use coupling agents such a tresyl chloride, pentafluoropyridine, cyanuric chloride, carbonyldiimidazole (CDI), or disuccinimidyl carbonate (DSC).[62] Figure 1.13 shows protein immobilization using hydroxyl groups activated with CDI. Hydroxyl group forms a reactive imidazole carbamate intermediate with CDI, which reacts with amines to produce a carbamate linkage. Polyethylene glycol related polymers are employed to immobilize protein via hydroxyl groups, containing not only the reactive group, but also presenting nonspecific abilities. Some polymers used to form covalent bonds with proteins are displayed in Figure 1.14.

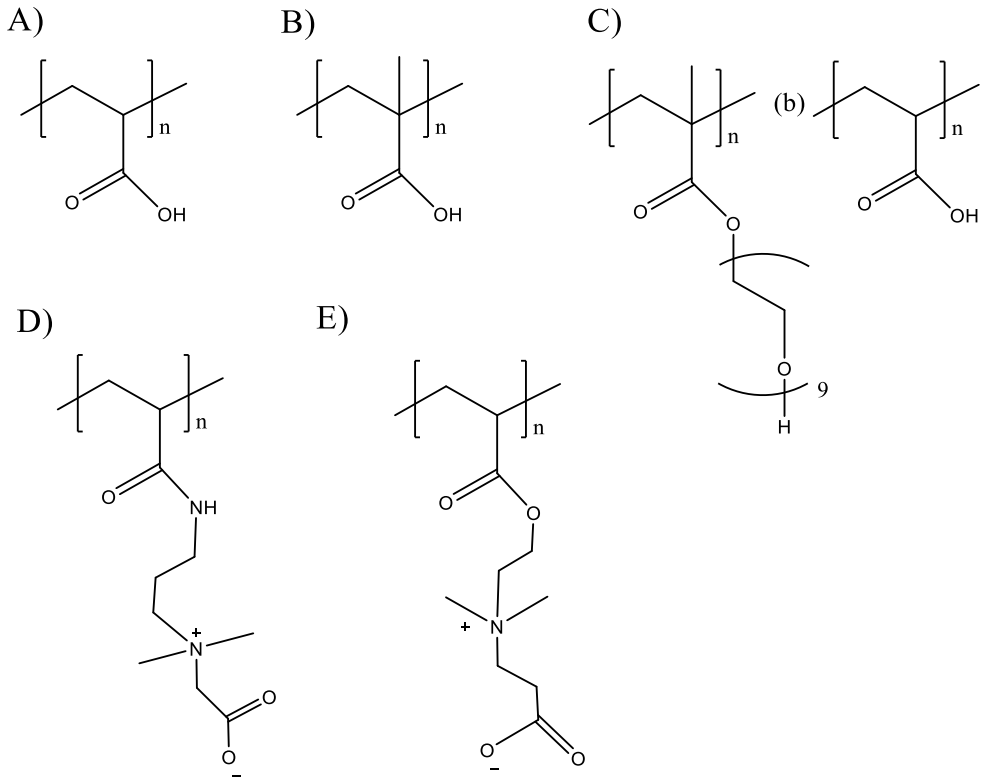

Figure 1.12. Chemical structures of polymers containing carboxylic acids used for covalent immobilization of proteins. A) Poly (acrylic acid).[63] B) Poly (methacrylic acid).[64] C) Poly (oligo(ethylene glycol)methacrylate-b-acrylic acid).[65] D) Poly (carboxybetaine acrylamide).[66] E) Poly (carboxybetaine methacrylate).[67]

1.1.3.2.3 Polymer brushes containing epoxide groups

In contrast with the previously described groups, epoxides allow direct immobilization via reaction with amines. As depicted in Figure 1.15, the reaction proceeds without activation or intermediate formation steps, and under mild conditions (room temperature, neutral pH). The most commonly used monomer to synthetize polymer brushes containing epoxide groups is glycidyl methacrylate (GMA). Despite its versatility, GMA is slightly hydrophobic, so homopolymers of GMA present nonspecific adsorption. Therefore, copolymers of GMA with hydrophilic monomers are preferred to build polymer brushes with epoxide groups. Figure 1.16 presents some polymers containing epoxide groups that have been used for protein covalent binding.

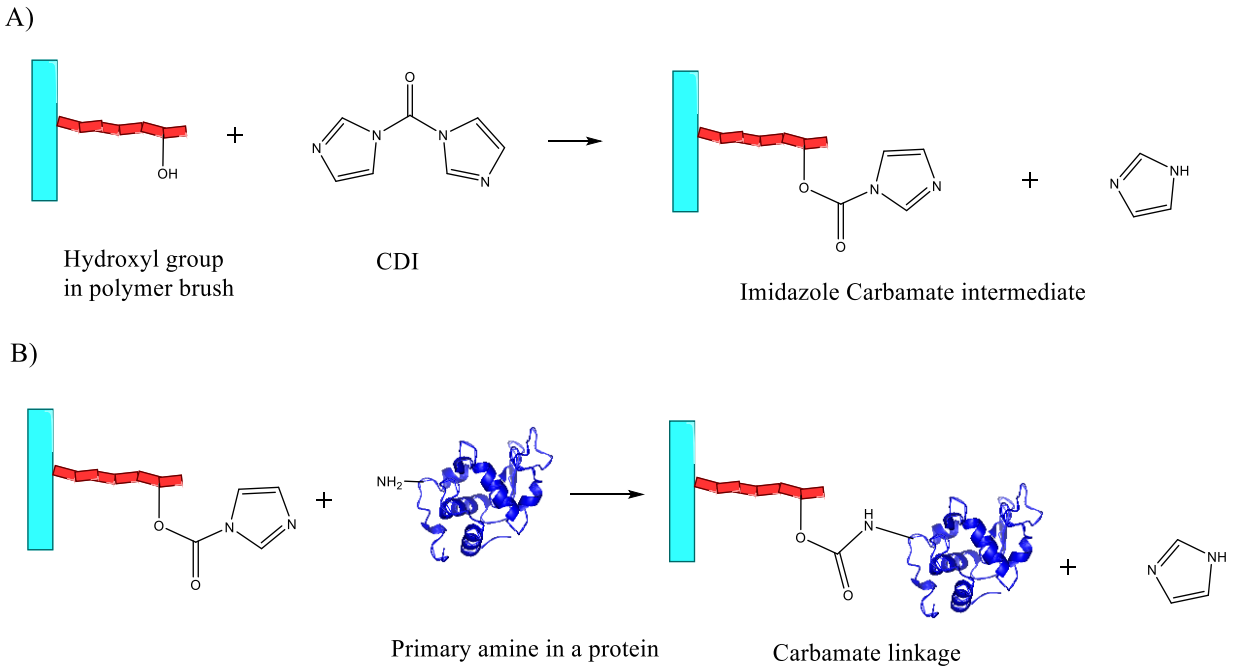

Figure 1.13. Protein binding using carbamate-activated hydroxyl groups in polymer brushes. A) Activation with CDI produces an intermediate imidazole carbamate. B) Protein is covalently immobilized via reaction with a primary amine.

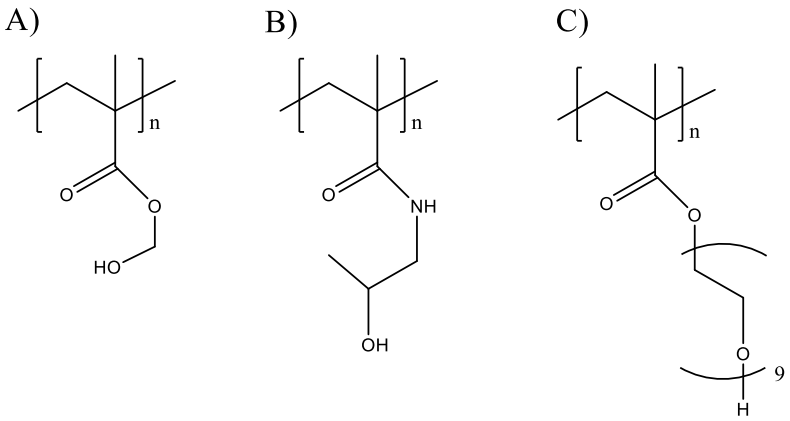

Figure 1.14. Chemical structures of polymers containing hydroxyl groups utilized for covalent binding of proteins. A) Poly (2-hydroxymethyl methacrylate).[62] B) Poly (N-(2-hydroxypropyl) methacrylamide).[68] C) Poly (oligo(ethylene glycol methacrylate)).[62]

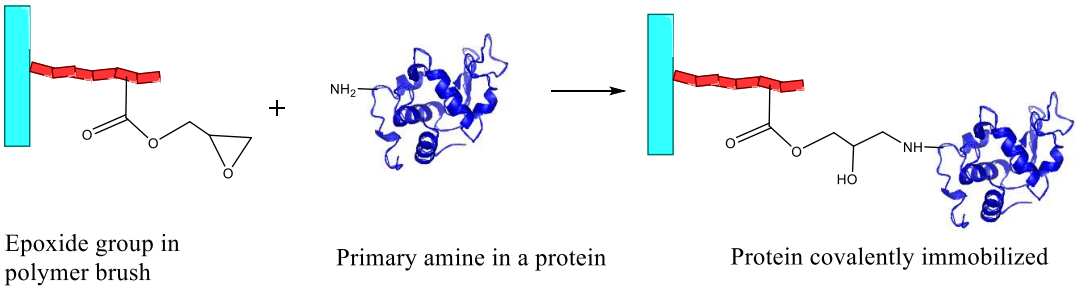

Figure 1.15. Direct protein immobilization using polymer brushes with epoxide groups.

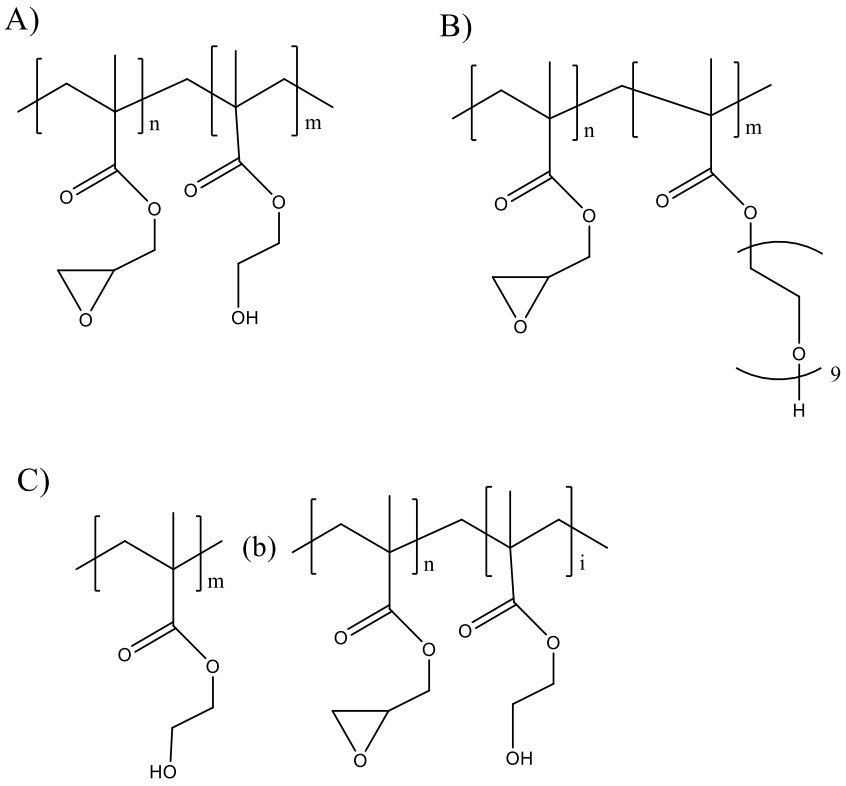

Figure 1.16. Chemical structures of polymers containing epoxide groups used for covalent immobilization of proteins. A) Poly(glycidyl methacrylate-co-(2-hydroxyethyl) methacrylate).[69] B) Poly(glycidyl methacrylate-co-oligo (ethylene glycol) methacrylate.[70] C) Poly[2-hydroxyethyl methacrylate-b-(glycidyl methacrylate-co-(2-hydroxyethyl) methacrylate)].[71]

1.1.3.2.4 Polymer brushes containing active ester groups

Like epoxide groups, polymer brushes containing active esters allow covalent protein immobilization without additional activation or coupling agents. N-Hydroxysuccinimide (NHS) ester is the most widely used active ester to react with amines in proteins (Figure 1.17).[72]

Polymerization of monomers containing active ester is demanding due to high reactivity of the side chain. Another drawback of using active esters in polymer brushes is the facility to hydrolyze demonstrated by this group of compounds.

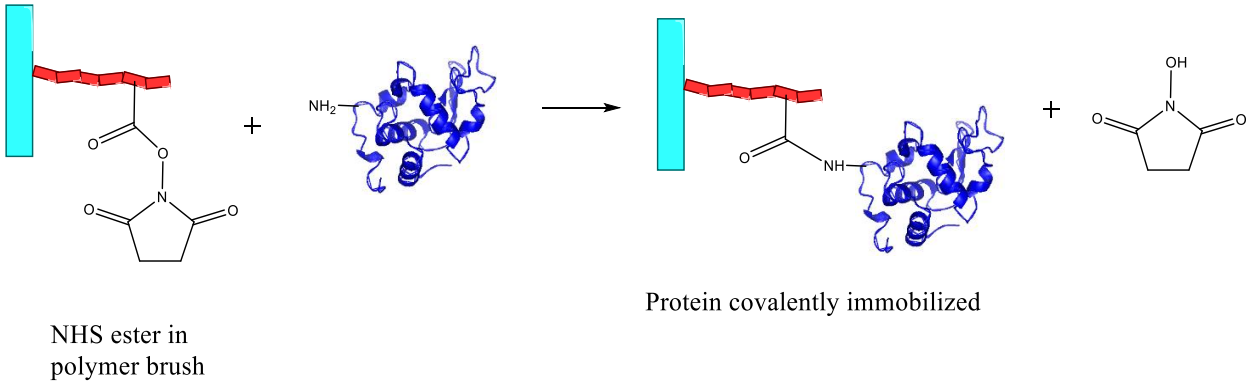

Figure 1.17. Direct protein immobilization using polymer brushes with NHS ester.

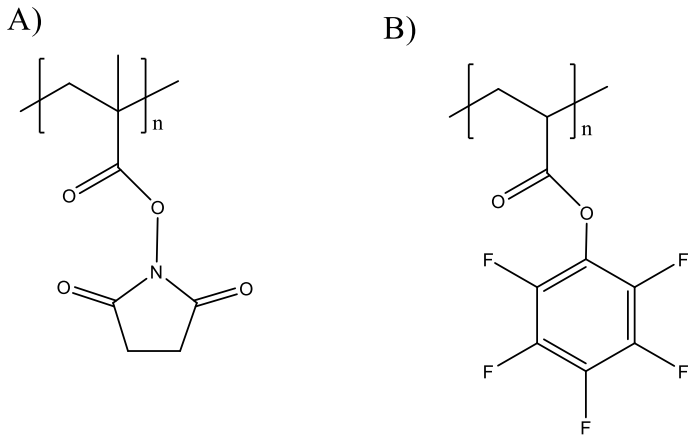

Figure 1.18. Chemical structures of polymers containing active ester groups used for covalent immobilization of proteins. A) Poly(methacryloyl succinimide).[72] B) Poly(pentafluorophenyl acrylate).[73]

1.1.3.3 Bonded phases for chromatographic separations

Initial stationary phases used for chromatographic separations consisted of liquids adsorbed onto solid supports. This approach was appropriate for gas chromatography; however, it is difficult to maintain a consistent liquid layer for techniques requiring high pressure and flow

rates (such as HPLC) . Stability of stationary phases was vastly improved with the introduction of chemically bonded stationary phases, in which alkylsilane reagents are covalently bound to solid supports. [74] Silanization has become the most used method for modifying silica surfaces as stationary phases for HPLC. The main advantage of this method is the high stability of the siloxane bonds of the silylant reagent and silanols on the silica surface. Despite this important advance, obtention of densely silanizated silica surface is difficult due to steric hindrance, resulting in around 50 % of unreacted silanols. Major problems for HPLC are caused by these exposed silanols on the silica surface: limited pH range (2–8 units) and interaction of residual silanols with some analytes via ion exchange.[75]

In order to take advantage of silica supports, it is necessary to improve surface functionalization. Polymer grafting have been successfully applied to silica-based chromatographic separations.[74] Availability of a broad variety of monomers with numerous functional groups allows one to finely-tune selectivity of a stationary phase to be appropriate for a given separation. Polymer brushes with high graft density sterically isolate silanols on the silica surface (Figure 1.19), avoiding interaction with analytes. Similarly, polymer chains can be developed to enhance silica resistance to a wider pH range. Further, one can take advantage of properties rarely present in other substrates. For instance, polymer brushes of poly(N-isopropylacrylamide) have been used to obtain thermoresponsive stationary phases,[76] in which separation is reached by changing the column temperature without modifying solvent composition.

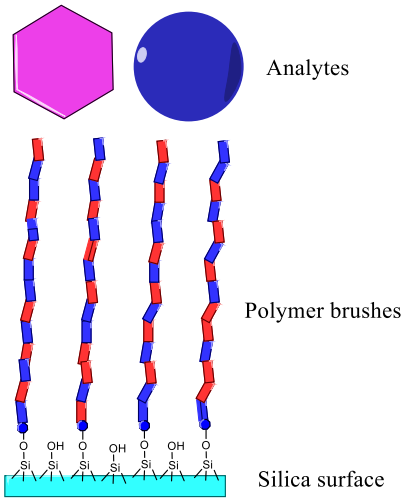

Figure 1.19. Scheme of polymer brushes on a silica surface preventing interaction of analytes with silanols.

As described in Table 1.1, several polymer brushes have been used to develop bonded stationary phases by selecting monomers with desirable properties for specific applications.

Table 1.1 Examples of polymer brushes used as bonded phases for chromatographic separations

Polymer	**Solid Support**	**Chromatographic Mode/Type**	**Analytes**	**Ref**
Poly(N-isopropylacrylamide)	Silica	Thermoresponsive HPLC	Hydrocortisone, dexamethasone, hydrocortisone acetate	76
Poly(2-(2-methoxyethoxy) ethyl methacrylate- co-oligo (ethylene glycol) methacrylate	Porous polymer monoliths	Thermoresponsive HPLC	Hydrocortisone, testosterone, medroxyprogesterone acetate	77
Polyacrylamide	Silica	HILIC	Glycoproteins	78
Poly(chloromethylstyrene-co-divinylbenzene)	Silica	HILIC	Vanillic acid, salicylic acid, puerarin	79
Poly(2-(dimethylamino) ethyl methacrylate)	Porous polymer monoliths	Salt and pH-responsive HPLC	Hydrocortisone, dexamethasone acetate, medroxyprogesterone acetate	80
Poly(GMA-co-N-isopropylacrylamide) modified with boronic acid	Silica	Thermoresponsive HILIC	Ovalbumin, and Horseradish peroxidase	81
Poly(N-[tris(hydroxymethyl) methyl]acrylamide)	Silica	HILIC	Uracil, cytosine, and ephedrine	82
Poly(pentaerythritol tetraglycidyl ether-co-ethylene imine)	Polymer monoliths	HILIC monolithic capillary	Thymidine, adenosine, uridine, cytidine, inosine	83
Poly(ethyl methacrylate-co-trimethylolpropane triacrylate)	Polymer monoliths	Reverse Phase monolithic capillary	Ribonuclease A, insulin, cytochrome, lysozyme, albumin	84
Poly(methyl methacrylate)	Silica	Hydrophobic Interaction Chromatography	Antibody-drug conjugates	85

1.2 Atom Transfer Radical Polymerization (ATRP)

Controlled/living radical polymerization (CRP) provides exceptional control over molecular weight, functional groups, polydispersity, and polymer architecture. CRP's most commonly used methods are Atom Transfer Radical Polymerization (ATRP), Nitroxide-mediated Radical Polymerization (NMR) and Reversible Addition−Fragmentation chain-Transfer polymerization (RAFT).[86] ATRP is one of the most important polymerization methods, showing a vertiginous growth over the last few decades.[87] ATRP was independently reported by Sawamoto[88] and Matyjaszewski/Wang[19] in 1995. Since then, ATRP has been widely employed because it facilitates polymerization of a greater variety of functional groups (alkyl, amino, epoxy, hydroxy, and vinyl) than can be present in monomers or initiators[29, 89-93].

In ATRP, a free radical ($P_n^{\bullet}$) is created from a reaction between an initiating alkyl halide/ macromolecular species (P_n-X) and an activator metallic complex (L_nM^z) with the reaction constant rate of activation (k_{act}), shown in Reaction (1) in Figure 1.20 (M^z represents the transition metal species in a oxidation state z and L_n is ligand). From that reaction, a deactivator organic complex is produced with a higher oxidation state ($L_nM^{z+1}X$) and a lower redox potential, which makes the reaction easily reversible and involves just one electron from halogen atom. The generated free radical can react with an unsaturated species (Reaction (2), Figure 1.20) to propagate the reaction, extending the polymer chain. The deactivator intermittently reacts with the growing radical in a opposite reaction (k_{deact}) to form a dormant species and activator. With these simultaneous reactions, it is possible to momentarily inhibit the addition of monomers units to the growing free radical, obtaining control over the polymerization.

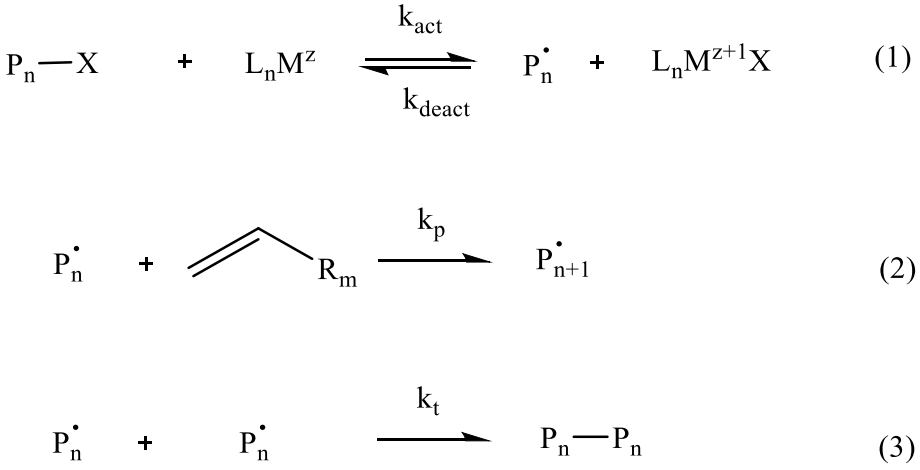

Figure 1.20 ATRP mechanism.

Appropriate design and selection of a catalyst (metal/ligand) and initiator (structure and halogen type) results in a polymerization process in which molecular weight increases linearly with conversion in agreement with a living process. Also, with the correct selection of reaction solvent and temperature, it is possible to control topography, composition, and functional groups using a great variety of polymerizable monomers.[94]

Monomers in ATRP are usually molecules with substituents that provide stability to the growing radical, such as styrene or methacrylates. Reaction of these monomers is satisfactory when the free radical concentration (growing species) is in equilibrium with the dormant species (initiator, monomer), generating polymers with controlled molecular weight and narrow polydispersity. Propagation velocity is specific for every type of monomer, therefore, reaction conditions such as initiator, catalyst and solvent, need to be optimized to keep the concentration of dormant species higher than radical species, without slowing down polymerization or reaching early termination (Reaction (3), Figure 1.20).

The amount of initiator in the reaction determines the number of concomitantly growing polymer chains. A faster initiation generates fewer termination and transfer reactions. Commonly, as initiators are used organic halides with similar structure of the monomers. Alkyl halides as initiators provide good control over molecular weight. Bromides are often preferred because of their higher reactivity, but chlorides allow a narrower polydispersity in chain length.[95] Choice in initiator defines polymer structure. For instance, an initiator with multiple alkyl halide groups creates a star polymer.[96] It is possible to use macroinitiators in ATRP, such as previously synthetized polymers with proper functionalization, to develop well-defined block copolymers.[97]

The catalyst is the most important component in ATRP, because it determines the equilibrium constant between active and dormant species ($K_{ATRP} = k_{act}/k_{deact}$).[98] Since K_{ATRP} governs polymerization rate, a small K_{ATRP} can slow down or stop polymerization. On the other hand, an extremely large K_{ATRP} speeds up the reaction, increasing polymer chain length distribution (polydispersity).

For ATRP, the transition metals need to meet several requirements. Its two oxidation states must be separated by only one electron, and the metallic center must have a reasonable affinity with the halogen involved. The metal's coordination sphere needs to be expandable so when it oxidizes, the halide can link to the catalyst structure.[22] It is required that the ligand strongly

complexes the catalyst. Finally, the complex needs to be at least partially soluble in reaction media, since polymerization can be carried on under homogeneous or heterogeneous conditions.[99]

The main role of a ligand is to stabilize the metallic salt and adjust catalytic activity of the metal to produce a controlled polymerization. The most used and efficient ligands in ATRP are nitrogenated bases[100]. An adequate ligand selection greatly influences catalyst effectiveness. Cu base catalyst have been extendedly applied to ATRP polymerizations.[101-102]

Besides previously described components, it is necessary to consider other important variables for a successful ATRP such as temperature, pressure, and oxygen concentration. Temperature is usually employed from room temperature to around 150 °C, allowing control over reaction velocity, molecular weight, and polydispersity. Molecular oxygen quickly reacts to capture radicals, forming stable peroxy radicals, and can oxidize transition metal. Oxygen's effects reduce reaction speed or could even halt radical polymerizations.[103] Therefore, oxygen must be limited in ATRP, often using complicated experimental set ups. In order to address this limitation, some modifications to initiation have been introduced, which has coined new ATRP techniques such inverse ATRP and AGET (activators generated by electron transfer) ATRP. In inverse ATRP, an initiator and metallic complex in its lower oxidation state are generated *in situ* from a conventional initiator and a metallic complex in its high oxidation state[104]. In AGET ATRP (section 1.2.1), catalyzing is performed by using an organic reducing agent to generate the metallic complex in its lower oxidation state from its higher oxidation state.[105] This more stable catalyst system suppresses the need for an oxygen-free reaction media, allowing simpler experimental procedures.

1.2.1 Activators generated by electron transfer for Atom Transfer Radical Polymerization (AGET ATRP)

As previously stated, AGET ATRP was introduced to overcome the need of a deoxygenated environment of normal ATRP. In this technique, the air sensitive activator in its lower oxidation state is substituted by a catalytic complex with the metal in its higher oxidation state, which permits adding the activator without initiating polymerization. Figure 1.21 shows the AGET ATRP mechanism using copper (Cu) as a catalyst. Polymerization is initiated by adding a reducing agent that reacts with the metallic complex ($L_nCu^{+2}X$) to generate the active species ($L_nC^{+1}X$), following a similar path to normal ATRP. All added reagents ($L_nC^{+2}X$, ATRP initiator and reducing agent)

are stable in the presence of oxygen, enabling better control over polymerization that starts only when the reducing agent is added to reaction media. Reducing agents used in AGET ATRP include tin(II)-ethylhexanoate[106], ascorbic acid[107], phenol[108], glucose[109] and methylaluminoxane.[110]

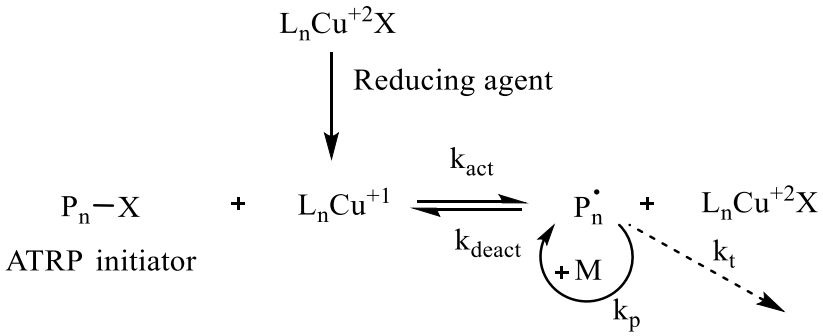

Figure 1.21 AGET ATRP mechanism.

Overall, the benefits of AGET include easy manipulation of the catalyst, tight control over the process, obtention of polymer chains with low polydispersity and minimal use of copper (less than 50 ppm).[94]

1.3 Glycoproteins

1.3.1 Glycosylation

Glycosylation is an enzymatic process that covalently attaches saccharides to amino acid side chains of a protein, generating a glycoprotein (Figure 1.22). The carbohydrate chains (glycans) can be anywhere from one up to hundreds of sugar units in length, branched or straight-chained. Glycosylation is a regulatory mechanism influencing several processes in proteins. Glycans can be used as receptors, playing an important role in cell attachment and cell-to-cell interactions. Due to their hydrophilic character, glycans can change protein solubility, thereby influencing its functions. The many possible combinations of monosaccharides give rise to a large variety of glycans, arising from differences in composition, linkage site, anomers, branching, and bonding with other compounds (proteins and lipids), among others.[111]

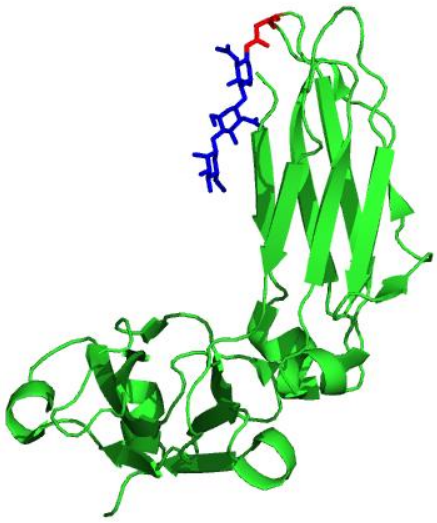

Figure 1.22. Crystal structure of human IgG1-Fc with glycan -$Man_9GlcNAc_2$- (blue) attached to N297 (red). Created with pyMOL, PDB file: 2WAH.

There are two main types of linkage of the glycans to the amino acids in glycoproteins: N-linked glycosylation (N-glycans, to the nitrogen atom of an amino acid) and O-linked glycosylation (O-glycans, to the oxygen atom of a hydroxyl group of an amino acid). In N-glycosylation, the oligosaccharide chain is bound to the amino group of asparagine (Asn), usually in the sequence Asn-X-Ser/Thr, where X can be any amino acid but proline. In O-glycosylation, the carbohydrates are linked to the hydroxyl group of serine (Ser) or threonine (Thr).

Glycans have both inside (intrinsic) and outside (extrinsic) cellular functions. For instance, as part of some immune system cells, N-glycans on the cell's surface determine migration behavior to specific sites where the cells are needed. Also, glycosylation plays a transcendental role in immunoglobulins' characteristic affinities by modifying their Fc fragments and other immune receptors. Structural conformation introduced by N-glycans affect not only the attachment site, but also hydrogen bonding, hydrophilic and hydrophobic interactions with other residues in the protein. Figure 1.23 shows IgG1-Fc residues interacting with different sugar units in the N-glycan covalently bound to asparagine 297. It is indicated that several amino acids in the Fc interact with a single saccharide, which contributes to folding structure of the entire molecule.[112]

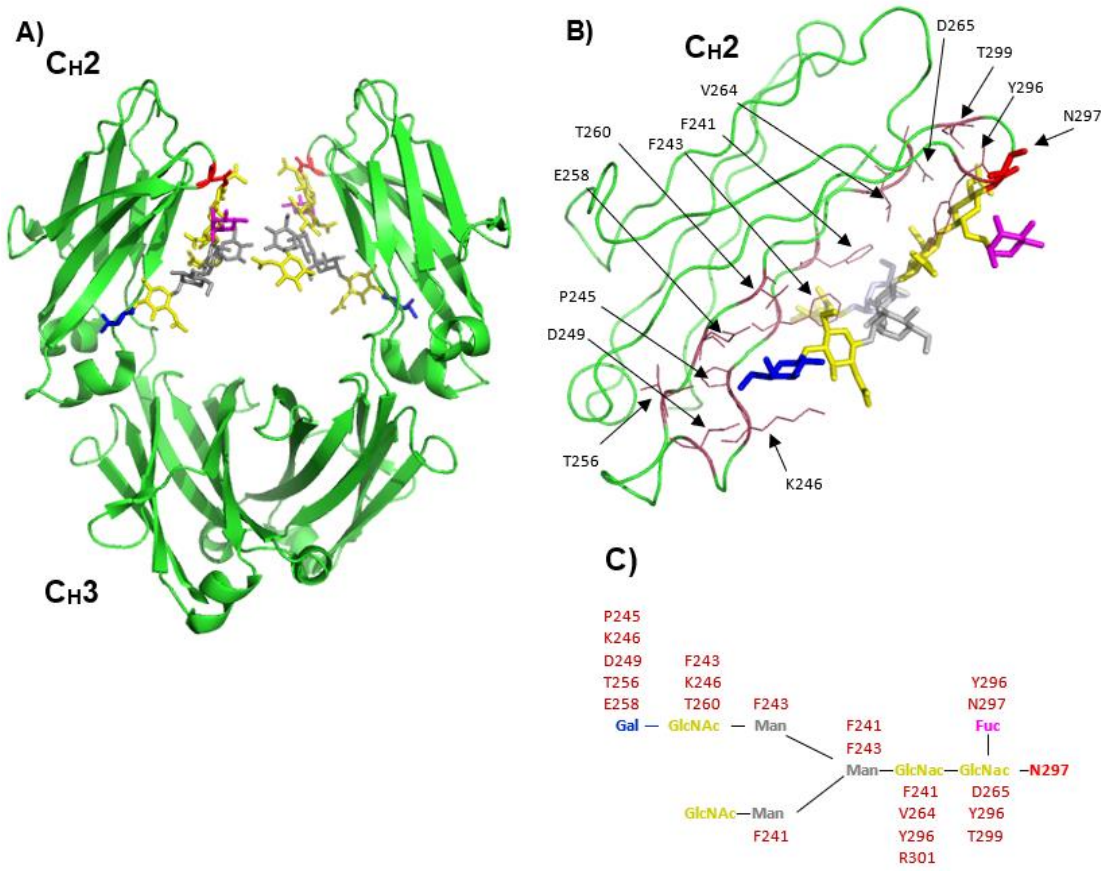

Figure 1.23. Crystal structure of a portion of the fragment crystallizable (Fc) region of human IgG1. A) The saccharides attached to N297 (red) are shown in yellow (GlcNAc), blue (Gal), grey (Man) and magenta (Fuc) (PDB file 1FC1). B) Contacts between the IgG1 C_H2 domain and the oligosaccharide. C) Glycan structure and residues interacting with saccharide units (red).

Glycan modification is a common characteristic in cancerous cells and may affect N-glycans and O-glycans. A variety of alterations in glycoproteins have been reported, showing repression or overexpression of specific sugar structures and the development of other glycan structures not usually found in normal cells. Some of the most common features in tumor cells include an increased branching of N-glycans, more sialic acid units, higher expression of specific carbohydrate antigens like sialyl-LewisX (SLecx), sialylLewisa (SLea), or polysialic acid.[113]

1.3.2 Structure analysis of glycoproteins

Due to their complexity, glycoprotein analysis is a very challenging field for analytical chemists and biochemists. Structural analysis of glycoproteins to elucidate glycosylation sites and glycan sequences is frequently a complicated process and may include multiple stages such extractions, separation and purifications, enzymatic or chemical cleavage, chemical derivatization and specialized assemblies and instrumentation.

1.3.2.1 Characterization of N-glycosylation by means of cleavage and mass spectrometry (MS)

In N-glycosylated proteins, polypeptide chains appear with the sequence Asn-X-Ser/Thr, where X can be any amino acid but proline, where the sugar chain is attached to the asparagine residue. In Figure 1.24 schematics of usual methodologies for N-glycoprotein analysis using mass spectrometry are shown. Two main procedures for glycoproteins can be performed using MS.

The first approach uses chemical or enzymatic cleavage of the intact glycan before an in-solution or in-gel proteolytic digestion. The polysaccharide chains can be released from the glycoprotein using peptide-N-glycosidase F (PNGase F), an enzyme that specifically cleavages the glycan in the Asn residue, producing the respective glycosylamines and converting Asn to aspartic acid (Asp). After the enzymatic digestion, the protein and the free glycan are analyzed separately. Deglycosylated protein is lysed in the gel or solution and the amino acids sequence can be determined by Electrospray Ionization Collision-Induced Dissociation mass spectrometry (ESI-CID). The released glycan may be characterized by ESI/MS, Matrix-assisted laser desorption/ionization (MALDI)[114] or High-Performance Anion-Exchange Chromatography Coupled with Pulsed Electrochemical Detection (HPAEC-PAD).[115] Hence, it is possible to obtain both the glycans' sequences and the binding sites that were previously occupied by them on the protein. Unfortunately, this approach does not identify which glycan was bound to which site.

In a second strategy, the intact proteolytic products are separated by high performance liquid chromatography (HPLC) before the MS analysis[116]. This method determines not only the glycan structure but also the specific glycosylation sites occupied by the carbohydrates in the protein. These two methods provide valuable information about glycan sequences and peptides. Both methodologies are, however, time-consuming and arduous.

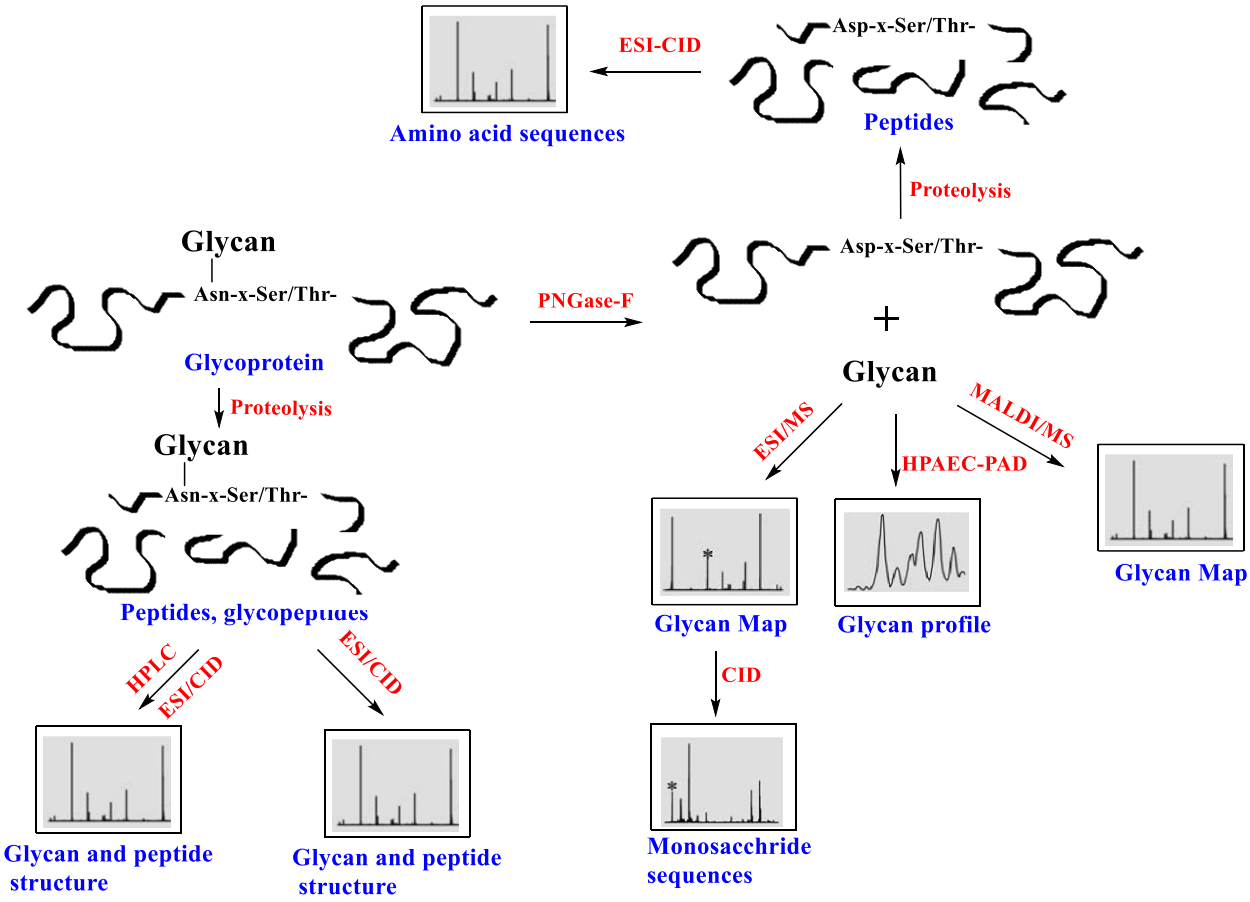

Figure 1.24. Most common methodologies for structural analysis of N-glycosylated proteins by MS.

1.3.2.2 Analysis of glycoproteins by Hydrophilic Interaction Liquid Chromatography (HILIC)

Hydrophilic Interaction Liquid Chromatography (HILIC) has been successfully used in separating hydrophilic compounds such as carbohydrates. It is considered a complementary technique to reverse phase chromatography (RPLC), since HILIC can retain polar analytes, and the aqueous-organic solvents used are advantageous to dissolve hydrophilic samples that are not soluble in the nonpolar mobile phases utilized in normal phase chromatography (NP).[117] Also, HILIC is appropriate to be used with mass spectrometry, given that prevailing organic solvent can enhance sensitivity.[118]

There has been an active discussion about retention mechanism in HILIC. Initially, it was proposed that polar analytes were retained by means of partitioning between a more hydrophobic mobile phase and a hydration layer created on the stationary phase, with contribution of other polar

interactions such as dipole-dipole.[119] Later findings have proved that the retention mechanism of HILIC is more elaborated than a straightforward liquid partitioning, as other mechanisms, like adsorption, electrostatic and hydrophilic interactions, and hydrogen bonding can also be present.[120]

HILIC has been successfully used for the analysis of glycosylation of proteins. Zhang et al, used acrylamide polymer brushes to obtain a HILIC stationary phase to separate glycoforms of intact Ribonuclease B, with excellent performance compared with commercial columns.[78] Periat et al, developed a new stationary phase based on silica functionalized with amide groups, for the analysis of protein biopharmaceuticals, under intact and digested conditions.[121] Tengattini et al, characterized intact semi-synthetic glycoproteins using different commercial amide HILIC columns (TSKgel Amide-80, XBridge BEH and AdvanceBio Glycan Mapping), being able to achieve good selectivity for different glycoforms.[122] Rinaldi et al, developed and evaluated a rapid HILIC-UV method for the analysis of glycoproteins, suitable for glycosylation characterization during synthesis.[123]

1.4 Thesis overview

The main purpose of this research is to create polymeric brushes for high performance in separation, extraction and analysis of protein analytes. Bonded phases were developed, optimized and characterized for two main applications: protein immobilization and HILIC stationary phase.

Chapter one introduces the synthetic processes, with an overview of the main features of utilized polymers and analyte characteristics in this work. In chapter two the coating process and characterization of magnetic particles, grafted with an epoxide-containing block copolymer is described. Performance of the obtained material was assessed by immunoprecipitation of BSA to determine specific and nonspecific binding properties. Also, in collaboration with Pfizer, magnetic particles were used to bind a model drug compound to capture a protein from a complex matrix.

Chapter three describes the development of a new HILIC bonded phase by means of a polyamide polymer, used for the analysis of an intact glycoprotein. The synthetized polymer brush was characterized and HPLC performance was tested using a model glycoprotein. Mass spectrometry compatibility was also assessed. In chapter four future directions for the polymeric materials developed in this work are discussed.

1.5 References

1. Ballauff, M.; Biesalski, M.; Muller, A. H. E., Polymer brushes. *Polymer* **2016,** *98*, 387.

2. Klok, H. A.; Genzer, J., Expanding the Polymer Mechanochemistry Toolbox through Surface-Initiated Polymerization. *ACS Macro Letters* **2015,** *4* (6), 636-639.

3. Kent, M. S., A quantitative study of tethered chains in various solution conditions using Langmuir diblock copolymer monolayers. *Macromolecular Rapid Communications* **2000,** *21* (6), 243-270.

4. Zdyrko, B.; Luzinov, I., Polymer brushes by the "grafting to" method. *Macromolecular rapid communications* **2011,** *32* (12), 859.

5. Kovaliov, M.; Allegrezza, M. L.; Richter, B.; Konkolewicz, D.; Averick, S., Synthesis of lipase polymer hybrids with retained or enhanced activity using the grafting-from strategy. *Polymer* **2018,** *137*, 338-345.

6. Sundaram, H. S.; Raghavachari, D., Controlled radical polymerization of tert-butyl acrylate at ambient temperature: Effect of initiator structure and synthesis of amphiphilic block copolymers. *Journal of Polymer Science, Part A: Polymer Chemistry* **2012,** *50* (5), 996-1007.

7. Lessard, B.; Maric, M., Optimization of 4-vinylpyridine nitroxide mediated controlled radical polymerization: Effect of initiator protection and complexation with C-60. *e-Polymers* **2012**.

8. Zhiyi, B.; Bruening, M. L.; Baker, G. L., Rapid growth of polymer brushes from immobilized initiators. *Journal of the American Chemical Society* **2006,** *128* (28), 9056-9060.

9. Chu, Z. a. Z. L. a. Z. W., Preparation and evaluation of maltose modified polymer-silica composite based on cross-linked poly glycidyl methacrylate as high performance liquid chromatography stationary phase. *Analytica Chimica Acta* **2018,** *1036*, 179--186.

10. Hua, D.; Tang, J.; Dai, L.; Pu, Y.; Cao, X.; Zhu, X., A strategy for synthesis of magnetic nanoparticles with "well-defined" polymers via reversible addition fragmentation chain transfer polymerization under ultrasonic irradiation. *Journal of nanoscience and nanotechnology* **2009,** *9* (11), 6681.

11. Belegrinou, S.; Malinova, V.; Masciadri, R.; Meier, W., Efficient Two-Step Synthesis of 11,11′-Dithiobis1-(2-bromo-2-methylpropionyloxy)undecane, a Conventional Initiator for Grafting Polymer Brushes from Gold Surfaces via ATRP. *Synthetic Communications* **2010,** *40* (20), 3000-3007.

12. Lattuada, M.; Hatton, T. A., Functionalization of monodisperse magnetic nanoparticles. *Langmuir : the ACS journal of surfaces and colloids* **2007,** *23* (4), 2158.

13. Zoppe, J. O. a. A. N. C. a. M. P. a. W. J. a. M. J. a. K. H. A., Surface-Initiated Controlled Radical Polymerization: State-of-the-Art, Opportunities, and Challenges in Surface and Interface Engineering with Polymer Brushes. *Chemical Reviews* **2017,** *117* (3), 1105--1318.

14. Si, G.; Zhang, S.; Pang, W.; Wang, F.; Tan, C., Stereoselective zwitterionic ring-opening polymerization of rac-lactide. *Polymer* **2018,** *154*, 148-152.

15. Dauginet-De Pra, L.; Demoustier-Champagne, S., Investigation of the electronic structure and spectroelectrochemical properties of conductive polymer nanotube arrays. *Polymer* **2005,** *46* (5), 1583-1594.

16. Hong Anh Ngo, T.; Tran, D. T.; Hung Dinh, C., Surface photochemical graft polymerization of acrylic acid onto polyamide thin film composite membranes. *Journal of Applied Polymer Science* **2017,** *134* (5), n/a-n/a.

17. Moriya, K.; Furuhashi, T.; Kajiwara, M., Syntheses of poly(bisphenoxyphosphazene) by cation polymerization: Effect of molecular weight and molecular weight distribution on the physical properties. 2005; Vol. 54, p 2452.

18. Choi, I. S.; Langer, R., Surface-initiated polymerization of l-lactide: Coating of solid substrates with a biodegradable polymer [3]. *Macromolecules* **2001,** *34* (16), 5361-5363.

19. Wang, J. S.; Matyjaszewski, K., Controlled/"Living" Radical Polymerization. Atom Transfer Radical Polymerization in the Presence of Transition-Metal Complexes. *Journal of the American Chemical Society* **1995,** *117* (20), 5614-5615.

20. Hawker, C.; Bosman, A.; Harth, E., New polymer synthesis by nitroxide mediated living radical polymerizations. *Chemical Reviews* **2001,** *101* (12), 3661-3668.

21. Baum, M.; Brittain, W. J., Synthesis of polymer brushes on silicate substrates via reversible addition fragmentation chain transfer technique. *Macromolecules* **2002,** *35* (3), 610-615.

22. Woodruff, S. R. a. D. B. J. a. T. N. V., Selecting the Optimal Reaction Conditions for Copper-Mediated Atom Transfer Radical Polymerization at Low Catalyst Concentration. *Progress in Controlled Radical Polymerization: Mechanisms and Techniques* **2019,** *1100*, 99--113.

23. Beziau, A. a. d. M. R. N. L. a. B. S. a. S. A. a. C. J. a. B. A. C. a. K. T. a. M. K., Combining ATRP and FRP gels: Soft gluing of polymeric materials for the fabrication of stackable gels. *Polymers* **2017,** *9* (6).

24. Tsarevsky, N. V.; Matyjaszewski, K., CHAPTER 8. Atom Transfer Radical Polymerization (ATRP). In *Fundamentals of Controlled/Living Radical Polymerization*, 2013; pp 287-357.

25. Braunecker, W. A.; Matyjaszewski, K., Controlled/living radical polymerization: Features, developments, and perspectives. *Progress in Polymer Science* **2007,** *32* (1), 93-146.

26. Degirmenci, M. a. T. A., Synthesis of Block Copolymers by Transformation of Free Radical Promoted Cationic Polymerization to Atom Transfer Radical Polymerization. *Polymer Journal* **2005,** *37* (9), 700--706.

27. Matyjaszewski, K.; Miller, P. J.; Shukla, N.; Immaraporn, B.; Gelman, A.; Luokala, B. B.; Siclovan, T. M.; Kickelbick, G.; Valiant, T.; Hoffmann, H.; Pakula, T., Polymers at interfaces: Using atom transfer radical polymerization in the controlled growth of homopolymers and block copolymers from silicon surfaces in the absence of untethered sacrificial initiator. *Macromolecules* **1999,** *32* (26), 8716-8724.

28. Otsu, T.; Ogawa, T.; Yamamoto, T., Solid-Phase Block Copolymer Synthesis by the Iniferter Technique. *Macromolecules* **1986,** *19* (7), 2087-2089.

29. Li, X.; Wang, M.; Wang, L.; Shi, X.; Xu, Y.; Song, B.; Chen, H., Block copolymer modified surfaces for conjugation of biomacromolecules with control of quantity and activity. *Langmuir* **2013,** *29* (4), 1122-8.

30. Ignatova, M.; Voccia, S.; Gilbert, B.; Markova, N.; Cossement, D.; Gouttebaron, R.; Robert Jerome, R.; Jerome, C., Combination of Electrografting and Atom-Transfer Radical Polymerization for Making the Stainless Steel Surface Antibacterial and Protein Antiadhesive. *Langmuir* **2005,** *22* (1), 255-262.

31. Huang, W.; Baker, G. L.; Bruening, M. L., Controlled Synthesis of Cross-Linked Ultrathin Polymer Films by Using Surface-Initiated Atom Transfer Radical Polymerization. *Angewandte Chemie International Edition* **2001,** *40* (8), 1510-1512.

32. Huang, X. a. D. L. J. a. W. M. J., Surface-Confined Living Radical Polymerization for Coatings in Capillary Electrophoresis. *Analytical Chemistry* **1998,** *70* (19), 4023--4029.

33. Yu, W. H.; Kang, E. T.; Neoh, K. G., Controlled grafting of well-defined epoxide polymers on hydrogen-terminated silicon substrates by surface-initiated ATRP at ambient temperature. *Langmuir : the ACS journal of surfaces and colloids* **2004,** *20* (19), 8294.

34. Zhao, B., Synthesis of binary mixed homopolymer brushes by combining atom transfer radical polymerization and nitroxide-mediated radical polymerization. *Polymer* **2003,** *44* (15), 4079-4083.

35. Zhao, B.; He, T., Synthesis of well-defined mixed poly(methyl methacrylate)/polystyrene brushes from an asymmetric difunctional initiator-terminated self-assembled monolayer. *Macromolecules* **2003,** *36* (23), 8599-8602.

36. Bin, Z.; Lei, Z., Nanoscale phase separation in mixed poly(tert-butyl acrylate)/polystyrene brushes on silica nanaoprticles under equilibrium melt conditions. *Journal of the American Chemical Society* **2006,** *128* (14), 4574-4575.

37. Ohm, C.; Welch, M. E.; Ober, C., Materials for biosurfaces. *J. Mater. Chem.* **2012,** *22* (37), 19343-19347.

38. Chen, S.; Li, L.; Zhao, C.; Zheng, J., Surface hydration: Principles and applications toward low-fouling/nonfouling biomaterials. *Polymer* **2010,** *51* (23), 5283-5293.

39. Krishnan, S. a. W. C. J. a. O. C. K., Advances in polymers for anti-biofouling surfaces. *Journal of Materials Chemistry* **2008,** *18* (29), 3405--3413.

40. Li, L.; Chen, S.; Zheng, J.; Ratner, B. D.; Jiang, S., Protein adsorption on oligo(ethylene glycol)-terminated alkanethiolate self-assembled monolayers: The molecular basis for nonfouling behavior. *The journal of physical chemistry. B* **2005,** *109* (7), 2934.

41. Ma, H.; Hyun, J.; Stiller, P.; Chilkoti, A., "Non-fouling" oligo(ethylene glycol)-functionalized polymer brushes synthesized by surface-initiated atom transfer radical polymerization. *Advanced Materials (FRG)* **2004,** *16* (4), 338-341.

42. Ladd, J.; Zhang, Z.; Chen, S.; Hower, J. C.; Jiang, S., Zwitterionic polymers exhibiting high resistance to nonspecific protein adsorption from human serum and plasma. *Biomacromolecules* **2008,** *9* (5), 1357.

43. Chen, H. a. Z. M. a. Y. J. a. Z. C. a. H. R. a. C. Q. a. C. Y. a. Z. J., Synthesis and characterization of antifouling poly(N - acryloylaminoethoxyethanol) with ultralow protein adsorption and cell attachment. *Langmuir* **2014,** *30* (34), 10398--10409.

44. Zhao, C.; Zhao, J.; Li, X.; Wu, J.; Chen, S.; Chen, Q.; Wang, Q.; Gong, X.; Li, L.; Zheng, J., Probing structure-antifouling activity relationships of polyacrylamides and polyacrylates. *Biomaterials* **2013,** *34* (20), 4714.

45. Zhao, C. a. Z. J., Synthesis and characterization of poly(N -hydroxyethylacrylamide) for long-term antifouling ability. *Biomacromolecules* **2011,** *12* (11), 4071--4079.

46. Liu, Q.; Singh, A.; Lalani, R.; Liu, L., Ultralow fouling polyacrylamide on gold surfaces via surface-initiated atom transfer radical polymerization. *Biomacromolecules* **2012,** *13* (4), 1086.

47. Ibanescu, S. A.; Nowakowska, J.; Khanna, N.; Landmann, R.; Klok, H. A., Effects of Grafting Density and Film Thickness on the Adhesion of Staphylococcus epidermidis to Poly(2-hydroxy ethyl methacrylate) and Poly(poly(ethylene glycol)methacrylate) Brushes. *Macromolecular Bioscience* **2016,** *16* (5), 676-685.

48. Zhao, C.; Li, L.; Wang, Q.; Yu, Q.; Zheng, J., Effect of film thickness on the antifouling performance of poly(hydroxy-functional methacrylates) grafted surfaces. *Langmuir : the ACS journal of surfaces and colloids* **2011,** *27* (8), 4906.

49. Yandi, W.; Mieszkin, S.; Martin-Tanchereau, P.; Callow, M. E.; Callow, J. A.; Tyson, L.; Liedberg, B.; Ederth, T., Hydration and Chain Entanglement Determines the Optimum Thickness of Poly(HEMA-co-PEG10MA) Brushes for Effective Resistance to Settlement and Adhesion of Marine Fouling Organisms. *ACS Applied Materials & Interfaces* **2014,** *6* (14), 11448-11458.

50. Yoshikawa, C. a. Q. J. a. H. C. F. a. S. Y. a. S. J. a. v. d. B. E., Non-biofouling property of well-defined concentrated polymer brushes. *Colloids and Surfaces B: Biointerfaces* **2015,** *127*, 213--220.

51. Schlenoff, J., Zwitteration: Coating Surfaces with Zwitterionic Functionality to Reduce Nonspecific Adsorption. *Langmuir* **2014,** *30* (32), 9625-9636.

52. Lica, C. G.; Segărceanu, M.; Pleșca, M.; Rikabi, A. A.; Nechifor, G., Synthesis of a new polymer poly(styrene sulfonic acid-co-4-vinylpyridine) for proton exchange membrane for fuel cell. *UPB Scientific Bulletin, Series B: Chemistry and Materials Science* **2014,** *76* (3), 151-158.

53. Masuda, S.; Minagawa, K.; Tsuda, M.; Tanaka, M., Spontaneous copolymerization of acrylic acid with 4-vinylpyridine and microscopic acid dissociation of the alternating copolymer. *European Polymer Journal* **2001,** *37* (4), 705-710.

54. Kudaibergenov, S. E.; Nuraje, N., Intra- and interpolyelectrolyte complexes of polyampholytes. *Polymers* **2018,** *10* (10), <xocs:firstpage xmlns:xocs=""/>.

55. Zhang, Z.; Zhang, M.; Chen, S.; Horbett, T. A.; Ratner, B. D.; Jiang, S., Blood compatibility of surfaces with superlow protein adsorption. *Biomaterials* **2008,** *29* (32), 4285-4291.

56. Bernards, M. T.; Cheng, G.; Zhang, Z.; Chen, S.; Jiang, S., Nonfouling polymer brushes via surface-initiated, two-component atom transfer radical polymerization. *Macromolecules* **2008,** *41* (12), 4216-4219.

57. Li, G.; Xue, H.; Gao, C.; Zhang, F.; Jiang, S., Nonfouling Polyampholytes from an Ion-Pair Comonomer with Biomimetic Adhesive Groups. *Macromolecules* **2010,** *43* (1), 14-16.

58. Dai, J.; Baker, G.; Bruening, M., Use of porous membranes modified with polyelectrolyte multilayers as substrates for protein arrays with low nonspecific adsorption. *Anal. Chem.* **2006,** *78* (1), 135-140.

59. Sun, L.; Dai, J.; Baker, G. L.; Bruening, M. L., High-capacity, protein-binding membranes based on polymer brushes grown in porous substrates. *Chemistry of Materials* **2006,** *18* (17), 4033-4039.

60. Sage, L., Protein biochips go high tech. *Analytical chemistry* **2004,** *76* (7), 137A.

61. Cullen, S. P.; Liu, X.; Mandel, I. C.; Himpsel, F. J.; Gopalan, P., Polymeric brushes as functional templates for immobilizing ribonuclease A: study of binding kinetics and activity. *Langmuir : the ACS journal of surfaces and colloids* **2008,** *24* (3), 913.

62. Trmcic-Cvitas, J.; Hasan, E.; Ramstedt, M.; Li, X.; Cooper, M. A.; Abell, C.; Huck, W. T. S.; Gautrot, J. E., Biofunctionalized protein resistant oligo(ethylene glycol)-derived polymer brushes as selective immobilization and sensing platforms. *Biomacromolecules* **2009,** *10* (10), 2885-94.

63. Qu, Z.; Xu, H.; Xu, P.; Chen, K.; Mu, R.; Fu, J.; Gu, H., Ultrasensitive ELISA Using Enzyme-Loaded Nanospherical Brushes as Labels. *Analytical Chemistry* **2014,** *86* (19), 9367-9371.

64. Wu, Y.; Nizam, M. N.; Ding, X.; Xu, F.-J., Rational Design of Peptide-Functionalized Poly(Methacrylic Acid) Brushes for On-Chip Detection of Protease Biomarkers. *ACS Biomaterials Science & Engineering* **2018,** *4* (6), 2018-2025.

65. Ma, J.; Luan, S.; Song, L.; Jin, J.; Yuan, S.; Yan, S.; Yang, H.; Shi, H.; Yin, J., Fabricating a Cycloolefin Polymer Immunoassay Platform with a Dual-Function Polymer Brush via a Surface-Initiated Photoiniferter-Mediated Polymerization Strategy. *ACS Applied Materials & Interfaces* **2014,** *6* (3), 1971-1978.

66. Brault, N. D.; White, A. D.; Taylor, A. D.; Yu, Q.; Jiang, S., Directly Functionalizable Surface Platform for Protein Arrays in Undiluted Human Blood Plasma. *Analytical Chemistry* **2013,** *85* (3), 1447-1453.

67. Zhang, Z.; Chen, S.; Jiang, S., Dual-Functional Biomimetic Materials: Nonfouling Poly(carboxybetaine) with Active Functional Groups for Protein Immobilization. *Biomacromolecules* **2006,** *7* (12), 3311-3315.

68. Rodriguez-Emmenegger, C.; Brynda, E.; Riedel, T.; Houska, M.; Subr, V.; Alles, A. B.; Hasan, E.; Gautrot, J.; Huck, W., Polymer Brushes Showing Non-Fouling in Blood Plasma Challenge the Currently Accepted Design of Protein Resistant Surfaces. *Macromol. Rapid Commun.* **2011,** *32* (13), 952-957.

69. Lei, Z.; Gao, J.; Liu, X.; Liu, D.; Wang, Z., Poly(glycidyl methacrylate- co -2-hydroxyethyl methacrylate) Brushes as Peptide/Protein Microarray Substrate for Improving Protein Binding and Functionality. *ACS Applied Materials & Interfaces* **2016,** *8* (16), 10174-10182.

70. Hu, W. a. L. Y. a. L. Z. a. L. C. M., Poly oligo(ethylene glycol) methacrylate-co-glycidyl methacrylate Brush Substrate for Sensitive Surface Plasmon Resonance Imaging Protein Arrays. *Advanced Functional Materials* **2010,** *20* (20), 3497--3503.

71. Ren, T.; Mao, Z.; Moya, S. E.; Gao, C., Immobilization of Enzymes on 2-Hydroxyethyl Methacrylate and Glycidyl Methacrylate Copolymer Brushes. *Chemistry – An Asian Journal* **2014,** *9* (8), 2132-2139.

72. Takasu, K.; Kushiro, K.; Hayashi, K.; Iwasaki, Y.; Inoue, S.; Tamechika, E.; Takai, M., Polymer brush biointerfaces for highly sensitive biosensors that preserve the structure and function of immobilized proteins. *Sens. Actuator B-Chem.* **2015,** *216*, 428-433.

73. Son, H.; Ku, J.; Kim, Y.; Li, S.; Char, K., Amine-Reactive Poly(pentafluorophenyl acrylate) Brush Platforms for Cleaner Protein Purification. *Biomacromolecules* **2018,** *19* (3), 951-961.

74. Faria, A.; Collins, C.; Jardim, I., State-of-the-Art in Immobilized Polymer Stationary Phases for High-Performance Liquid Chromatography. *J. Braz. Chem. Soc.* **2009,** *20* (8), 1385-1398.

75. Kirkland, J. J., Development of some stationary phases for reversed-phase high-performance liquid chromatography. *Journal of chromatography. A* **2004,** *1060* (1-2), 9.

76. Nagase, K. a. K. J. a. K. A. a. A. Y. a. K. H. a. O. T., High stability of thermoresponsive polymer-brush-grafted silica beads as chromatography matrices. *ACS Applied Materials and Interfaces* **2012,** *4* (4), 1998--2008.

77. Li, N.; Qi, L.; Shen, Y.; Li, Y.; Chen, Y., Thermoresponsive Oligo(ethylene glycol)-Based Polymer Brushes on Polymer Monoliths for All-Aqueous Chromatography. *ACS Appl. Mater. Interfaces* **2013,** *5* (23), 12441-12448.

78. Zhang, Z. a. W. Z. a. W. M. J., Polyacrylamide brush layer for hydrophilic interaction liquid chromatography of intact glycoproteins. *Journal of Chromatography A* **2013,** *1301*, 156--161.

79. Dai, X.; He, Y.; Wei, Y.; Gong, B., Preparation of hydrophilic polymer-grafted polystyrene beads for hydrophilic interaction chromatography via surface-initiated atom transfer radical polymerization. *Journal of Separation Science* **2011,** *34* (22), 3115-3122.

80. Shen, Y.; Qi, L.; Wei, X.; Zhang, R.; Mao, L., Preparation of well-defined environmentally responsive polymer brushes on monolithic surface by two-step atom transfer radical polymerization method for HPLC. *Polymer* **2011,** *52* (17).

81. Ma, H.; Jiang, L.; Hajizadeh, S.; Gong, H.; Lu, B.; Ye, L., Nanoparticle-supported polymer brushes for temperature-regulated glycoprotein separation: investigation of structurefunction relationship. *J. Mater. Chem. B* **2018,** *6* (22), 3770-3781.

82. Bui, N. T. H.; Jiang, W.; Sparrman, T.; Irgum, K., Synthesis of poly(N -[tris(hydroxymethyl)methyl]acrylamide) functionalized porous silica for application in hydrophilic interaction chromatography. *Journal of Separation Science* **2012,** *35* (23), 3257-3269.

83. Chen, Y.; Shu, Y.; Yang, Z.; Lv, X.; Tan, W.; Chen, Y.; Ma, M.; Chen, B., The preparation of a poly (pentaerythritol tetraglycidyl ether-co-poly ethylene imine) organic monolithic capillary column and its application in hydrophilic interaction chromatography for polar molecules. *Analytica Chimica Acta* **2017,** *988*, 104-113.

84. Schlemmer, B.; Bandari, R.; Rosenkranz, L.; Buchmeiser, M. R., Electron beam triggered, free radical polymerization-derived monolithic capillary columns for high-performance liquid chromatography. *Journal of Chromatography A* **2009,** *1216* (13), 2664-2670.

85. Chen, T.-H.; Yang, Y.; Zhang, Z.; Fu, C.; Zhang, Q.; Williams, J. D.; Wirth, M. J., Native Reversed-Phase Liquid Chromatography: A Technique for LCMS of Intact Antibody-Drug Conjugates. *Analytical chemistry* **2019,** *91* (4), 2805.

86. Braunecker, W. A. a. M. K., Controlled/living radical polymerization: Features, developments, and perspectives. *Progress in Polymer Science (Oxford)* **2007,** *32* (1), 93--146.

87. Matyjaszewski, K., Atom Transfer Radical Polymerization (ATRP): Current status and future perspectives. *Macromolecules* **2012,** *45* (10), 4015-4039.

88. Kato, M.; Kamigaito, M.; Sawamoto, M.; Higashimura, T., Polymerization of Methyl Methacrylate with the Carbon Tetrachloride/Dichlorotris-(triphenylphosphine)ruthenium(II)/ Methylaluminum Bis(2,6-di-tert-butylphenoxide) Initiating System: Possibility of Living Radical Polymerization. *Macromolecules* **1995,** *28* (5), 1721-1723.

89. Oh, J. K. a. M. K. a. M. K., Preparation of poly(oligo(ethylene glycol) monomethyl ether methacrylate) by homogeneous aqueous AGET ATRP. *Macromolecules* **2006,** *39* (9), 3161--3167.

90. Liu, X. H. a. Z. Q. Y. a. D. W. L. a. Z. Y. G. a. D. C., A novel copper catalyst containing a hydroxyl functional group: A facile strategy to prepare block copolymers of vinyl monomer and ϵ-caprolactone: Via tandem reverse ATRP and ROP. *Polymer Chemistry* **2017,** *8* (32), 4752--4760.

91. Matyjaszewski, K. a. H. D. a. J. W. a. P. J. a. K. A., Grafting from surfaces for everyone : ARGET ATRP in the presence of air. *Langmuir* **2007,** *23* (8), 4528--4531.

92. Catalo, F. a. G. J. R. a. T. A. S. M. a. S. A. C. a. C. J. F. J., Facile synthesis of well-controlled poly(glycidyl methacrylate) and its block copolymers via SARA ATRP at room temperature. *Polymer Chemistry* **2015,** *6* (10), 1875--1882.

93. Lutz, J. F. a. B. H. G. a. W. K., Combining atom transfer radical polymerization and click chemistry: A versatile method for the preparation of end-functional polymers. 2005; Vol. 26, pp 514--518.

94. Boyer, C. a. C. N. A. a. J. K. a. N. D. a. N. T. K. a. A. N. N. M. a. O. S. a. S. S. a. Y. J., Copper-mediated living radical polymerization (atom transfer radical polymerization and copper(0) mediated polymerization): From fundamentals to bioapplications. *Chemical Reviews* **2016,** *116* (4), 1803--1949.

95. Lin, C. Y.; Coote, M. L.; Gennaro, A.; Matyjaszewski, K., Ab initio evaluation of the thermodynamic and electrochemical properties of alkyl halides and radicals and their mechanistic implications for atom transfer radical polymerization. *Journal of the American Chemical Society* **2008,** *130* (38), 12762.

96. Burdyńska, J.; Cho, H. Y.; Mueller, L.; Matyjaszewski, K., Synthesis of star polymers using ARGET ATRP. *Macromolecules* **2010,** *43* (22), 9227-9229.

97. Hhne, S. a. U. P., Synthesis of functional block copolymers and terpolymers containing polyglycidyl methacrylate blocks. *Journal of Polymer Science, Part A: Polymer Chemistry* **2015,** *53* (5), 675--684.

98. Tang, W.; Tsarevsky, N. V.; Matyjaszewski, K., Determination of Equilibrium Constants for Atom Transfer Radical Polymerization. *Journal of the American Chemical Society* **2006,** *128* (5), 1598-1604.

99. Min, K. a. M. K., Atom transfer radical polymerization in aqueous dispersed media. *Central European Journal of Chemistry* **2009,** *7* (4), 657--674.

100. Tang, W.; Kwak, Y.; Braunecker, W.; Tsarevsky, N. V.; Coote, M. L.; Matyjaszewski, K., Understanding atom transfer radical polymerization: effect of ligand and initiator structures on the equilibrium constants. *Journal of the American Chemical Society* **2008,** *130* (32), 10702.

101. Krishnan, R.; Srinivasan, K. S. V., Room temperature atom transfer radical polymerization of glycidyl methacrylate mediated by copper(I)/N-alkyl-2-pyridylmethanimine complexes. *Macromolecules* **2004,** *37* (10), 3614-3622.

102. Zhang, Q. a. W. P. a. L. Z. a. M. R. a. G. J. a. A. A. a. W. C. a. H. D. M., Aqueous copper-mediated living polymerization: Exploiting rapid disproportionation of CuBr with Me6TREN. *Journal of the American Chemical Society* **2013,** *135* (19), 7355--7363.

103. Enciso, A. E.; Fu, L.; Russell, A. J.; Matyjaszewski, K., A Breathing Atom-Transfer Radical Polymerization: Fully Oxygen-Tolerant Polymerization Inspired by Aerobic Respiration of Cells. *Angewandte Chemie International Edition* **2018,** *57* (4), 933-936.

104. Bencherif, S. A. a. S. D. J. a. S. A. a. H. F. a. H. J. O. a. W. N. R. a. M. K., Nanostructured hybrid hydrogels prepared by a combination of atom transfer radical polymerization and free radical polymerization. *Biomaterials* **2009,** *30* (29), 5270--5278.

105. AGET ATRP of Poly poly(ethylene glycol) methyl ether methacrylate Catalyzed by Hydrophobic Iron(III)-Porphyrins. *Macromolecular Chemistry and Physics* **2015,** *216* (20), 2032--2039.

106. Jakubowski, W.; Matyjaszewski, K., Activator generated by electron transfer for atom transfer radical polymerization. *Macromolecules* **2005,** *38* (10), 4139-4146.

107. Ke, M.; Haifeng, G.; Matyjaszewski, K., Preparation of homopolymers and block copolymers in miniemulsion by ATRP using activators generated by electron transfer (AGET). *Journal of the American Chemical Society* **2005,** *127* (11), 3825-3830.

108. Matyjaszewski, K.; Jakubowski, W.; Ke, M.; Tang, W., Diminishing catalyst concentration in atom transfer radical polymerization with reducing agents. *Proceedings of the National Academy of Sciences of the United States of America* **2006,** *103* (42), 15309.

109. Jakubowski, W.; Matyjaszewski, K., Activators Regenerated by Electron Transfer for Atom-Transfer Radical Polymerization of (Meth)acrylates and Related Block Copolymers. *Angewandte Chemie International Edition* **2006,** *45* (27), 4482-4486.

110. Yamamura, Y.; Matyjaszewski, K., Methylaluminoxane as a Reducing Agent for Activators Generated by Electron Transfer ATRP. *Journal of Macromolecular Science, Part A* **2007,** *44* (9), 1035-1039.

111. Reis, C. A.; Osorio, H.; Silva, L.; Gomes, C.; David, L., Alterations in glycosylation as biomarkers for cancer detection. *Journal of Clinical Pathology* **2010,** *63* (4), 322.

112. An, Z., *Therapeutic monoclonal antibodies : from bench to clinic*. Hoboken, N.J. : John Wiley & Sons: Hoboken, N.J., 2009.

113. Peracaula, R.; Barrabes, S.; Sarrats, A.; Rudd, P.; de Llorens, R., Altered glycosylation in tumours focused to cancer diagnosis. *Dis. Markers* **2008,** *25* (4-5), 207-218.

114. Šagi, D.; Kienz, P.; Denecke, J.; Marquardt, T.; Peter-Katalinić, J., Glycoproteomics of N -glycosylation by in-gel deglycosylation and matrix-assisted laser desorption/ionisation-time of flight mass spectrometry mapping: Application to congenital disorders of glycosylation. *PROTEOMICS* **2005,** *5* (10), 2689-2701.

115. Guignard, C.; Jouve, L.; Bogéat-Triboulot, M. B.; Dreyer, E.; Hausman, J.-F.; Hoffmann, L., Analysis of carbohydrates in plants by high-performance anion-exchange chromatography coupled with electrospray mass spectrometry. *Journal of Chromatography A* **2005,** *1085* (1), 137-142.

116. Wuhrer, M.; Deelder, A. M.; Hokke, C. H., Protein glycosylation analysis by liquid chromatography–mass spectrometry. *Journal of Chromatography B* **2005,** *825* (2), 124-133.

117. Buszewski, B.; Noga, S., Hydrophilic interaction liquid chromatography (HILIC)--a powerful separation technique. *Analytical and Bioanalytical Chemistry* **2012,** *402* (1), 231-247.

118. Tetaz, T.; Detzner, S.; Friedlein, A.; Molitor, B.; Mary, J.-L., Hydrophilic interaction chromatography of intact, soluble proteins. *Journal of Chromatography A* **2011,** *1218* (35), 5892-5896.

119. Alpert, A. J., Hydrophilic-interaction chromatography for the separation of peptides, nucleic acids and other polar compounds. *Journal of Chromatography A* **1990,** *499* (C), 177-196.

120. Guo, Y., Recent progress in the fundamental understanding of hydrophilic interaction chromatography (HILIC). *The Analyst* **2015,** *140* (19), 6452.

121. Periat, A.; Fekete, S.; Cusumano, A.; Veuthey, J.-L.; Beck, A.; Lauber, M.; Guillarme, D., Potential of hydrophilic interaction chromatography for the analytical characterization of protein biopharmaceuticals. *Journal of Chromatography A* **2016,** *1448*, 81-92.

122. Tengattini, S.; Domínguez-Vega, E.; Temporini, C.; Bavaro, T.; Rinaldi, F.; Piubelli, L.; Pollegioni, L.; Massolini, G.; Somsen, G. W., Hydrophilic interaction liquid chromatography-mass spectrometry as a new tool for the characterization of intact semi-synthetic glycoproteins. *Analytica Chimica Acta* **2017,** *981*, 94-105.

123. Rinaldi, F.; Tengattini, S.; Calleri, E.; Bavaro, T.; Piubelli, L.; Pollegioni, L.; Massolini, G.; Temporini, C., Application of a rapid HILIC-UV method for synthesis optimization and stability studies of immunogenic neo-glycoconjugates. *Journal of Pharmaceutical and Biomedical Analysis* **2017,** *144*, 252-262.

CHAPTER 2. HIGH MAGNETIZATION ULTRA-STABLE FERRIMAGNETIC PARTICLES FOR IMMUNOPRECIPITATION AND DRUG BINDING EVALUATION

2.1 Abstract

Magnetic particles are attractive for immunoprecipitation due to their stability, biocompatibility and fast extraction capability. Common structure of magnetic beads includes an iron core embedded in a polymer with a reactive group such NHS ester or epoxide to allow binding of antibodies. The purpose of the present work is to obtain ultra-stable magnetic Fe_3O_4 particles with high magnetization and improved binding capabilities. As an initial stage, commercially available magnetic nanoparticles were coated with silica by a modified Stöber process and heat treated. It was established that calcination at 600 °C under vacuum produces an impermeable shell, resistant to subsequent surface initiation processes. TEM analysis revealed a 50 nm thick silica layer, smothered after the temperature treatment. Fe_3O_4@SiO_2 particles were aggregated into 1 μm sized agglomerates during coating process because of the residual magnetism of the starting material. Silica surface was grafted using aqueous AGET-ATRP with a two steps block copolymer of polyhydroxyethyl acrylamide, to reduce protein adsorption, and polyglycidyl methacrylate, to covalent binding of antibodies. Resulting polymer coated particles exhibited excellent dispersion in aqueous solution. Magnetization measurements determined that reported particles are almost three times more magnetic that commercial Dynabeads. Immunoprecipitation of fluorescent labeled BSA showed a 2-fold binding capacity compared to Dynabeads, with similar non-specific binding. Also, it was demonstrated that these beads can be used for protein pull out, attaching a specific engineered drug compound to the particles through amine group.

2.2 Introduction

Magnetic nanoparticles (MNPs) are widely used in multiple fields, including magnetic inmunoprecipitations,[1] protein purification,[2] ferrofluids,[3] drug delivery[4] and biosensors.[5] Application for bio-separations are based in their magnetic properties that allow for a facile recovery of biomolecules from complex matrices. Naked iron oxide (Fe_3O_4) particles are highly reactive and can be easily oxidized in air, losing their magnetic properties. Accordingly, magnetic

particles are generally coated to improve their chemical resistance. Most used covering processes include grafting of or coating of the surface with a broad type of compounds, such as biomolecules, surfactants, and polymers, or using an inorganic layer such as silica, metal oxides or sulfides.[6] Surface coating not only produces more stable iron oxide particles, but also allows subsequent funcionalization.[7]

Stöber based methods are widely used to obtain silica-coated Fe_3O_4 particles.[8] However, the addition of nonmagnetic silica to the surface frequently produces a reduction of the magnetization of small magnetic particles.[9] Research efforts have been focused in coating larger ferrimagnetic particles to enhance their magnetization extraction efficiency.[10-11] Furthermore, silica layer obtained by Stöber method is not completely impermeable and shows microporous,[12-13] so iron core is not entirely protected against oxidation. Since Fe_3O_4 is susceptible to acid dissolution, hydrochloric acid (HCl) can be used to evaluate stability and quality of the silica layer of coated magnetic particles. Previously utilized approaches to obtain acid-resistant silica-coated MNPs include addition of an intermediate hydrophobic silica layer (using dimethyldiethoxysilane)[14] and silane post-modification with (3-aminopropyl)triethoxysilane.[15] However, these methods produce particles that can only resist HCl concentrations up to 1 mol/L.

Silanes are extensively employed as modifiers for silica surfaces. Noncorrosive ethoxy silanes are preferred to minimize damage of the silica coating, although, they do not provide a dense surface coverage.[17] Contrarily, chlorosilanes afford much dense surface functionalization, feature that makes them very useful in fields like chromatography where highly coated surfaces are essential.[16] However, attachment of chlorosilanes requires more aggressive reaction conditions, thus, an appropriate silica coating is essential, restricting their use to pure silica or very well coated surfaces.

Utilization of MNPs as capture agents requires binding specificity and efficacy, conferred by inclusion of active groups on the surface. Such groups allow direct interaction with the target molecules by electrostatic forces and/or hydrogen bonds, like in the case of amino-modified surfaces,[17] or indirectly through immobilization of molecules like antibodies.[18] Functional groups that enable attachment of bioactive molecules on surfaces throughout formation of covalent bonds include N-hydroxysuccinimide (NHS) ester,[19] and epoxide.[20] NHS esters are not stable in aqueous conditions and suffer from hydrolysis, compromising their binding capacity over time.[21] On the

other hand, epoxy groups are stable in aqueous media and are very reactive to amines and sulfhydryl groups.[22]

Epoxide functionalization of silica coated magnetic nanoparticles can be made by grafting with epoxide-containing polymers such polyglycidyl methacrylate (PGMA).[23] However, PGMA is hydrophobic, presenting non-specific absorption of undesirable molecules,[24] being necessary to copolymerize it to improve this drawback. Hydrophilic polymers such as poly (meth)acrylates and polyacrylamides have been used to obtain antifouling[25] and low protein adsorption surfaces,[26] with adequate mechanical resistance. Consequently, a copolymer of PGMA with a hydrophilic low adsorption polymer can be used to graft MNPs in order to improve their anti-biofouling functionality, obtaining a material with high reactivity with low non-specific binding.

Magnetic nanoparticles have attracted attention in biomedical applications due to their low toxicity and biocompatibility.[27] In magnetic resonance imaging, MNPs are used as enhancing contrast agents.[28-29] As drug delivery systems, MNPs are guided with an external magnetic field to target a desired area, minimizing side effects and controlling doses for chemotherapy.[30-32] Different synthetic methodologies are used to functionalize drug molecules onto MNP's surface, these include, amines, acids, epoxy, hydroxyl, thiol, azide, aldehyde and hydrazide.[33] In vitro tests, have shown that MNPs have potential in drug development to evaluate specific drug-target interactions.[34]

Phosphodiesterases (PDEs) are the only known enzymes that catalyze degradation of cAMP and cGMP, key intracellular messengers to multiple cellular functions. PDEs include 11 families, PDE1 to PDE11, with specific functionalities across brain regions.[35] PDE2A inhibitors have demonstrated potential to improve cognitive and social functions in rodents.[36] Pyrazolopyrimidine derivative compounds have been studied as potent inhibitors of PDE2A, showing strong binding capacity and selectivity[37], making them good candidates for in-vitro evaluation of drug-target relations with MNPs.

In this work, commercial iron particles were silica-coated and thermally treated under vacuum to obtain an impermeable surface, tolerating HCl concentration up to 11 M. Enhanced resistance, permits surface functionalization with nitric acid under reflux and aggressive chlorosilanes. Using "grafting from" approach with AGET ATRP,[38-39] a uniform low biofouling block copolymer with PGMA and polyhydroxyethyl acrylamide (PHEAA), was synthetized. Copolymer binding performance was evaluated using immunoprecipitation of Bovine Serum

Albumin. Also, as an attractive application, PDE2 inhibitor was bound to the MNPs via amine coupling, to extract and elute PDE2 from a complex lysate matrix.

2.3 Experimental

2.3.1 Materials

Deionized water was obtained using a Milli-Q Gradient equipment to a final conductivity of 0.055 mS. Fe_3O_4 nanoparticles (50 nm – 100 nm) were obtained from Nanostructured & Amorphous Materials, Inc. Ethanol (200 proof) was acquired from Decon Laboratories. Tetraethyl orthosilicate (TEOS, 97%), branched polyethylenimine (PEI, Mw ~ 25,000 Mn 10,000), N-hydroxyethyl acrylamide (HEAA, 97%), glycidyl methacrylate (GMA, 97%), $CuCl_2$ (99.995%), phosphate buffered saline (PBS, tablet), 2-Amino-2-(hydroxymethyl)-1,3-propanediol (TRIS, 99.9%), ammonium hydroxide solution (28 %), and sodium dodecyl sulfate (SDS, 98.5 were purchased from Sigma Aldrich. Protein free T-20 blocking buffer, hydrochloric acid (37 %), Dynabeads M-270 epoxide and toluene (99.5%) were distributed by Thermo Fisher Scientific. Sodium L-Ascorbate (98 %) were obtained from TCI chemicals. Tris(2-dimethylaminoethyl) amine (Me6Tren, 97%) was a product of Alfa Aesar. Chloromethyl phenylethyl dimethylchlorosilane (98 %) was procured from Gelest. 1 µm silica particles were obtained from Superior Silica. Fluorescent Bovine Serum Albumin (LBSA, Alexa Fluor® 555 or 488 conjugate) and BSA antibody (Anti-BSA, 70-BC67) were purchased from Fitzgerald. PDE2 and PDE2 inhibitor (drug) were provided by Pfizer.

2.3.2 Silica coating

2 g of Fe_3O_4 were dispersed in 400 mL ethanol with sonication (Branson 3800) for 3 h. Next, the particles were magnetically separated, and dried under vacuum at 60 °C for 2 h. 1 g of the dried solid was suspended into a solution of 200 mL of water and 2 g of PEI. This dispersion was sonicated and overhead stirred (Chemglass) for 8 h, followed by separation via centrifugation. 500 mg of the PEI treated Fe_3O_4 was transfer to 500 mL of water and sonicated with overhead stirring for 15 min. Then, 200 mL of ethanol were added and sonicated/stirred for extra 5 min. The stirrer was removed, and sonication alone was allowed for 5 min. Then, 10 mL of TEOS were added, and sonication was extended for 1 h. Fe_3O_4 particles were magnetically extracted, rinsed three times with ethanol and dried under vacuum at 60 °C for 2 h. 250 mg of the silica coated

particles were sonicated and stirred for 15 min in a mixture of 800 mL of ethanol and 160 mL of water. Stirring was stopped and 16.6 mL of NH_4OH and 2 mL of TEOS were added. Sonication only was continued for 1 h. Finally, the silica coated magnetic particles were magnetically extracted and dried at 60 °C under vacuum for 2 h.

2.3.3 Thermal treatment

500 mg of dry silica coated material were transferred to a quartz boat and placed inside of a tube oven (MTI corporation, model OTF-1200 X). The tube was sealed and purged with nitrogen for 3 min and vacuumed for 2 min; four more purge/vacuum cycles were performed leaving the tube under active vacuum before starting the heat treatment.

2.3.4 HCl resistance evaluation

Heat treated particles were placed in a tared 20 mL Scintillation glass vial to measure initial mass. 10 mL of 37 % HCl were added and the capped vial was sonicated for 1 h at room temperature. Afterwards, supernatant was magnetically removed. Vial was rinsed with DI water until neutral pH. Container was vacuum dried at 60 °C until constant weight. Mass loss percentage was calculated as in (Equation 2.1).

$$\% \text{ mass loss} = \frac{m_s\text{-}(m_{tf}\text{-}m_v)}{m_s} \text{ x } 100 \qquad \text{(Equation 2.1)}$$

where: m_s: mass of sample before acid, g
m_{tf}: mass of vial and sample dried, g
m_v: mass of the empty vial, g

2.3.5 AGET ATRP surface initiation

500 mg of acid tested Fe_3O_4@SiO_2 were suspended in 10 mL of 37 % HCl and sonicated for 1 h. Then, material was washed with deionized water until neutral pH. Next, 250 mL of 1.5 M HNO_3 was added and refluxed during 24 h. Particles were washed five times with deionized water and once with ethanol, followed by drying at 60 °C under vacuum for 2 h. In a dried round bottom flask, 500 mg of particles were dispersed in 100 mL of dried toluene under a nitrogen atmosphere.

2 mL of chloromethyl phenylethyl dimethylchlorosilane and 100 µL of butylamine were incorporated. The mixture was refluxed for 3 h. After reaction completion, the particles were washed twice with toluene and twice with acetonitrile and dried at 60 °C.

2.3.6 Polymer grafting

Water and ethanol were purged with nitrogen under sonication for 15 min to remove dissolved oxygen. In a 50 mL two necked round bottom flask equipped with a homemade sealed overhead stirrer, 200 mg of surface-initiated particles and 15 mL of ethanol were sonicated until dispersion. Then, a mixture of 6.3 g of HEAA (53 mmol) and 14 mL of water was added to the flask and sonication with nitrogen sparging was applied for 10 min. A solution of 40 mg of $CuCl_2$ (0.295 mmol), 80 µL of Me6Tren (0.298 mmol) in 2.5 mL of water was incorporated. The reaction was started by addition of 2.5 mL of water containing 27 mg of sodium ascorbate (0.136 mmol). The reaction flask was transfer to a water bath at 35 °C, nitrogen flow was suspended, and polymerization was allowed for 120 min under hermetic conditions. Upon completion, PHEAA coated particles were magnetically extracted, washed thrice with water, and once with ethanol.

For the second copolymer layer, in a 50 mL two necked round bottom flask equipped with a homemade sealed overhead stirred, 100 mg of PHEAA coated particles were suspended in 18 mL of ethanol, 13 mL of water with 0.9 g of HEAA and sonicated with nitrogen purging for 10 min. A solution of 15 mg of $CuCl_2$ (0.1104 mmol), 29 µL of Me6Tren (0.1079 mmol) in 3 mL of water was transferred to the reaction flask. After homogenization, 1.05 mL of glycidyl methacrylate (3.73 mmol) were added. Polymerization at room temperature was initiated with 10 mg of sodium ascorbate (0.0505 mmol) dissolved in 2 mL of water and allowed for 20 min under nitrogen (no flowing) and stirring. Epoxide containing magnetic particles were rinsed once with acetonitrile, twice with ethanol followed by two water rinses. Particles were completely dried under vacuum at room temperature.

2.3.7 Transmission Electron Microscope Analysis

1 mg of material was suspended in 500 µL of solvent (ethanol for silica coatings and water for polymer coatings). 5 µL of the slurry was transferred to a F/C 300 mesh Cu grid (TED PELLA Inc.). TEM micrographs were acquired in a FEI Tecnai G2 20 Transmission Electron Microscope.

2.3.8 Infrared Analysis

Samples were grinded with dried KBr, in an agate mortar to get a 0.2 % homogeneous fine powder. 50 mg of the mixture were hydraulically compressed to form a pellet. IR spectra were measured using a FT-IR spectrometer (Tensor 37, Bruker)

2.3.9 Magnetic Characterization

A sample of 5 mg was introduced into a SQUID straw, and a four-quadrant scan was done using an MPMS-3 magnetometer at 300 K. For correcting the residual magnetic moment of the equipment at zero magnetic field, an identical scan using a gadolinium gallium garnet was performed.

2.3.10 Fluorescence Analysis

Fluorescence measurements were performed in an Edinburgh Instruments FLS980 Steady State Fluorescence Spectrometer.

2.3.11 Antibody binding Capacity

5 mg of epoxide coated beads were suspended in 1 mL of PBS 1X containing 0.1 mg of Anti-BSA, incubation for 3 h was performed on a horizontal shaker at 750 rpm. After binding, 50 µL of supernatant were transferred to a new vial containing 500 µL of T-20 blocking buffer, reaction was allowed for 1 h. Magnetic extracted beads were washed three times with PBS 1X and then incubated for 1 h in 1 mL of fluorescent BSA (0.1 g/L in PBS 1X). Particles were rinsed 3 times with TRIS buffer (20 mM, pH 8.2). Elution was performed for 30 min with 20 µL of 2 % SDS. 10 µL of final supernatant were diluted with PBS 1X to 2 mL for fluorescence quantitation.

2.3.12 Non-specific Binding

3 mg of epoxide magnetic beads were incubated in 600 µL of T-20 blocking buffer for 1 h. Particles were magnetically extracted and rinsed 3 times with PBS 1X and 100 µL of fluorescent BSA (40 mg/mL in PBS 1X), allowing binding for 1 h. Particles were washed 6 times with TRIS buffer (20 mM, pH 8.2). Elution was performed as for antibody capacity.

2.3.13 Drug Binding

10 mg of epoxy coated beads were suspended in 450 µL of pH 8.9 buffer containing 0.2 M sodium tetraborate and 1 M ammonium sulfate in a 1.5 mL vial. Then, 25 µL of inhibitor compound solution in DMSO (50 mM) were added and allowed to bind for 3 h under shaker at 750 rpm. Upon completion, supernatant was removed under magnetic extraction and beads were incubated in 500 µL of T-20 blocking buffer for 1 h at 750 rpm. Blocked beads were rinsed three times with 50m M TRIS buffer pH 8.2 containing 1 % (m/v) SDS and 0.5 % (m/v) Tween 20. Three more were made with PBS 1X and one with Trizma buffer 50 mM (MgCl2 1.3 mM and Brij 35 0.01 %).

2.3.14 HeLa lysate clean-up

HeLa lysate vials containing between 2.8 mg and 5 mg in 500 µL of PBS buffer were centrifuged at 14000g for 10 min to remove cell debris, utilizing the supernatant for binding experiments.

2.3.15 Chromatographic measurements

A Waters Acquity I-Class UHPLC system (Waters Corporation, Milford, MA) was used for chromatographic separations, with a column ACQUITY UPCL BEH300 C4 1.7 µm (Waters Corporation, Milford, MA).

2.3.16 PDE2 Protein extraction

10 mg of drug bound beads were placed in 500 µL of PDE2 protein or HeLa lysate solution (pH 7.5) containing Trizma 50 mM, $MgCl_2$ 1.3 mM and Brij 35 0.01 %. Binding was carried out at room temperature for 1.5 h in a horizontal shaker at 750 rpm. After protein binding, beads were magnetically extracted and rinsed five times with 20mM Tris buffer containing 0.1 % Tween. Rinsed beads were suspended in 150 µL of 20 mM Tris buffer (0.1 % Tween) and quantitatively transferred to a 200 µL PCR tube. TRIS buffer was removed, and 100 µL of 0.1 % SDS was added and a first extraction was performed for 30 min. Supernatant was collected and analyzed. Beads were rinsed 3X with PBS 1X buffer and protein elution was made using 60 µL of 2 % SDS (0.2 % TFA) were added and elution was performed for 30 min.

2.4 Results and Discussion

2.4.1 Coating of magnetic particles

Commercial iron particles were first coated with a silica layer and after surface initiation, grafted using AGET ATRP, with epoxide containing block polymer as depicted in Figure 2.1. Individual stages are discussed in this section.

2.4.1.1 Silica Coating

Initially, iron particles are coated with PEI, to produce a positive zeta potential, enhancing suspension, and allowing subsequent silica deposition. Silica coating is obtained using a modified two steps Stöber procedure.[40] TEM micrograph in Figure 2.2A reveals a rough topography of the 50 nm silica layer. When these particles are treated with 37 % HCl under sonication, the iron core is dissolved, leaving an empty shell as depicted in Figure 2.2B. This finding exposes the porous nature of the synthetized silica layer.

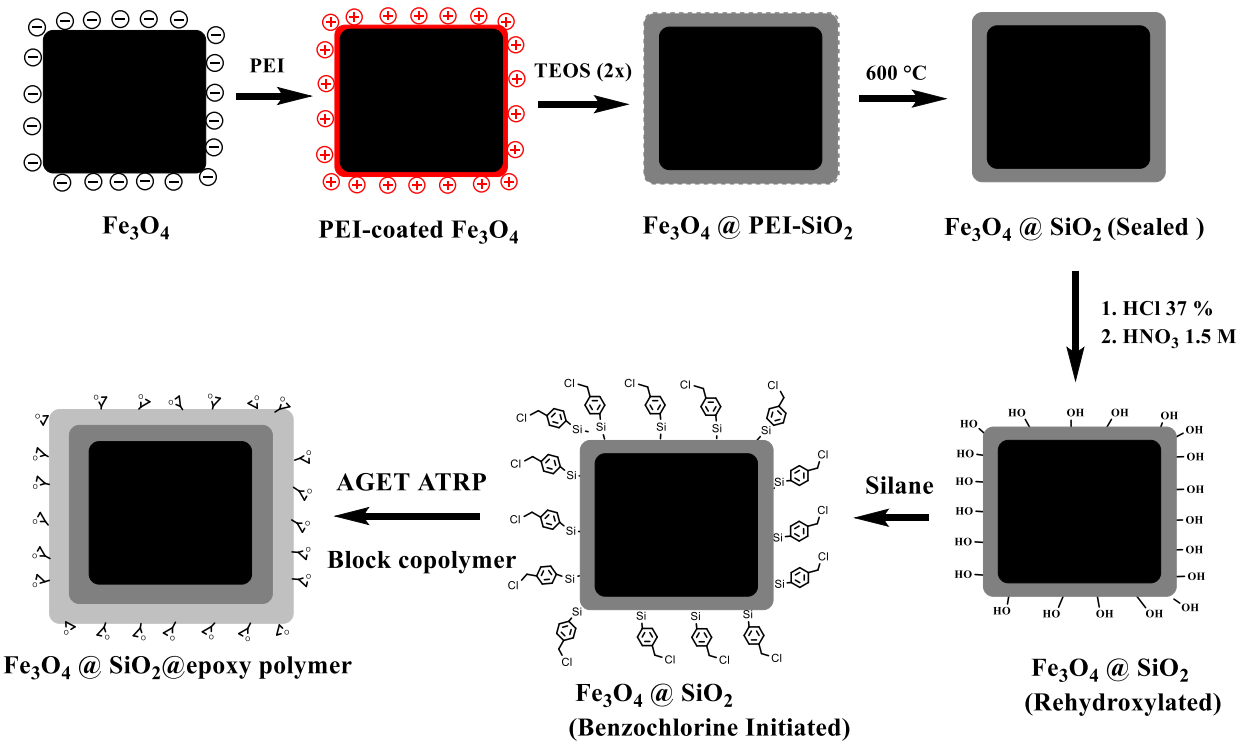

Figure 2.1 Scheme of coating process of magnetic particles.

It has been proved that thermal treatment seals silica cracks and condenses the siloxane groups creating an impermeable and denser shell. [41-43] However, if iron oxide is heated under an oxygen environment, it oxidizes, losing its magnetic properties.[44] So, the material needs to be heat treated under free oxygen atmosphere. This can be achieved in a tube furnace, pre-purged with nitrogen and maintained at high vacuum along the cycle. Silica heat treatment includes annealing in a wide range of temperatures (800 °C – 1200 °C) and calcination (400 °C – 600 °C). [41-43] Accordingly, evaluated thermal cycles included annealing and calcination at T_A and T_C temperatures during t_A and t_C times, respectively as described in Figure 2.3. Percentage of mass loss after HCl exposure was used as indication of silica layer permeability.

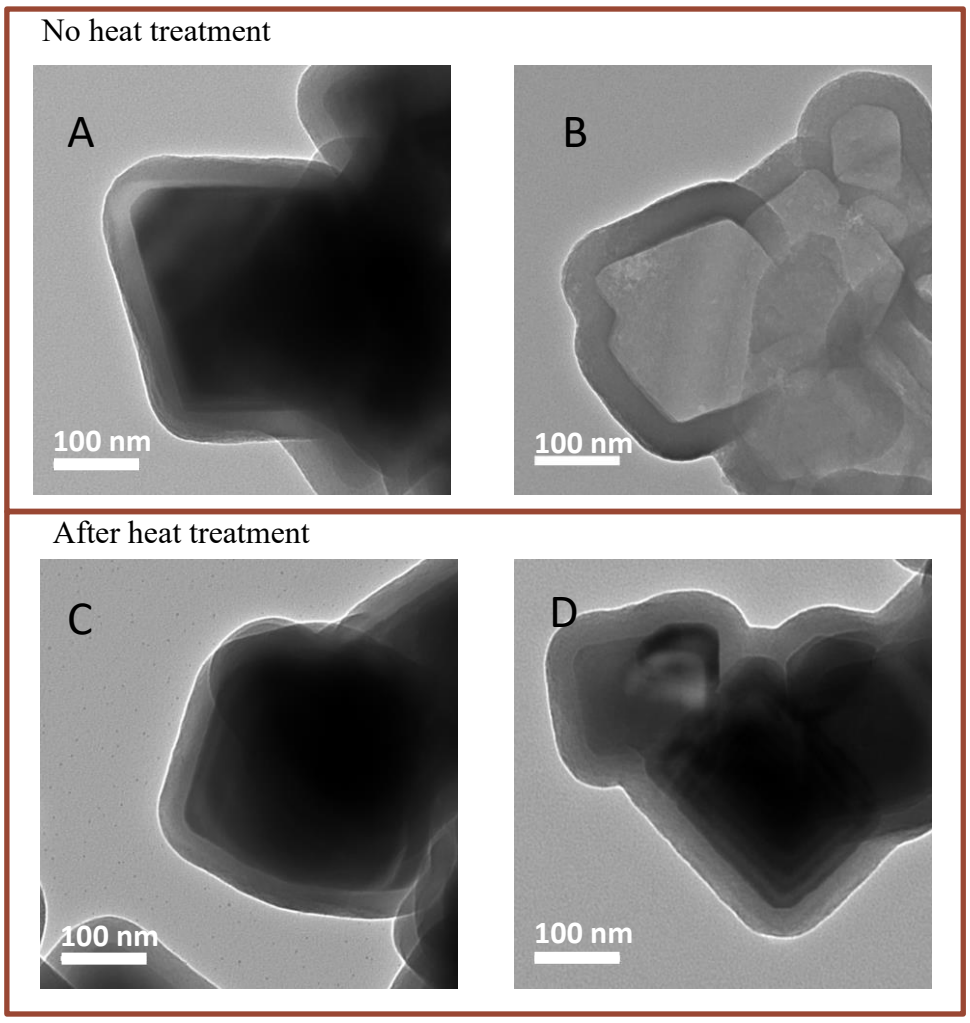

Figure 2.2.TEM micrographs of Fe_3O_4@SiO_2. (A) Before thermal treatment. (B) After sonicating in 37 % HCl for 1 h. (C) After calcinating at 600 °C for 3 h. D) After heat treatment and sonication in 37 % HCl for 1 h.

Initially, annealing at 1050 °C (without calcination) was evaluated during 10 min and 30 min (Table 2.1, programs 1 and 2), but obtained particles were completely dissolved in HCl. Addition of calcination at 600 °C (program 3) slightly improved permeability, though only 20 % of the material survived the acid. Annealing at 800 °C (programs 4 and 5), exhibited lower mass loss in acid. Also, it was appreciated that longer calcination time at 600 °C enhances silica porosity. Hence, only calcination for longer time (program 6) was evaluated, given the lowest mass loss among examined programs. These results can be explained by calcination's capacity to remove excess reagents from Stöber process (ethanol, water, ammonia), making silica denser and sealing pores. Annealing temperatures, on the other hand, can make silica softer, allowing subtle deformation, that for a thin layer (about 50 nm) could yield to exposed iron cores, make them susceptible to acid attack. After effective heat treatment, silica layer is smoother and thinner (presumably denser) as appreciated in Figure 2.2C, preventing oxidation of Fe_3O_4 under strong acid conditions (Figure 2.2D).

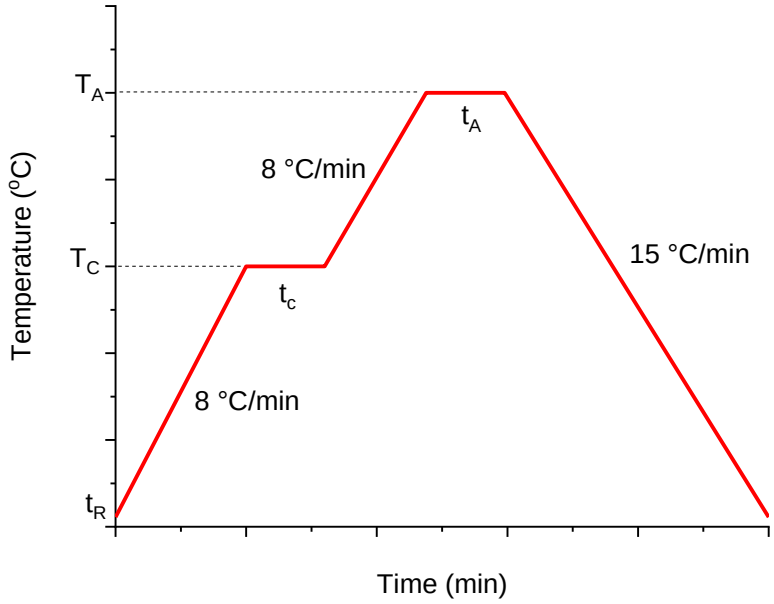

Figure 2.3. Evaluated heat treatment for Fe_3O_4@SiO_2 particles included two stages, calcination at T_C during t_C time and annealing at T_A during t_A time. Heating up and cooling down rates were kept constant between vacuum tube furnace specifications. Mass loss in HCl after every tested program was used to assess its effectiveness.

Particles tend to stick together during silica coating due to their residual magnetic moment, producing aggregates of around 1 µm of size as shown in Figure 2.4. Despite the large size of the particles, surface area is high, a desirable feature for binding purposes.

Table 2.1 Heat treatment optimization programs. T_C and T_A are calcinating and annealing temperatures at times t_C and t_A, respectively. Empty boxes indicate that the step was omitted.

Program	**T_C [°C]**	**T_C [min]**	**T_A [°C]**	**T_A (min)**	**% Mass loss**
1	---	---	1050	10	92 ± 3.5
2	---	---	1050	30	97 ± 2.8
3	600	20	1050	10	80 ± 5.6
4	600	20	800	40	48 ± 3.8
5	600	120	800	40	18 ± 2.5
6	600	180	---	---	12 ± 1.7

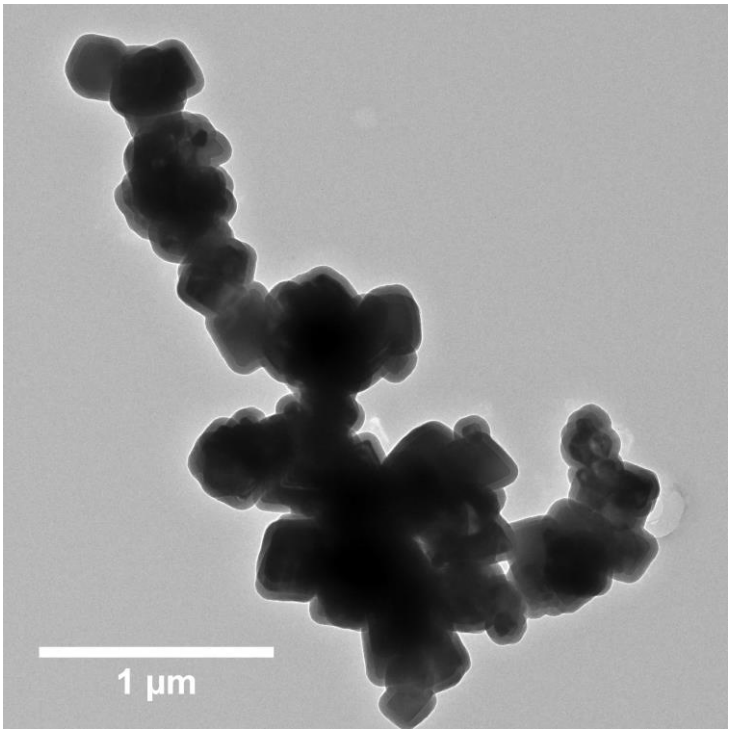

Figure 2.4. TEM micrograph of Fe_3O_4@SiO_2 particles after heat treatment and acid test. Aggregation is obtained due to magnetic properties of starting material.

2.4.1.2 Surface initiated AGET ATRP

Calcinated silica coated magnetic particles can withstand re-hydroxylation under acidic reflux conditions (1.5 M HNO_3 for 24 h) and the following chlorosilane modification to incorporate ATRP initiators. GMA is used as epoxide containing polymer, but its hydrophobicity hinders obtention of a low biofouling surface. Polyacrylamides were selected to form a copolymer with GMA, due to their high hydrophilic character and biocompatibility. Polyacrylamide (PAAM) shows very good non-specific absorption behavior,[25] but it undergoes hydrolysis under aqueous conditions, producing acrylic acid.[45] On the other hand, poly-N-Hydroxyethyl acrylamide (PHEAA) is higher resistant to degradation than PAAM and demonstrates low biofouling.[46-48] Hence, a copolymer of PGMA and PHEAA was chosen to develop a more hydrophilic surface with high binding capacity.

Since, obtention of silica coated magnetic particles is time-consuming, optimization of surface initiated AGET ATRP was made using 1 µm SiO_2 particles, with same silane functionalization. The goal was to synthetize a dense and smooth polymer layer with a thickness of at least 10 nm,[49-50] to obtain a surface with low non-specific absorption and high binding capacity. Initially, copolymerization of GMA and HEAA was carried out using 0.4 M of both monomers. These polymerization conditions produced particle aggregation as seen in Figure 2.5A, and free polymer growing in solution after only 10 min of reaction. Aggregates formation was slightly improved by lowering monomer concentrations to 0.1 M and extending the reaction time to 20 min, but surface was still irregular and polymer thickness was only 3 nm (Figure 2.5B).

Controlled ATRP reactions require proper selection of initiator.[51] Selection of benzyl chloride as initiator was made considering that chlorine initiators provide slower reaction rates compared with bromide initiators,[52] and bromide initiators are less stable and need to be used in short time after functionalization. So, a change in initiator would not help to improve reaction control. Since methacrylates are more ATRP reactive than acrylamides,[53] the difference in reaction rates for GMA and HEAA presents an important problem for this copolymerization. Living character of ATRP provides a way to not only obtain block copolymers, but also, to “change initiator”, since halogens at end chains become initiators for next polymerization.[54-56] Hence, a block copolymer would be helpful to control the PGMA-co-PHEAA polymerization.

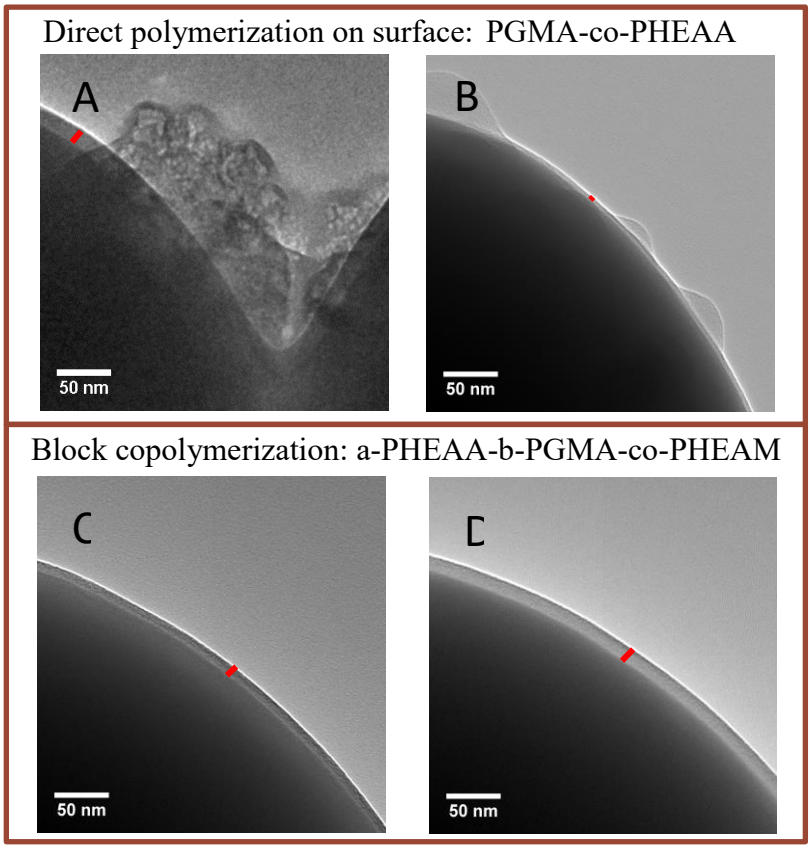

Figure 2.5. TEM micrographs of 1µm silica particles grafted with polymer. A) SiO_2@ PGMA-co-PHEAA ([monomers] = 0.4 M, 10 min reaction) B) SiO_2@ PGMA-co-PHEAA ([monomers] = 0.1 M, 20 min reaction. C) SiO_2@ PHEAA (1 M, 60 min), D) SiO_2@ PHEAA-b-PGMA-co-PHEAA (0.15 M, 20 min).

Optimized conditions allowed to grow an 8 nm PHEAA layer (Figure 2.5C), producing hydrophilic particles with improved water dispersity. Next, a second layer of PGMA-co- PHEAA was added to the PHEAA surface. Using 0.2 M monomer concentrations the reaction was controlled during 20 min, with no appreciable aggregation, adding 5 nm of epoxy containing polymer (Figure 2.5D). Variation in molar ratio of monomers were subsequently evaluated with similar polymerization control in all experiments. LBSA was directly bound to the surface and intensity of obtained color was used as qualitative indication of binding performance (see Figure 2.6). As presented in Table 2.2. a 1:1 molar ratio (0.2 M of each monomer) permits a balance between binding capacity and particle hydrophilicity.

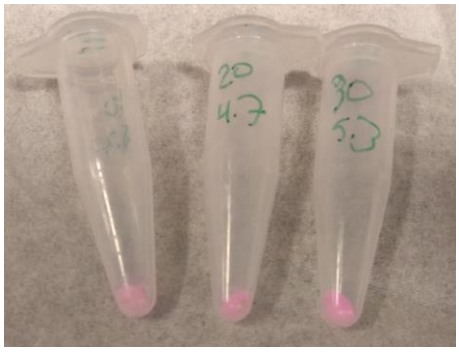

Figure 2.6. Vials containing silica polymer beads with LBSA bound directly to epoxide on the surface.

Table 2.2. Label Fluorescence test. 0.1g/L LBSA was incubated for 2 h directly with silica polymer beads. Intensity was qualitatively evaluated to asses binding performance.

[HEAA] mol/L	**[GMA] mol/L**	**Fluorescence from LBSA**	**Suspension in water**
0.2	0.03	No visible	Complete
0.2	0.09	No visible	Complete
0.2	0.12	fair	Complete
0.2	0.2	Very good	Complete
0.4	0.2	good	Complete
0.8	0.2	Fair	Complete
1	0.2	No visible	Complete
1.2	0.2	No visible	Complete

Applying this optimized polymerization to the silica coated magnetic particles needed a modification to the experimental set up, because a magnetic stirrer causes aggregation and without a homogenization mechanism the particles would stick against the bottom of reaction flask. Also, the reaction requires to be carried out under a nitrogen atmosphere. A home-made overhead stirring system provided appropriated experimental conditions to full fit these requirements. A small magnet was attached to one end of a long glass rod as shown in Figure 2.7A. A condenser was connected to a two necked reaction flask, placing the stirrer inside and using the condenser inlet for nitrogen purge (Figure 2.7B). Top of the condenser was sealed using an extension with an outlet for nitrogen and an overhead stirred with a magnet provided the agitation (Figure 2.7C)

The optimized method allowed to obtain a controlled polymerization over the silica coated magnetic particles. As revealed in Figure 2.8B, PHEAA layer is smooth and around 8 nm, in agreement with the polymerization on the 1 µm silica particles. The second polymerization increases the homogeneous polymer thickness to around 13 nm, as presented in Figure 2.8C. These TEM micrographs demonstrate that the block copolymerization approach was effective to obtain a controlled growing of PGMA-co-PHEAA.

2.4.1.3 Infrared Spectroscopy characterization

In Figure 2.9 are displayed the chemical structures for the components of coated material: iron core (magnetite), silica coating (SiO_2) and block copolymer (PGMA and PHEAA). Fourier-transform infrared spectroscopy confirms chemical composition of material along coating process. Figure 2.10, presents FT-IR spectra of material after main steps. Magnetite (Fe_3O_4) absorption band can be located around 800 cm^{-1} and 500 cm^{-1}. [57-58] Silica coating produces additional peaks at 1080 cm^{-1} due to Si-O-Si stretching and at 1050 cm^{-1} to 1250 cm^{-1} by Fe-O-Si stretching vibration. [59-60] PHEAA composition is verified by characteristic carbonyl vibration of at 1728 cm^{-1},[61] and amide absorption band at N-H stretching at 3300 cm^{-1} – 3500 cm^{-1}. One of the most important features of the surface is the presence of the epoxide ring at 908 cm^{-1}, [62] an intact oxirane group in the final material is vital for binding with amine groups in proteins.

2.4.2 Magnetic characterization

A faster magnetic extraction, compared with other separation techniques as centrifugation, makes very attractive the material presented in this work. The particles must have high magnetization in the presence of an external magnetic field to reduce waiting time and maximize recovery. Figure 2.11, shows variation of magnetization during the different coating stages. It is possible to appreciate a decrement in magnetic saturation, starting with more than 90 emu/g for Fe_3O_4, then after silica coverage is reduced to 56 emu/g and finally becomes 45 emu/g for polymer coated particles. This variation is mainly due to the addition of non-magnetic materials (silica and polymer) and possible minimal oxidation of iron during heat treatment. It is necessary to point out that plotted moment values are per mass unit, and since silica and polymer cause a net diminution in material density, a unit mass of coated material has less magnetic iron cores compared with pure Fe_3O_4.

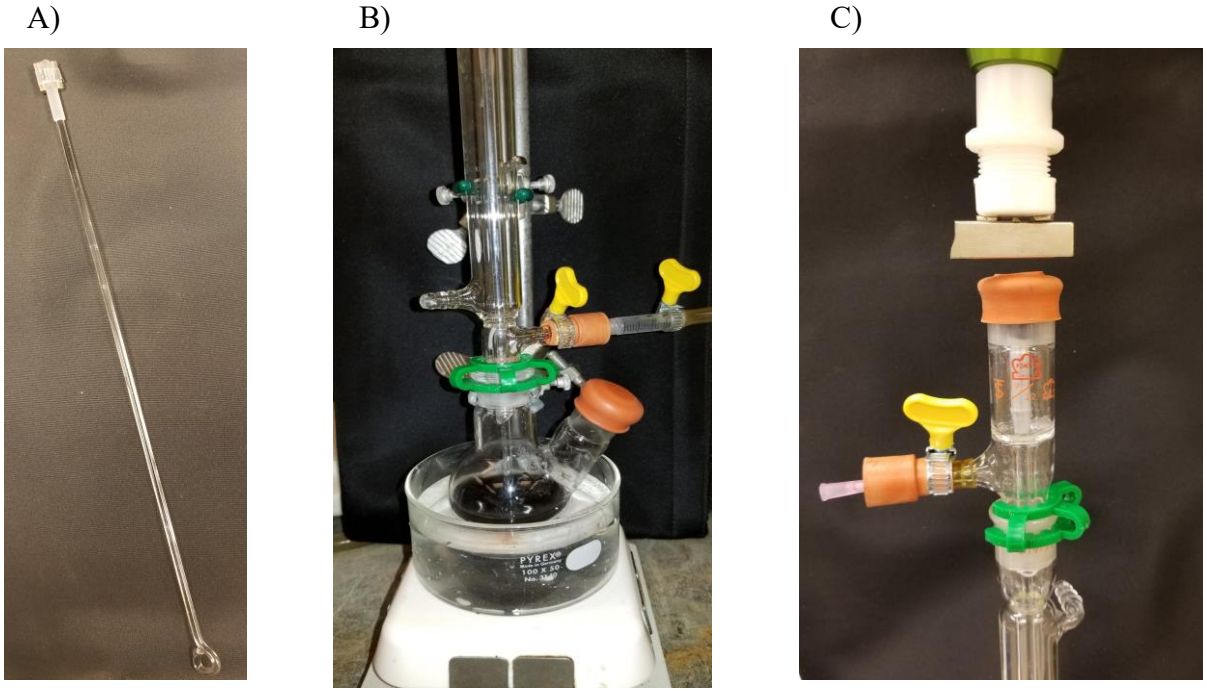

Figure 2.7. Experimental set up for AGET ATRP of magnetic particles. A) Glass stirrer with magnet at the top, placed inside condenser. B) Two-neck reaction flask connected to condenser with nitrogen inlet. C) Top of condenser with nitrogen outlet. Overhead stirrer with magnet attached allows sealed mixing.

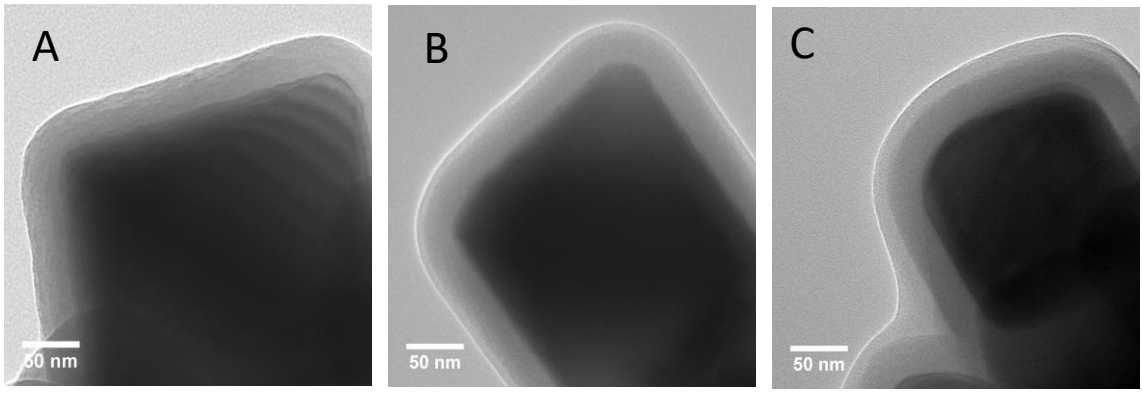

Figure 2.8. TEM micrographs of polymerization process of silica coated magnetic particles. A) Initial Fe_3O_4@SiO_2 chlorosilane initiated. B) Fe_3O_4@SiO_2@PHEAA after first AGET-ATRP polymerization. C) Fe_3O_4@SiO_2@PHEAA-b-PGMA-PHEAA, final block copolymer.

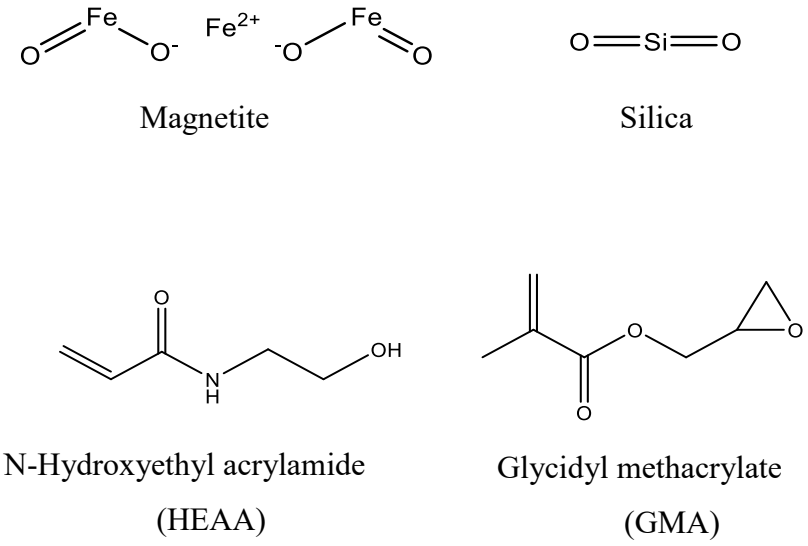

Figure 2.9. Chemical structures of components of epoxide magnetic beads.

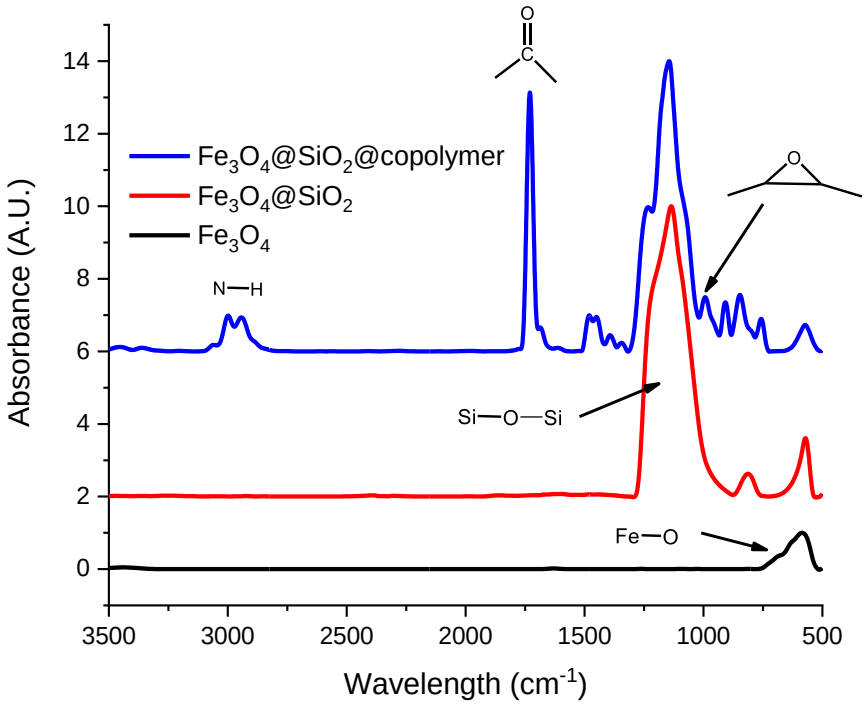

Figure 2.10. FT-IR spectra of iron oxide (Fe_3O_4), silica coated iron after calcination ($Fe_3O_4@SiO_2$), and after block copolymerization ($Fe_3O_4@SiO_2$@copolymer). Silica peak (1100 cm^{-1} – 1000 cm^{-1}) absorbance was used for normalization of spectra.

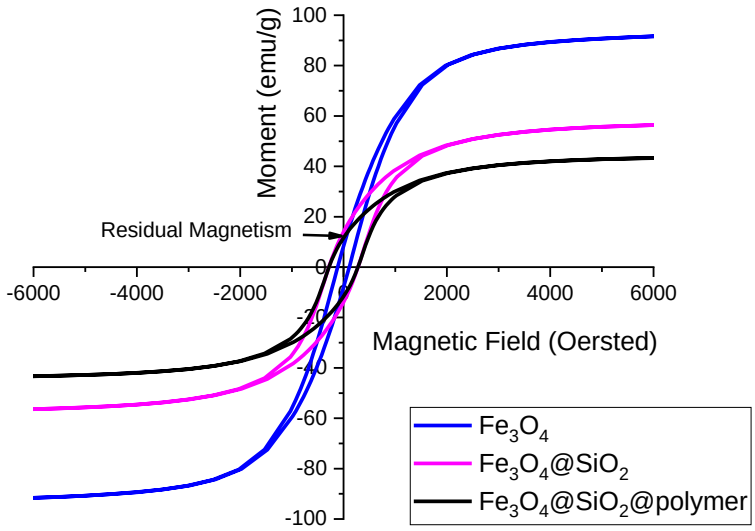

Figure 2.11. Magnetic hysteresis loops of variation of magnetization during coating stages, reduction of magnetic saturation is mainly due to addition of layers of non-magnetic materials and changes in material density

Another evident feature displayed in Figure 2.11, is the residual magnetic moment, intrinsic to starting material and almost constant during coating steps. This characteristic causes aggregation of particles during coating, hindering obtention of singly silica coated particles as pictured in TEM micrographs of Figure 2.4. Some efforts have been made to obtain individually silica coated magnetic particles;[10-11] however, such coating processes give very low yields and require several synthesis steps. Figure 2.12 compares magnetic hysteresis loops of the epoxy magnetic beads obtained in this work with two commercially available extraction beads: Dynabeads M-270 epoxy and BcMag. Particles developed here, have a higher magnetic saturation (45 emu/g) contrasted with Dynabeads (32 emu/g) and BcMag (19 emu/g). This feature permits to use smaller particle size for a higher surface area, keeping a fast removal from suspension.

2.4.3 Binding performance for immunoprecipitation

As a basic test of binding capacity, common immunoprecipitation test was performed. BSA antibody was bound to the surface at different binding times, particles were blocked and incubated for 1 h with LBSA. Eluted LBSA from beads was quantified via fluorescence measurements. Similar protocols were followed with commercial beads and results are pictured in Figure 2.13. Saturation of all studied particles is reached around 4 h, although silica coated magnetic

nanoparticles exhibit higher binding capacity (1.83 µg BSA/mg) than Dynabeads and BcMag (approximately 0.9 µg BSA/mg).

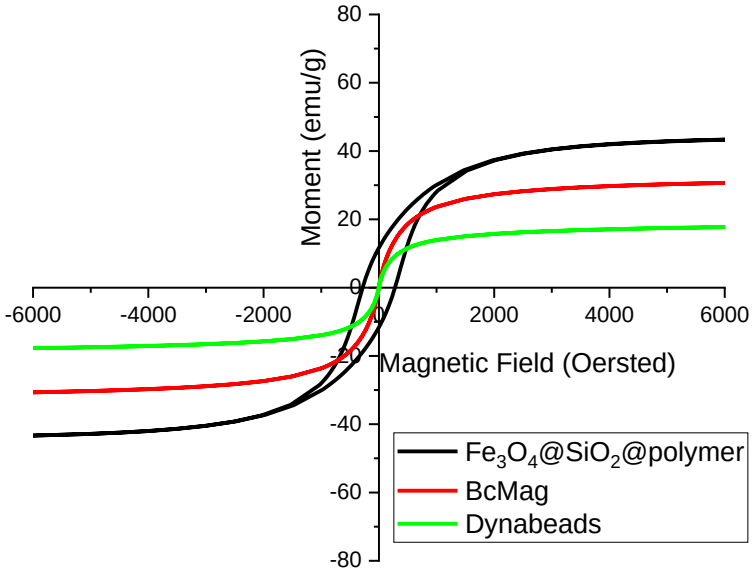

Figure 2.12. Magnetic hysteresis loops, comparison of epoxide magnetic beads (Fe_3O_4@SiO_2@polymer) and commercial beads.

Despite this difference, it is important to point out that the comparison is made per mass of particles, and it could be unfair for noticeable differences in density and surface area. Therefore, it was investigated the non-specific binding of all the beads to contrast them with their specific bindings, in order to obtain the signal to noise ratio (SNR) as a fair comparison. As shown in Table 2.3, Fe_3O_4@SiO_2@copolymer particles have 1.85 times more SNR compared to Dynabeads and almost 16-fold contrasted against BcMag, despite the fact BcMag have higher surface area. This could be attributed to the obtained block copolymer, with high graft density and long chains (more than 10 nm), improving resistance to protein absorption.[63]

There are notable differences in structure of compared particles, Dynabeads and BcMag are similar in morphology. Dynabeads are 2.7 µm polystyrene spheres inserted with superparamagnetic iron nanoparticles (Figure 2.14). BcMag are silica coated magnetic particles, with smaller size and have only 1 nm of epoxide linker (Figure 2.15).[64] Lower non-specific binding of the magnetic particles reported by this work can be attributed to the longer dense polymer layer (13 nm), which avoids interaction of proteins with silanols present on silica surface.

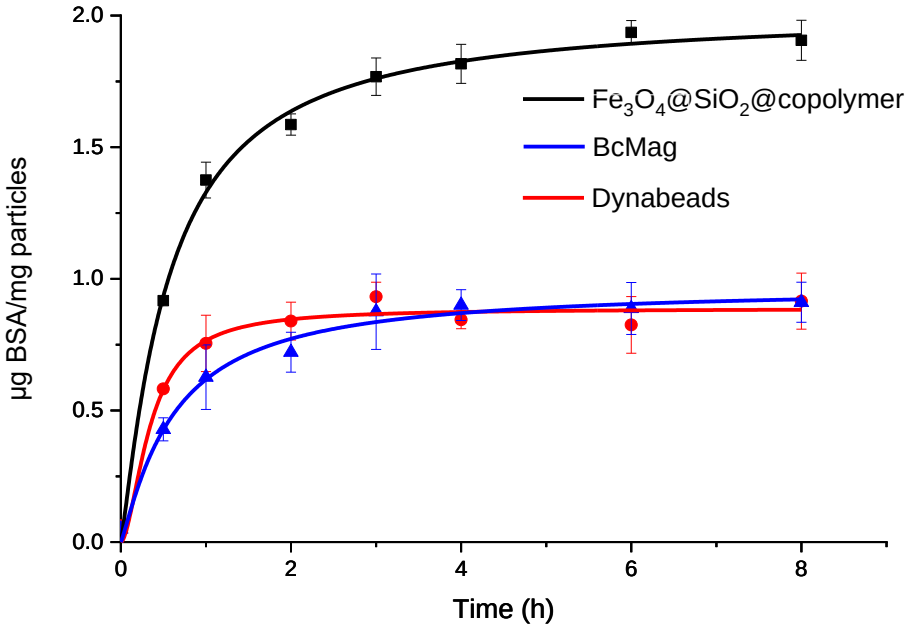

Figure 2.13. BSA antibody binding kinetics measured via eluted fluorescent BSA. All concentrations were 0.1 µg/µL.

Table 2.3. Comparison of specific and non-specific binding of fluorescent BSA for silica coated magnetic particles and commercial beads. Signal to noise ratio (SNR) was calculated as the quotient of specific/non-specific. Binding time was 4 h for all assays.

Beads	**Specific binding (µg/mg)**	**nonspecific binding (µg/mg)**	**SNR**	**Surface area (m^2/g)**
BcMag	0.91 ± 0.08	0.225 ± 0.005	4.05 ± 0.35	100
Dynabeads M-270	0.92 ± 0.11	0.026 ± 0.003	34.69 ± 5.7	2 to 5
Fe_3O_4@SiO_2@copolymer	1.83 ± 0.04	0.029 ± 0.004	64.21 ± 8.01	10

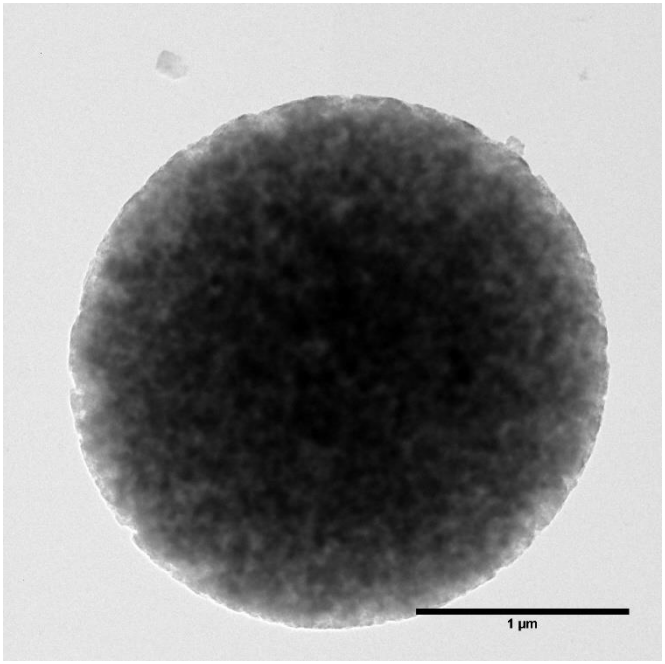

Figure 2.14. TEM micrograph of Dynabeads M-270 epoxy.

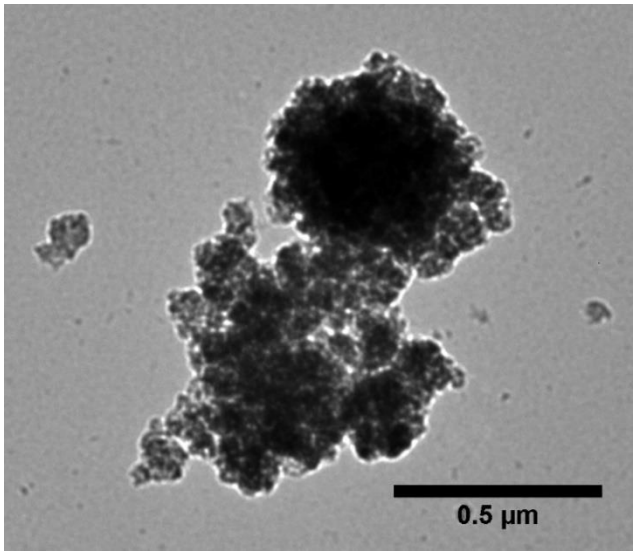

Figure 2.15. TEM micrograph of BcMag beads.

2.4.4 Drug – protein binding

A more interesting application of the reported magnetic extraction beads is to study their use as a mean to evaluate drug-protein interaction. Essentially, the idea is to investigate target protein pull out using a drug compound immobilized on the particles. It has been found that trifluromethyl drug compounds can strongly bind to phosphodiesterase 2A (PDE2A) enzyme, inhibiting its activity (Figure 2.16A). At first, the drug compound must be attached to the surface via a covalent bond. Since used PDE2A drug shown in Figure 2.16B, does not have an active group to react with the epoxide groups, it was necessary to create a linker with an amino group that allows the binding. Inclusion of an amino PEG chain was selected because its low biofouling properties (Figure 2.16C).

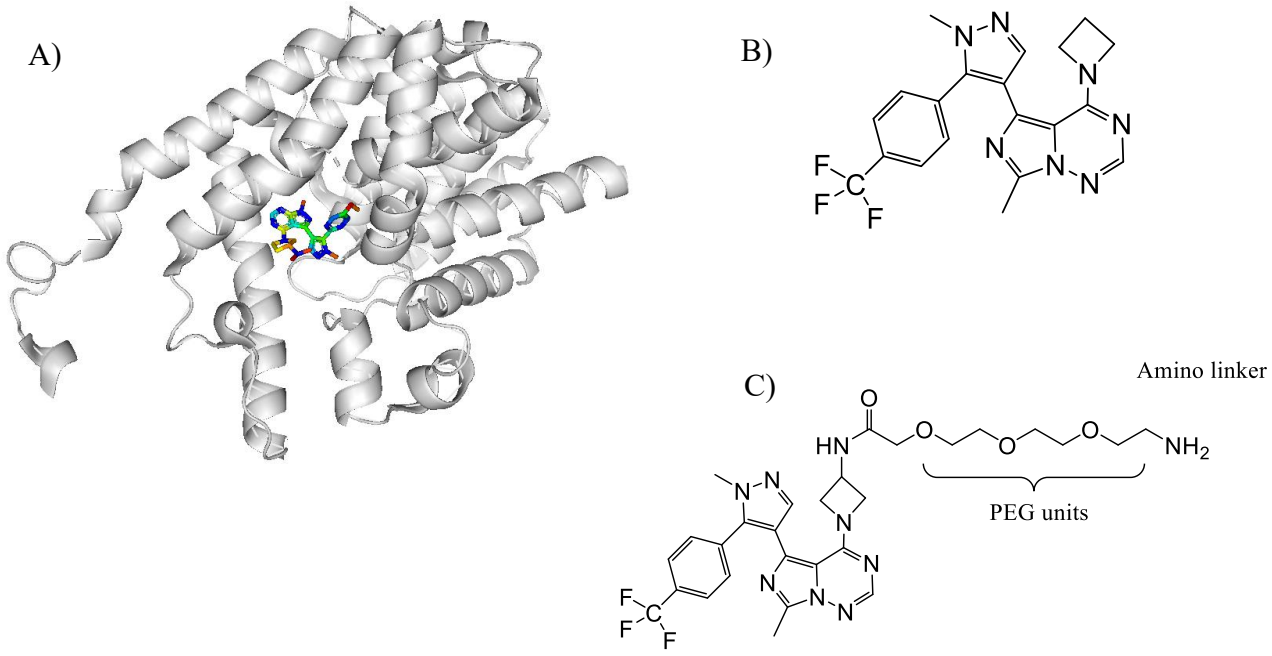

Figure 2.16 A) Phosphodiesterase 2A (PDE2A) with trifluorimethyl drug (rainbow chain) filling induced pocket on x-ray structure PDB code 5U7L. B) PDE2A inhibitor (PF-05085727, Pfizer). C) PDE2A inhibitor with a 3-PEG units amino linker.

2.4.4.1 Evaluation of the effect of linker length in protein binding

It was necessary to evaluate how long the linker chain needs to be to facilitate interaction of the drug active site with the binding pocket of the PDE2A (Figure 2.16A). Three different PEG linker lengths (3, 6 and 12 units) were studied, comparing the relative amount of PDE2A that can be eluted from every group of particles, after being incubated with standard PDE2 2 µg/mL in Trizma buffer. PDE2 analysis was made using RPHPLC, a standard sample of PDE2 50 µg/mL in Trizma 50 mM was ran to obtain a model chromatogram (Figure 2.17A). As can be appreciated in Figure 2.17B, eluted PDE2 from beads with various PEG lengths drugs, does not show a significant difference. For remaining experiments, drug with 6 PEG units was used.

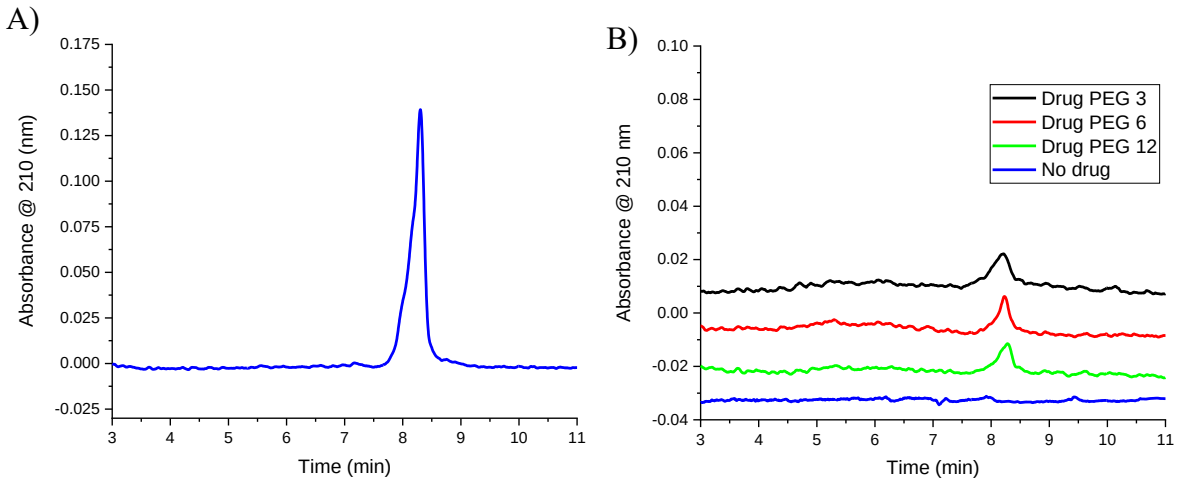

Figure 2.17. HPLC chromatograms for: A) PDE2 standard 50 µg/mL in buffer (Trizma 50 mM). B) PDE2 eluted in 2 % SDS from beads with different PEG units drugs bound and from beads with drug. Conditions: Flow rate: 200 µL/min. Solvents: A: H_2O (0.1 % TFA), B: ACN (0.1 % TFA); flow rate: 200 µL/min; injection: 30 µL (3 times 10 µL during stacking conditions (25 % B). Gradient: 0 – 1 min: 25 % 1-14 min 25 % B to 90 % B. Column temperature: 60 °C

2.4.4.2 Correlation of initial concentration with amount of eluted PDE2

For quantifying PDE2, a calibration curve was obtained with PDE2 standards in 2 % SDS (0.2 % TFA), since those are the elution conditions utilized with the particles (Figure 2.18). It can be seen a good correlation of peak area and protein concentration, confirmed by the correlation coefficient close to 1. This calibration plot was used to determine recovered PDE2 from binding experiments.

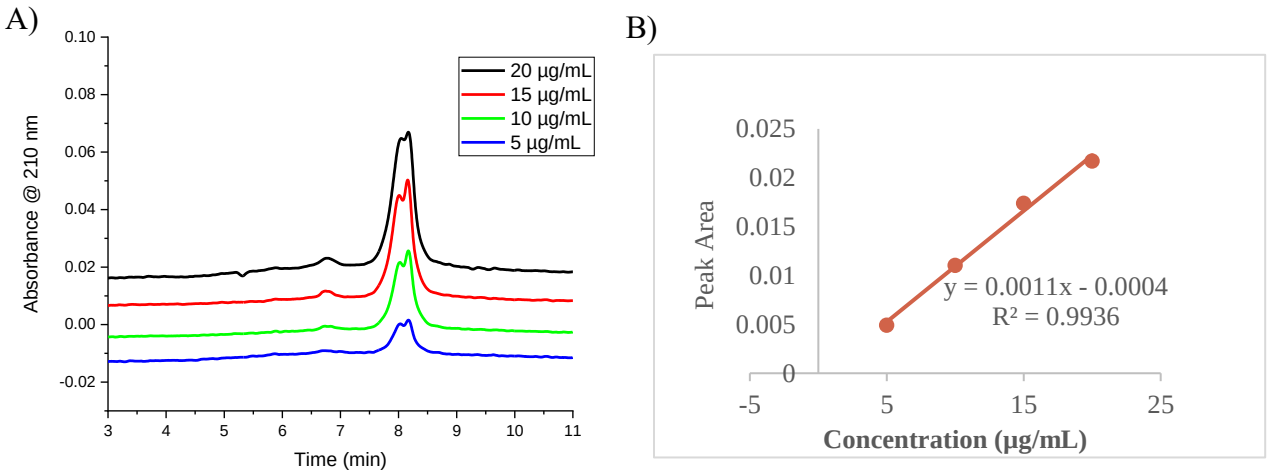

Figure 2.18. PDE2 standard curve in 2 % SDS (0.2 % TFA). A) HPLC chromatograms for PDE2 standards in 2 % SDS (0.2 % TFA), conditions as described in Figure 2.17. B) Calibration plot of PDE2 in 2 % SDS (0.2 % TFA).

To stablish the relation between the PDE2 concentration used during incubation with drug-bound beads and the amount eluted, four different initial concentrations of PDE2 in Trizma buffer (1 µg/mL, 1.5 µg/mL, 2 µg/mL, and 4 µg/mL) were utilized for binding experiments. Chromatograms of eluted PDE2 from those different initial PDE2 concentrations shown in Figure 2.19, show that binding of PDE2 is correlated with the solution initial concentration. Also, according with these results, for the analytical method used in this work, PDE2 released when initial concentration is lower than 1.5 µg/ml is not detected.

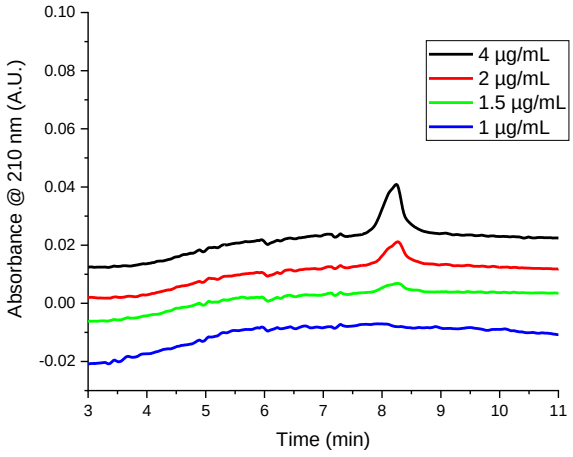

Figure 2.19. HPLC chromatograms for eluted PDE2 from beads incubated with different initial standard concentrations. (Note that labeled concentrations correspond to PDE2 initially incubated with beads, chromatograms do show PDE2 released)

PDE2 recovery can be calculated using the peak area and obtained calibration curve. For instance, for the initial PDE2 concentration of 4 µg/mL, the peak area of the eluted protein is 0.0077 (Figure 2.19), and the concentration in 60 µL of extract is:

$$[\text{PDE2}] = \frac{0.0077 + 0.0004}{0.0011} = 7.36\ \mu\text{g/mL}$$

The mass of PDE2 released is 7.36 µg/ml x 0.06 mL = 0.4416 µg. Since, solution used for binding was in 500 µL, recovery can be calculated as follows:

$$\text{Recovery} = \frac{0.4416\ \mu\text{g}}{4\ \mu\text{g/mL}\ \text{x}\ 0.5\ \text{mL}} \text{x}100 = 22.08\ \%$$

These findings show that protein recovery could be enhanced adjusting binding parameters as incubation time, however, in more complex matrixes increasing the binding time longer than used here (1.5 h) potentially increases not specific absorption.

2.4.4.3 Reuse of drug-bound magnetic particles

The ability of the covalently drug-bound beads to be reused for multiple analysis, makes them more attractive. To assess this, beads used in a previous experiment were prepared for a second extraction by additional washes with 2 % SDS and subsequently rinses with Trizma buffer to remove any surfactant. Once clean, the particles were used again for extraction of PDE2 at initial concentration of 2 µg/mL and eluted PDE2 was analyzed. As presented in Figure 2.20, PDE2 released from reused drug-bound beads is comparable with the first extraction, demonstrating that the drug immobilization is stable enough for being reused at least one more time.

2.4.4.4 Non-specific absorption of the surface without drug bound

It is necessary to stablish if capturing of PDE2 is due to interaction with drug and not to adsorption into polymer layer. Hence, it is critical to evaluate the non-specific binding by the surface. Epoxy magnetic particles were incubated with blocking buffer to deactivate the epoxide groups, and no drug was bound. Next, the blocked particles (10 mg) were incubated with HeLa lysate (section 2.3.14) during 1.5 h. Same procedure was applied for Dynabeads. Elution from

both type of beads was made with 2 % SDS and HPLC analysis was performed. Chromatograms for the extracts shows no visible PDE2 protein, (Figure 2.21). Non-specific binding is higher for Dynabeads compared with magnetic particles reported here, however such a complex matrix contains species that can be absorbed on the surface, which is appreciable between 2 min and 6 min as a raised baseline for the copolymer beads.

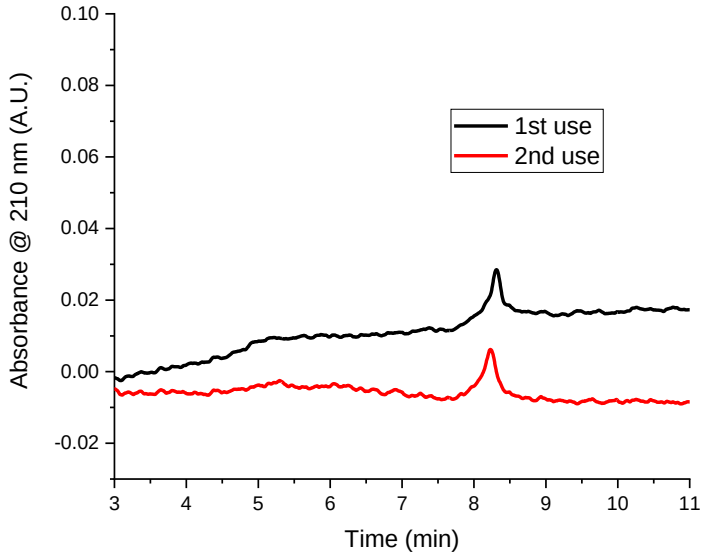

Figure 2.20. HPLC chromatograms for released PDE2 from beads reused twice. HPLC conditions as described previously.

2.4.4.5 PDE2 binding from HeLa lysate with drug-bound particles

Amount of PDE2 found in HeLa lysates was too low for being detected by the HPLC method utilized in this work. The main purpose of this part of the research is to evaluate the influence of a more complex matrix in binding PDE2. Hence, HeLa lysates was spiked with 2 µg/mL of PDE2 for these experiments.

Preliminary binding experiments with HeLa lysates showed that washes with Tween 0.1 % were not completely effective to remove species adsorbed on the surface, evident in extracts exhibiting a large variety of extra peaks. During elution conditions studies, lower SDS concentrations were used and non or very low amounts of PDE2 were obtained. Considering these

discoveries, it was proposed to use a preliminary stringency rinse using 0.1 % SDS during 20 min (same time used for final elution) to minimize adsorbed species during final elution. After that initial wash, the elution with 2 % SDS was utilized as previously described. Improved protocol was applied also to Dynabeads. From chromatograms for reported beads in Figure 2.22A is noticeable that stringency wash removed an important amount of absorbed species and no visible PDE2 bound to the drug (blue line), while elution with 2 % SDS shows the characteristic peak for PDE2 around 8 min (red line). Results for Dynabeads in Figure 2.22B, it is also evident the removal of a higher amount of non-specific binding to the surface with the stringency wash (blue line). However, the expected peak for PDE2 is not visible in the final elution solution and a considerable number of extra peaks is present (red line).

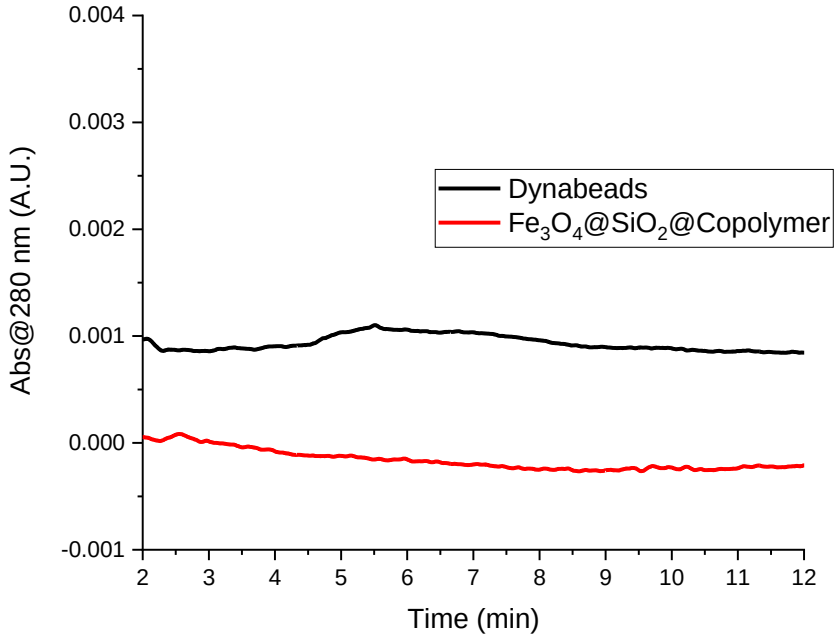

Figure 2.21. HPLC chromatograms for elution with 2 % SDS (60 µL) from beads with surface previously blocked (no drug), incubated with HeLa lysate spiked with PDE2. HPLC conditions as described previously.

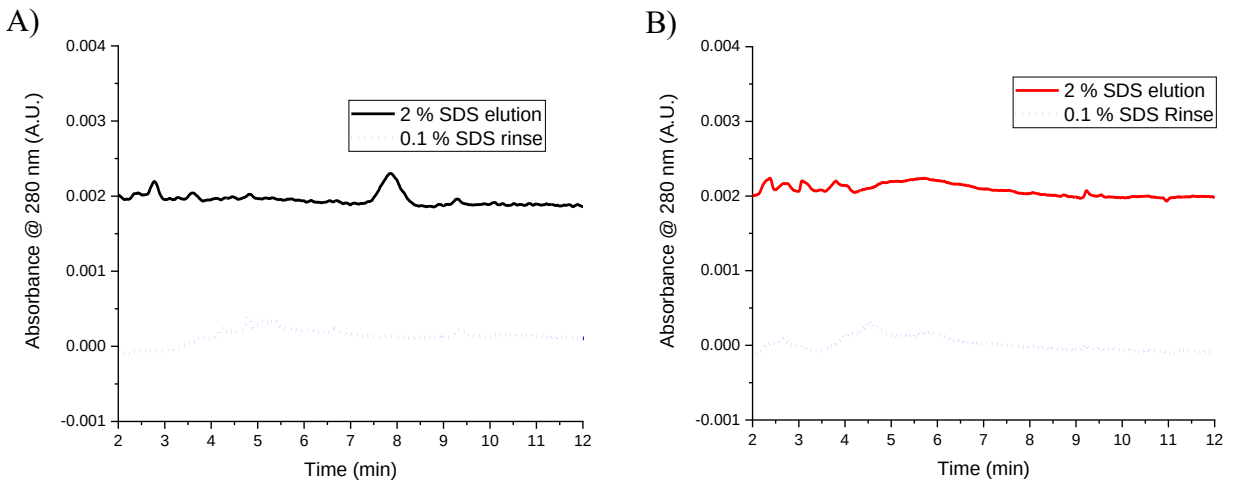

Figure 2.22. HPLC chromatograms for a previous rinse with 0.1 % SDS (blue line, bottom) and elution with 2 % SDS (red line, top) from beads with inhibitor bound, after incubation with HeLa lysate spiked with PDE2: A) Fe_3O_4@SiO_2@copolymer and B) Dynabeads M-270 epoxy. HPLC conditions as described previously.

2.5 Conclusions

Commercially available magnetic nanoparticles were coated with silica using a modified two steps Stöber and heat treated to obtain a strong acid resistant surface. Large Fe_3O_4 particles have high magnetization and can be easily extracted with regular neodymium magnets. Impervious silica coating can be functionalized with chlorosilanes to obtain ATRP initiator on the surface. A two steps AGET ATRP, permits control over the copolymerization of monomers with different reactivity to produce a hydrophilic layer preserving binding capacity of epoxide groups. Composition analysis and TEM showed a successful optimized stepwise coating process. Immunoprecipitation performance of the reported particles indicated higher binding capacity in short time and lower nonspecific binding compared with some commercial extraction beads. Versatility of the particles reported in this work, allowed binding of a drug via amino linker reaction with epoxide groups, being possible to extract the target protein PDE2 from a complex matrix of HeLa lysate, showing better performance than commercial beads with low non-specific binding.

2.6 References

1. Tang, D. a. Y. R. a. C. Y. a. A. H., Magnetic-core/porous-shell CoFe2O4/SiO2 composite nanoparticles as immobilized affinity supports for clinical immunoassays. *Advanced Functional Materials* **2007,** *17* (6), 976--982.

2. Lee, J. a. C. J., Facile and high-efficient immobilization of histidine-tagged multimeric protein G on magnetic nanoparticles. *Nanoscale Research Letters* **2014,** *9* (1), 664.

3. Philipse, A. P. a. B. M. P. B. V. a. P. C., Magnetic Silica Dispersions: Preparation and Stability of Surface-Modified Silica Particles with a Magnetic Core. *Langmuir* **1994,** *10* (17), 92--99.

4. Tokajuk, G.; Niemirowicz, K.; Deptuła, P.; Piktel, E.; Cieśluk, M.; Wilczewska, A. Z.; Dąbrowski, J. R.; Bucki, R., Use of magnetic nanoparticles as a drug delivery system to improve chlorhexidine antimicrobial activity. *International Journal of Nanomedicine* **2017,** *12*, 7833-7846.

5. Baniukevic, J. a., Magnetic gold nanoparticles in SERS-based sandwich immunoassay for antigen detection by well oriented antibodies. *Biosensors and Bioelectronics* **2013,** *43* (1), 281--288.

6. Wu, W.; He, Q.; Jiang, C., Magnetic Iron Oxide Nanoparticles: Synthesis and Surface Functionalization Strategies. *Nanoscale Research Letters* **2008,** *3* (11), 397-415.

7. Poole, C. F., New trends in solid-phase extraction. *Trends in Analytical Chemistry* **2003,** *22* (6), 362-373.

8. Stber, W. a. F. A. a. B. E., Controlled growth of monodisperse silica spheres in the micron size range. *Journal of Colloid and Interface Science* **1968,** *26* (1), 62--69.

9. Sun, Y. a. D. L. a. G. Z. a. D. Y. a. M. M. a. X. L. a. Z. Y. a. G. N., An improved way to prepare superparamagnetic magnetite-silica core-shell nanoparticles for possible biological application. *Journal of Magnetism and Magnetic Materials* **2005,** *285* (1-2), 65--70.

10. Marcelo, G. a. P. E. a. C. T. a. P. C., Stabilization in water of large hydrophobic uniform magnetite cubes by silica coating. *Journal of Physical Chemistry C* **2011,** *115* (51), 25247--25256.

11. Park, J. a. P. M. D. a. G. M. C., Silica encapsulation of ferrimagnetic zinc ferrite nanocubes enabled by layer-by-layer polyelectrolyte deposition. *Langmuir* **2015,** *31* (11), 3537--3545.

12. Parnell, S. R.; Washington, A. L.; Parnell, A. J.; Walsh, A.; Dalgliesh, R. M.; Li, F.; Hamilton, W. A.; Prevost, S.; Fairclough, J. P. A.; Pynn, R., Porosity of silica Stöber particles determined by spin-echo small angle neutron scattering. *Soft Matter* **2016,** *12* (21), 4709--4714.

13. Li, S.; Wan, Q.; Qin, Z.; Fu, Y.; Gu, Y., Unraveling the Mystery of Stöber Silica's Microporosity. *Langmuir* **2016,** *32* (36), 9180--9187.

14. Wang, D.; Guan, K.; Bai, Z.; Liu, F., Facile preparation of acid-resistant magnetite particles for removal of Sb(Ⅲ) from strong acidic solution. *Science and Technology of Advanced Materials* **2016,** *17* (1), 80-88.

15. Bai, Y.; Cui, Y.; Paoli, G. C.; Shi, C.; Wang, D.; Zhou, M.; Zhang, L.; Shi, X., Synthesis of amino-rich silica-coated magnetic nanoparticles for the efficient capture of DNA for PCR. *Colloids and Surfaces B: Biointerfaces* **2016,** *145*, 257-266.

16. Zhang, Z. a. W. Z. a. W. M. J., Polyacrylamide brush layer for hydrophilic interaction liquid chromatography of intact glycoproteins. *Journal of Chromatography A* **2013,** *1301*, 156--161.

17. Bai, Y.; Cui, Y.; Paoli, G.; Shi, C.; Wang, D.; Shi, X., Nanoparticles Affect PCR Primarily via Surface Interactions with PCR Components: Using Amino-Modified Silica-Coated Magnetic Nanoparticles as a Main Model. *ACS Appl. Mater. Interfaces* **2015,** *7* (24), 13142-13153.

18. Yang, C.-C.; Yang, S.-Y.; Ho, C.-S.; Chang, J.-F.; Liu, B.-H.; Huang, K.-W., Development of antibody functionalized magnetic nanoparticles for the immunoassay of carcinoembryonic antigen: a feasibility study for clinical use.(Report). *Journal of Nanobiotechnology* **2014,** *12* (1).

19. Pirani, P.; Patil, U.; Apsunde, T.; Trudell, M.; Cai, Y.; Tarr, M., Protein surface labeling reactivity of N -hydroxysuccinimide esters conjugated to Fe 3 O 4 @SiO 2 magnetic nanoparticles. *An Interdisciplinary Forum for Nanoscale Science and Technology* **2015,** *17* (9), 1-11.

20. Sung, D. a. P. S. a. J. S., Facile immobilization of biomolecules onto various surfaces using epoxide-containing antibiofouling polymers. *Langmuir* **2012,** *28* (9), 4507--4514.

21. Wong, S. Y.; Putnam, D., Overcoming limiting side reactions associated with an NHS-activated precursor of polymethacrylamide-based polymers. *Bioconjugate chemistry* **2007,** *18* (3), 970.

22. Thierry, B.; Jasieniak, M.; de Smet, L. C. P. M.; Vasilev, K.; Griesser, H. J., Reactive epoxy-functionalized thin films by a pulsed plasma polymerization process. *Langmuir : the ACS journal of surfaces and colloids* **2008,** *24* (18), 10187.

23. Krishnan, R. a. S. K. S. V., Controlled/“Living” Radical Polymerization of Glycidyl Methacrylate at Ambient Temperature. *Macromolecules* **2003,** *36* (6), 1769--1771.

24. Krishnan, S. a. W. C. J. a. O. C. K., Advances in polymers for anti-biofouling surfaces. *Journal of Materials Chemistry* **2008,** *18* (29), 3405--3413.

25. Zhao, C.; Zhao, J.; Li, X.; Wu, J.; Chen, S.; Chen, Q.; Wang, Q.; Gong, X.; Li, L.; Zheng, J., Probing structure-antifouling activity relationships of polyacrylamides and polyacrylates. *Biomaterials* **2013,** *34* (20), 4714.

26. Chen, H. a. Z. M. a. Y. J. a. Z. C. a. H. R. a. C. Q. a. C. Y. a. Z. J., Synthesis and characterization of antifouling poly(N - acryloylaminoethoxyethanol) with ultralow protein adsorption and cell attachment. *Langmuir* **2014,** *30* (34), 10398--10409.

27. Mou, X.; Ali, Z.; Li, S.; He, N., Applications of Magnetic Nanoparticles in Targeted Drug Delivery System. *J. Nanosci. Nanotechnol.* **2015,** *15* (1), 54-62.

28. Lee, N.; Hyeon, T., Designed synthesis of uniformly sized iron oxide nanoparticles for efficient magnetic resonance imaging contrast agents. *Chem. Soc. Rev.* **2012,** *41* (7), 2575-2589.

29. Peng, E.; Wang, F.; Xue, J. M., Nanostructured magnetic nanocomposites as MRI contrast agents. *J. Mater. Chem. B* **2015,** *3* (11), 2241-2276.

30. Wu, M.; Liu, J.; Hu, C.; Li, D.; Yang, J.; Wu, Z.; Yang, L.; Chen, Y.; Fu, S.; Wu, J., Olaparib nanoparticles potentiated radiosensitization effects on lung cancer. *International journal of nanomedicine* **2018,** *13*, 8461.

31. van de Ven, A. L.; Tangutoori, S.; Baldwin, P.; Qiao, J.; Gharagouzloo, C.; Seitzer, N.; Clohessy, J. G.; Makrigiorgos, G. M.; Cormack, R.; Pandolfi, P. P.; Sridhar, S., Nanoformulation of Olaparib Amplifies PARP Inhibition and Sensitizes Deficient Prostate Cancer to Radiation. *Molecular cancer therapeutics* **2017,** *16* (7), 1279.

32. Pandya, S. R.; Singh, M., Preparation and characterization of magnetic nanoparticles and their impact on anticancer drug binding and release processes moderated through a 1 st tier dendrimer. *RSC Adv.* **2016,** *6* (44), 37391-37402.

33. El-Boubbou, K., Magnetic iron oxide nanoparticles as drug carriers: preparation, conjugation and delivery. *Nanomedicine (London, England)* **2018,** *13* (8), 929.

34. Asadi, N.; Annabi, N.; Mostafavi, E.; Anzabi, M.; Khalilov, R.; Saghfi, S.; Mehrizadeh, M.; Akbarzadeh, A., Synthesis, characterization and in vitro evaluation of magnetic nanoparticles modified with PCL–PEG–PCL for controlled delivery of 5FU. *Artificial Cells, Nanomedicine, and Biotechnology* **2018,** *46* (sup1), 938-945.

35. Kelly, M. P.; Brandon, N. J., Differential function of phosphodiesterase families in the brain: gaining insights through the use of genetically modified animals. *Progress in Brain Research* **2009,** *179* (C), 67-73.

36. Boess, F. G.; Hendrix, M.; van Der Staay, F.-J.; Erb, C.; Schreiber, R.; van Staveren, W.; de Vente, J.; Prickaerts, J.; Blokland, A.; Koenig, G., Inhibition of phosphodiesterase 2 increases neuronal cGMP, synaptic plasticity and memory performance. *Neuropharmacology* **2004,** *47* (7), 1081-1092.

37. Helal, C. J.; Arnold, E. P.; Boyden, T. L.; Chang, C.; Chappie, T. A.; Fennell, K. F.; Forman, M. D.; Hajos, M.; Harms, J. F.; Hoffman, W. E.; Humphrey, J. M.; Kang, Z.; Kleiman, R. J.; Kormos, B. L.; Lee, C.-W.; Lu, J.; Maklad, N.; McDowell, L.; Mente, S.; O'Connor, R. E.; Pandit, J.; Piotrowski, M.; Schmidt, A. W.; Schmidt, C. J.; Ueno, H.; Verhoest, P. R.; Yang, E. X., Application of Structure-Based Design and Parallel Chemistry to Identify a Potent, Selective, and Brain Penetrant Phosphodiesterase 2A Inhibitor. *J. Med. Chem.* **2018,** *60* (13).

38. Jiang, L. a. Z. X. a. W. G. a. L. X. a. W. W. a. Q. J., Preparation and characterization of poly(glycidyl methacrylate)-grafted magnetic nanoparticles: Effects of the precursor concentration on polyol synthesis of Fe 3 O 4 and PMDETA 0 CuBr 2 0 ratios on SI-AGET ATRP. *Applied Surface Science* **2015,** *357*, 1619--1624.

39. Sun, H.; Wang, T.; Zhou, Y.; Li, P.; Kong, Y., Synthesis of well-defined amphiphilic block copolymers via AGET ATRP used for hydrophilic modification of PVDF membrane. *Journal of Applied Polymer Science* **2015,** *132* (24), n/a-n/a.

40. Park, J.; Porter, M. D.; Granger, M. C., Silica Encapsulation of Ferrimagnetic Zinc Ferrite Nanocubes Enabled by Layer-by-Layer Polyelectrolyte Deposition. *Langmuir* **2015,** *31* (11), 3537-3545.

41. Gorsd, M. N. a. P. L. R. a. B. M. N., Synthesis and Characterization of Hollow Silica Spheres. *Procedia Materials Science* **2015,** *8*, 567--576.

42. Newby, J. J. a. L. M. A. a. R. B. a. W. M. J., Annealing of silica to reduce the concentration of isolated silanols and peak tailing in reverse phase liquid chromatography. *Journal of Chromatography A* **2011,** *1218* (31), 5131--5135.

43. Chabanov, A. A. a. J. Y. a. N. D. J., Elimination of cracks in self-assembled photonic band gap crystals. **2003,** *55455*, 18--21.

44. Kemp, S. J.; Ferguson, R. M.; Khandhar, A. P.; Krishnan, K. M., Monodisperse magnetite nanoparticles with nearly ideal saturation magnetization. *RSC Adv.* **2016,** *6* (81), 77452-77464.

45. Caulfield, M. J. a. H. X. a. Q. G. G. a. S. D. H., Degradation on polyacrylamides. Part I. Linear polyacrylamide. *Polymer* **2003,** *44* (5), 1331--1337.

46. Zhao, C. a. P. K. a. A. L. M. a. L. Z. a. H. R. a. C. H. a. L. X. a. L. L. a. Z. G. a. C. Y. a., Antifouling and biodegradable poly(N-hydroxyethyl acrylamide) (polyHEAA)-based nanogels. *RSC Advances* **2013,** *3* (43), 19991--20000.

47. Narumi, A. a. C. Y. a. S., Poly(N-hydroxyethylacrylamide) prepared by atom transfer radical polymewater-solublerization as a nonionic, water-soluble, and hydrolysis-resistant polymer and/or segment of block copolymer with a well-defined molecular weight. *Macromolecular Chemistry and Physics* **2009,** *210* (5), 349--358.

48. Zhao, C. a. Z. J., Synthesis and characterization of poly(N -hydroxyethylacrylamide) for long-term antifouling ability. *Biomacromolecules* **2011,** *12* (11), 4071--4079.

49. Higaki, Y. a. K. M. a. M. D. a. T. A., Anti-fouling behavior of polymer brush immobilized surfaces. *Polymer Journal* **2016,** *48* (4), 325--331.

50. Kostina, N. Y. a. R.-E. C. a. H. M. a. B. E. a. M. J., Non-fouling hydrogels of 2-hydroxyethyl methacrylate and zwitterionic carboxybetaine (meth)acrylamides. *Biomacromolecules* **2012,** *13* (12), 4164--4170.

51. Tang, W.; Kwak, Y.; Braunecker, W.; Tsarevsky, N. V.; Coote, M. L.; Matyjaszewski, K., Understanding atom transfer radical polymerization: effect of ligand and initiator structures on the equilibrium constants. *Journal of the American Chemical Society* **2008,** *130* (32), 10702.

52. Matyjaszewski, K.; Shipp, D. A.; Wang, J. L.; Grimaud, T.; Patten, T. E., Utilizing halide exchange to improve control of atom transfer radical polymerization. *Macromolecules* **1998,** *31* (20), 6836-6840.

53. Peng, C. H.; Kong, J.; Seeliger, F.; Matyjaszewski, K., Mechanism of halogen exchange in ATRP. *Macromolecules* **2011,** *44* (19), 7546-7557.

54. Li, X.; Wang, M.; Wang, L.; Shi, X.; Xu, Y.; Song, B.; Chen, H., Block copolymer modified surfaces for conjugation of biomacromolecules with control of quantity and activity. *Langmuir* **2013,** *29* (4), 1122-8.

55. Li, Y. a. A. S. P. a. J. X. a. Z. S., Direct synthesis of well-defined quaternized homopolymers and diblock copolymers via ATRP in protic media. *Macromolecules* **2003,** *36* (22), 8268--8275.

56. Kagawa, Y. a. M. H. a. O. M. a. Z. J., Preparation of block copolymer particles by two-step atom transfer radical polymerization in aqueous media and its unique morphology. *Polymer* **2005,** *46* (4 SPEC. ISS.), 1045--1049.

57. Roca, A. G. a. M. M. P. a. S. C. J., Synthesis of Monodispersed Magnetite Particles From Different Organometallic Precursors. *IEEE Transactions on Magnetics* **2006,** *42* (10), 3025--3029.

58. Cabrera, L. a. G. S. a. M. N. a. M. M. P. a. H. P., Magnetite nanoparticles: Electrochemical synthesis and characterization. *Electrochimica Acta* **2008,** *53* (8), 3436--3441.

59. Marcelo, G.; Perez, E.; Corrales, T.; Peinado, C., Stabilization in Water of Large Hydrophobic Uniform Magnetite Cubes by Silica Coating. *Journal of Physical Chemistry C* **2011,** *115* (51), 25247-25256.

60. Martinez, J. R. a. R. F. a. V. Y. V. a. P.-R. F. a. G.-H. J., Infrared spectroscopy analysis of the local atomic structure in silica prepared by sol-gel. *Journal of Chemical Physics* **1998,** *109* (17), 7511--7514.

61. Gunes, D. a., Poly(N-hydroxyethyl acrylamide)-b-polystyrene by combination of ATRP and aminolysis processes. 2013; Vol. 127, pp 2684--2689.

62. Edmondson, S. a. H. W. T. S., Controlled growth and subsequent chemical modification of poly(glycidyl methacrylate) brushes on silicon wafers. *Journal of Materials Chemistry* **2004,** *14*, 730.

63. Yoshikawa, C. a. H. S. a. H. T. a. H. C. F. a. K. H., Non-biofouling property of well-defined concentrated poly(2-hydroxyethyl methacrylate) brush. *Materials Letters* **2012,** *83*, 140--143.

64. Inc, B. BcMag DEAE Magnetic Beads. http://www.bioclone.us/DEAE-magnetic-beads-particle-resin-matrix.html (accessed 04/28/2019).

CHAPTER 3. POLYACRYLAMIDES AS BONDED PHASES FOR INTACT GLYCOPROTEIN ANALYSIS BY HYDROPHILIC INTERACTION LIQUID CHROMATOGRAPHY

3.1 Abstract

Glycosylation modifications are related to some diseases; hence, glycan characterization is used as a biomarker for early detection. Most analytical methods for glycosylation involve enzymatic or chemical cleavage and labeling, becoming time-consuming and cumbersome. Utilizing intact proteins allows for faster analysis. Hydrophilic interaction liquid chromatography (HILIC) has been successfully applied for intact glycoprotein analysis. According to previous studies, polyacrylamide (PAAM)-grafted silica particles as stationary phases show enhanced HILIC resolution for glycosylation of proteins. However, PAAM is susceptible to hydrolysis. In this work, poly N-hydroxymethyl acrylamide (PHMAA) was selected as a HILIC bonded phase based on better performance and hydrolysis resistance compared with polyacrylamide, poly N-hydroxyethyl acrylamide and poly Tris acrylamide Surface-initiated polymerization of PHMAA was monitored by transmission electron microscopy (TEM), revealing that an optimized procedure produces reproducible, smooth and low polydispersity layers appropriate for HPLC. PHMAA as a HILIC bonded phase was characterized with a model glycoprotein (Ribonuclease B) and standard hydrophilic analytes such as adenosine, guanosine, adenine, uracil and cytosine. The bonded phase exhibited augmented resolution, run to run reproducibility, resistance to degradation and mass spectrometry (MS) coupling capabilities.

3.2 Introduction

Glycosylation is an important post-translational modification produced by enzymes in cells, where individual sugar units are arranged to form unique sequences.[1] In the human genome it is estimated that around two percent of genes encode for proteins involved in some way with glycosylation, and near fifty percent of cellular proteins are glycosylated.[2] Consequently, it is not unexpected that several genetic alterations have been detected across many glycosylation routes.[3, 4] Identification of different glycoforms is crucial in fields such as drug discovery and development, and study of biomarkers for early detection of disease.[5, 6]

Standard analytical methods for glycosylation characterization are time consuming and laborious, commonly involving enzymatic or chemical cleavage, labeling of polysaccharide chains and separation via capillary electrophoresis or hydrophilic interaction liquid chromatography (HILIC) coupled with mass spectrometry (MS).[7, 8] In many cases, these methods are not able to identify glycosylation sites in the protein sequence. Hence, analysis of intact glycoproteins allows not only faster characterization, but also establishment of the glycosylation site.

HILIC has been utilized for the characterization of intact glycoproteins with acceptable performance.[9-11] Previous work in our group used polyacrylamide to obtain a HILIC stationary phase to separate glycoforms of intact Ribonuclease B, with excellent performance compared with commercial columns.[12] Additionally, packing difficulties were overcome growing the polymer after packing the surface initiated silica particles, instead of packing pre-polymerized particles. [13] Even though polyacrylamide columns exhibited enhanced resolution, stability was poor as columns only maintained resolution for around one month.[14]

In theory, any hydrophilic polymer can be used as a HILIC stationary phase. Most commonly used HILIC polymers include vinylic units, [15-18] due to availability of a large number of monomers with functionalities than allow fine tuning of hydrophilicity, and mainly because of their compatibility with the versatile Atom Transfer Radical Polymerization. Main problems associated with limitations for commercial applications of such novel bonded phases are related with reproducibility of the polymerization and chemical or mechanical stability of polymer layers. Additionally, obtention of reproducible columns is hindered by packing related issues with polymer swelling, and in-column approach proposed previously[13] is can be less attractive to manufacturers due to difficulty of sequential production.

In this study different acrylamides were initially evaluated as HILIC stationary phases for intact glycoproteins characterization. During selection, both HPLC performance for the model glycoprotein Ribonuclease B and stability were considered. These preliminary studies showed a superior performance of poly N-hydroxymethyl acrylamide among tested polymers, being selected for a more detailed optimization and characterization. Polymerization conditions were carefully tuned to obtain a smooth polymer layer with low polydispersity, evaluated by means of transmission electron microscopy (TEM). Moreover, the packing procedure was optimized to minimize polymer swelling, obtaining adequate operational backpressures.

3.3 Experimental

3.3.1 Materials

Deionized water was obtained using a Milli-Q Gradient equipment to a final conductivity of 0.055 mS. Ethanol (EtOH) (200 proof) was acquired from Decon Laboratories. Acrylamide (AAM, 99.9 %), N-hydroxyethyl acrylamide (HEAA, 97%), and $CuCl_2$ (99.995%) were purchased from Sigma Aldrich. Methanol (MeOH), dimethyl sulfoxide (DMSO) and ethylene glycol were acquired from Thermo Fisher Scientific. Sodium L-Ascorbate (98 %) were obtained from TCI chemicals. Tris(2-dimethylaminoethyl) amine (Me_6TREN, 97%) was a product of Alfa Aesar. Trimethylchlorosilane (98 %) and chloromethyl phenylethyl dimethylchlorosilane (98 %) was procured from Gelest. 1.5 µm silica particles were obtained from Superior Silica.

3.3.2 Silica thermal treatment

5 g of 1.5 µm of silica were calcinated at 600 °C for 12 h. Once at room temperature, particles were sonicated in 600 mL of deionized water until maximum suspension (1 h to 3 h). Silica was collected under centrifugation and rinsed twice with ethanol. After dried at 60 °C for 3 h, SiO_2 was transferred to a crucible and calcinated at 600 °C for 12 h. Temperature was raised to 1050 °C and kept during 3 h. After cooling down, particles were transferred to a glass container for storage.

3.3.3 Silica particles rehydroxylation

5 g of heat-treated silica particles were sonicated in 500 mL of 1.5 M HNO_3 in a 1000 mL reaction flask until complete suspension. Reaction flask was transfer to a hot plate and an open condenser was attached. Reflux was performed for 15 h. Particles were washed with deionized water until neutral pH of the rinse water was reached. Then SiO_2 particles were rinsed once with ethanol, followed by drying at 60 °C under vacuum for 3 h.

3.3.4 AGET ATRP surface initiation

In a water free 1000 mL round bottom flask, 5 g of rehydroxylated particles were dispersed in 500 mL of dried toluene under sonication, with nitrogen purging. Under nitrogen atmosphere, 10 mL of ((chloromethyl)phenylethyl)dimethylchlorosilane and 500 µL of butylamine were incorporated. The mixture was refluxed under nitrogen for 3 h once boiling was reached. With

nitrogen flowing, condenser was removed, and 10 mL of trimethylchlorosilane were added. Condenser was placed back, and reflux was performed for three more hours. Heat source was suspended, and reaction flask cooled under nitrogen overnight. Surface initiated particles were washed twice with toluene and twice with acetonitrile and dried at 60 ˚C.

3.3.5 AGET ATRP polymerization

Water and ethanol were purged with nitrogen under sonication for 15 min to remove dissolved oxygen. In a 100 mL round bottom flask, 0.45 g of surface-initiated silica particles and 15 mL of ethanol were sonicated until dispersion. Then, 13.3 mL of water were added with respective monomer. Nitrogen was bubbled while keeping sonication for 15 min. Sonication temperature was controlled at 35 °C during the whole process.

A solution of 40.0 mg of $CuCl_2$ (0.295 mmol), 80 µL of Me6Tren (0.298 mmol) in 2.5 mL of water was incorporated. The reaction was started by addition of 2.5 mL of water containing 20.0 mg of sodium ascorbate (0.1 mmol). Nitrogen purging was kept for 10 min, and then a balloon was set to obtain a seal environment and avoid oxygen to reach reaction solution. Polymerization was allowed for respective time under sonication, controlling temperature. Upon completion, reaction solution was transferred to a 50 mL centrifuge tube and polymer grafted particles were separated by centrifugation. If not stated, all centrifugation steps were done at 7500 rpm for 1 min.

Particles were washed twice with water using vortex, and one more time under sonication for 5 min, using centrifugation for separation. Sonication for 30 min in 40 mL of Ethylene glycol was done. Centrifugation at 6000 rpm during 3 min was used to separate potential free polymer suspended in ethylene glycol from silica particles. Afterwards, particles were resuspended in 40 mL of deionized water and sonicated for 15 min. Suspension was filtered through a 2 µm mesh stainless steel grid. Filtered solution was centrifuged and resuspended in ethanol with sonication for 5 min. A final suspension/wash/centrifugation step was performed with acetone. Rinsed particles were dried at room temperature under vacuum.

3.3.6 Transmission Electron Microscope Analysis

1 µg of material was suspended in 500 µL of water. 5 µL of the slurry was transferred to a F/C 300 mesh Cu grid (TED PELLA Inc.). TEM micrographs were acquired in a FEI Tecnai G2 20 Transmission Electron Microscope.

3.3.7 Infrared Analysis

Samples were grinded with dried KBr, in an agate mortar to get a 0.2 % homogeneous fine powder. 50 mg of the mixture were hydraulically compressed to form a pellet. IR spectra were measured using a FT-IR spectrometer (Tensor 37, Bruker).

3.3.8 Dynamic Light Scattering

Suspensions were prepared in selected solvents in a concentration to obtain a stable slurry, with an adequate mass of particles for measurements with low polydispersity indexes. The instrument used was a Wyatt DynaPro Plate Reader II (Wyatt technology Corp, CA, USA).

3.3.9 Column packing

Packing slurry was prepared sonicating polymer grafted particles in 2 mL of selected solvent mixture. For a 50 x 2.1 mm column, 0.26 g of particles were used, while for a 30 mm x 2.1 mm column, 0.16 g of polymer coated particles were utilized. Once complete suspension was reached (approx. 30 min), slurry was transferred to a reservoir column (150 x 4.6 mm) attached to respective column. Packing with solvent mixture used for the slurry was made under sonication until collected volume of solvent passing through the column was at least 5 mL. Solvent was switched to acetonitrile and packing was extended for 20 min. Pressure was kept at maximum pump capacity (17.5 kpsi) during all packing steps. Column was detached from reservoir and top cap was placed.

3.3.10 Chromatographic analysis

A Waters Acquity I-Class UHPLC system (Waters Corporation, Milford, MA) was used for chromatographic separations, with UV detection at 215 nm. Solvent A was H_2O (0.1% TFA) and solvent B was acetonitrile (0.1% TFA). Column temperature was 30 °C. For UHPLC-MS analysis, Waters Acquity UHPLC system was connected to a Thermo LTQ Velos mass spectrometer. Solvent A was water with 0.1% TFA and solvent B acetonitrile with 0.1 % TFA. Column temperature was 30 °C.

3.4 Results and Discussion

3.4.1 Silica particles grafting and column packing processes

Compared with the previously proposed "in-situ" polymerization[19], in which polymer grows on particles already packed into the column, an "ex-situ" reaction has two main challenges. First, during the reaction particles in solution must be well-suspended and the polymerization rate controlled to minimize free polymer formation and polymer layer polydispersity. With these attributes controlled, even surface topography, homogeneous polymer thickness and low aggregates are observed. Second, for packing polymer-grafted particles, it is necessary to form a stable and well-suspended slurry, which for hydrophilic polymer brushes is an aqueous mixture. Unfortunately, water forms a hydration layer that swells the polymer coating, which causes high backpressure during packing, restricting solvent flow and resulting in a loosely-packed bed.

3.4.1.1 Polymerization improvement

Since polyacrylamides are very hydrophilic, AGET ATRP for such polymers is normally performed in aqueous mixtures. Water-based media ensure good solubility for acrylamide monomers, and stable suspension for grafted particles. However, initial benzylchloride silane surface modified particles are hydrophobic, and do not suspend in pure water. Also, ATRP in aqueous solvents can be difficult to control due to "disproportionation" of copper-ligand complex,[20] causing precipitation of elemental metal and speeding up the reaction rate. Therefore, for AGET-ATRP of SI-particles, mixtures of alcohols and water were selected, within a range of 30 % to 40 % alcohol. Isopropanol (IPA) provides very good suspension for initial particles, but reaction rate is not high enough to produce an adequate polymer length in short time (< 2 h), requiring a monomer concentration of at least 2.5 M. Methanol on the other hand, is faster and less than 1 M monomer is necessary. Particle shown in Figure 3.1, was obtained grafting 1.5 µm SiO_2 with AGET ATRP in methanol 40 %, with a monomer concentration of 0.4 M. As can be seen, obtained surface topography is smooth and no aggregation was observable. Despite this, a small amount of metallic copper was obtained at the end of reaction, requiring additional rinses in aqueous 0.1 % TFA to remove.

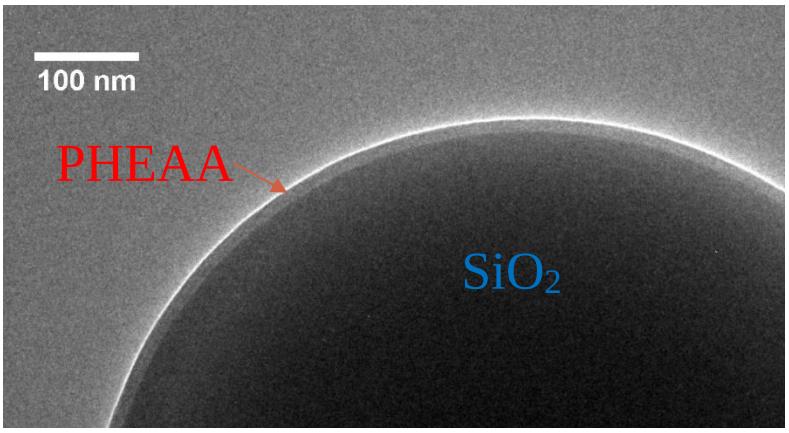

Figure 3.1. TEM micrograph of 1.5 µm SiO_2 grafted with poly (N-hydroxyethyl)acrylamide, HEAA in 40 % methanol. Reaction conditions: [HEAA] 0.4 M, solvent: methanol 40 %, temperature: 35 °C, reaction time: 120 min. Polymer thickness is around 12 nm.

An obvious next step was to evaluate an intermediate solvent between IPA and methanol: ethanol. AGET ATRP was implemented in 30 % ethanol, being necessary to use a higher monomer concentration 1.5 M and shortening reaction time to prevent Cu precipitation. As seen in Figure 3.2, polymer layer obtained under described conditions yields a homogenous surface, with particle aggregation minimized and no visible precipitated copper. Based on these findings with HEAA, all further polymerizations were conducted using ethanol as solvent, adjusting solvent composition (30 % to 40 %) and monomer concentration around 1 M based on each monomer's ATRP polymerization rates. Additionally, polymerization protocol was further improved by, initially suspending the hydrophobic SI-particles in pure ethanol under sonication and addition of water, monomer, ligand-Cu, and sodium ascorbate at reaction start.

3.4.1.2 Free polymer removal

Even under optimized polymerization conditions, formation of free polymer in solution is possible (Figure 3.3). Thus, free polymer removal is important previous packing steps, to obtain a stable packing bed. Free polymer is less dense than coated particles, so it is possible to separate it under selective centrifugation. Initially, water and water/ethanol mixtures, were unsuccessfully tested to obtain free polymer suspended with silica particles completely separated by centrifugation. At low rotor speeds a considerable amount of grafted silica particles stayed in suspension with the free polymer, and at high rotor velocities, both were completely sedimented. According with Stoke's law (Equation 3.1),[21] sedimentation velocity can be adjusted also changing

solvent, which implies a variation in viscosity (η) and density (ρ) of the medium. Consequently, the use of a solvent with higher viscosity decreases sedimentation velocity of particles and free polymer, allowing a finer tune by changing rotor speed to achieve a more complete separation. Hence, it was necessary to find a solvent in which polyacrylamides grafted particles were suspended, with higher viscosity than water (0.89 cP)[22]. Ethylene glycol exhibits a complete and stable suspension of the polymer coated particles, with a viscosity of 16.1 cP and similar specific densities (water 0.999 , ethylene glycol 1.111)[22]. Rotor speed and centrifugation time were carefully varied until only few particles were visible in the supernatant, obtaining better results at 6000 rpm during 3 min. Efficiency of free polymer removal was visually evaluated by TEM.

$$V = \frac{d^2(\rho\text{-}L)\,a}{18\,\eta} \qquad \text{Equation 3.1}$$

where: *V:* sedimentation velocity

d: diameter of the particle

ρ: particle density

L: medium density

η: viscosity of the medium

a: acceleration

In addition to free polymer issues, it is necessary to consider that silica particles obtained by Stöber process can be forming aggregates, even though manufacturers do their best to offer a product with a narrow size distribution. As depicted in Figure 3.4, silica particles can be fused together, causing packing problems. It is clear that those defects are not caused by polymerization, and also it is important to mention that the point of contact of the particles (red arrows in Figure 3.4) do not represent any type of crosslinking of the particles, those are created by the drying process of the suspension deposited on the TEM grids. In order to minimize aggregated particles in the columns, the particles are suspended in water and filtered using a stainless-steel grid with a 2 μm mesh, and filtrate is used for packing. Even after filtering, those contact point are always seen when particles dry in the TEM grid.

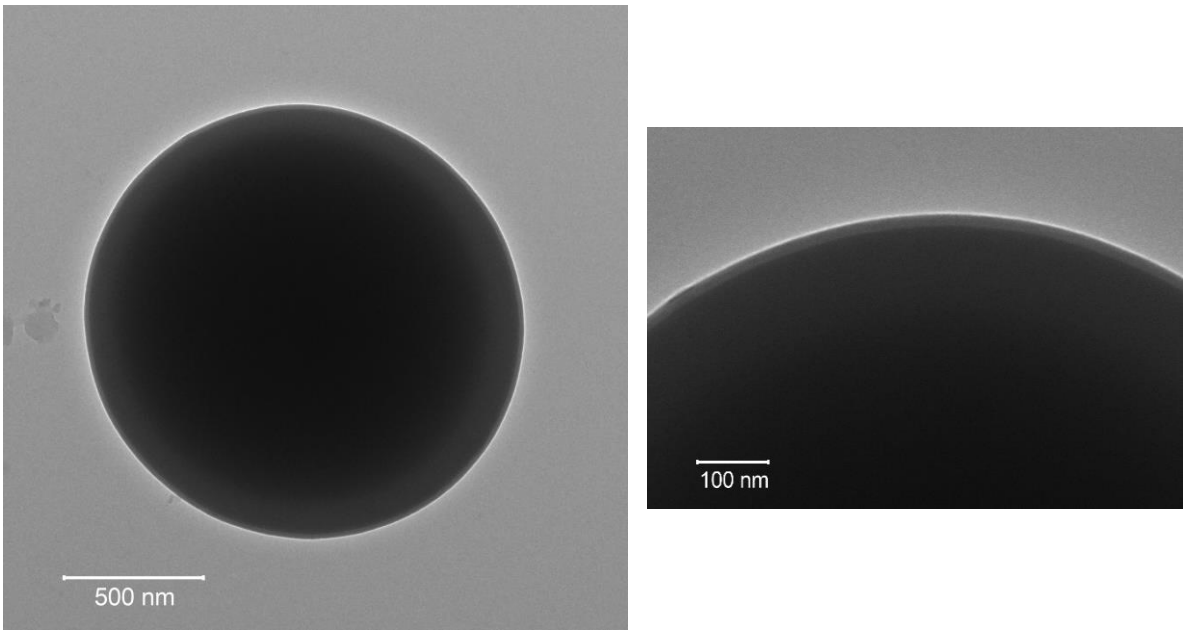

Figure 3.2. TEM micrograph of 1.5 µm SiO_2 grafted with poly (N-hydroxyethyl) acrylamide, HEAA in 30 % ethanol. Reaction conditions: [HEAA] 1.5 M, solvent: ethanol 30 %, temperature: 35 °C, reaction time: 90 min. Polymer thickness: 15 nm.

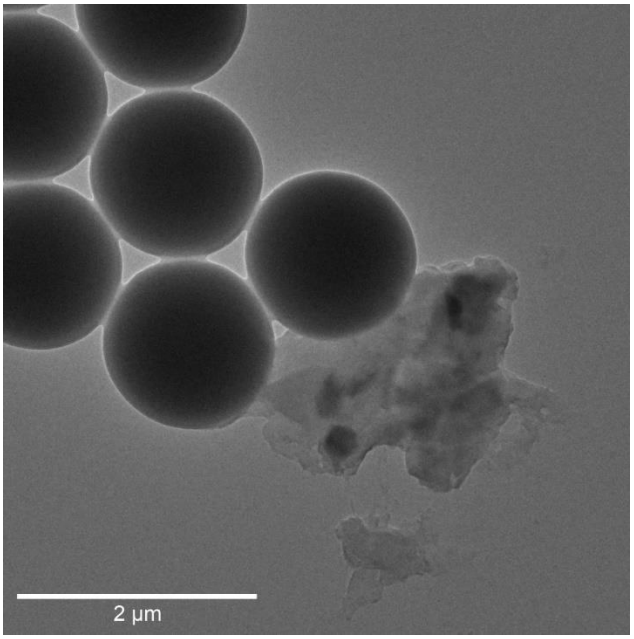

Figure 3.3. TEM micrograph of free polymer formed during AGET ATRP.

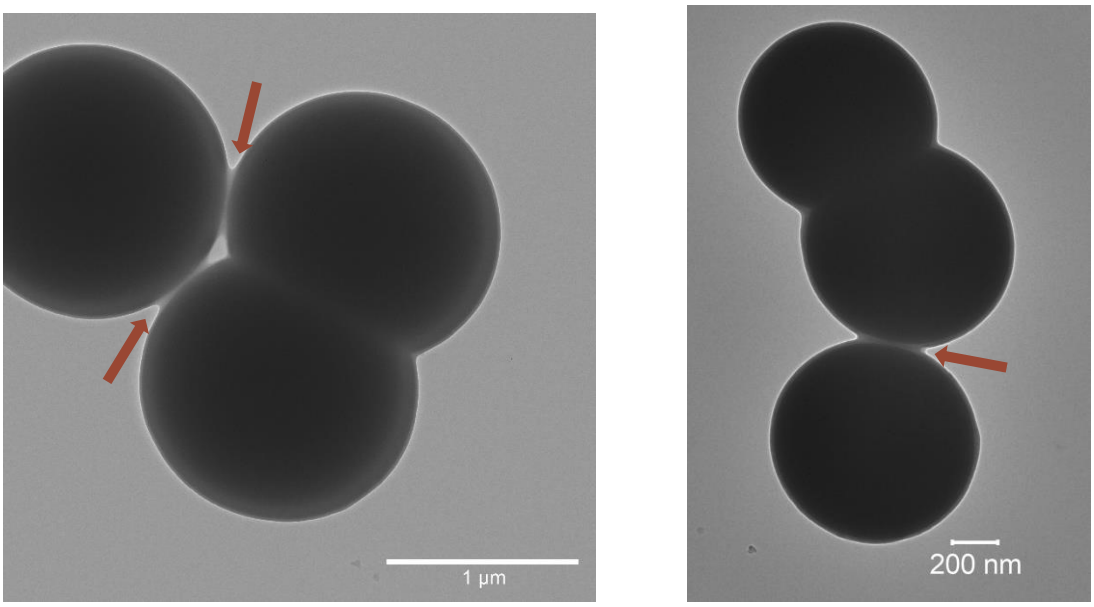

Figure 3.4. TEM images of defects found in silica particles. Right: 1.5 µm SiO_2@PHMAA, Left: 1 µm SiO_2@PHMAA. Red arrows represent contact points of polymer layers, created during drying of the suspension on TEM grids.

3.4.1.3 Polymer grafted particles packing improvement

As previously discussed, polyacrylamides undergo swelling when in contact with water containing solvents. On the other hand, aqueous solvents provide a stable and complete suspension of polyacrylamide grafted particles. To overcome this difficulty, a greater percentage of hydrophobic solvent was added to the packing solvent. The scheme showed in Figure 3.5 describes the principle behind this approach, where a less swollen polymer layer during packing produces a tighter packed bed.

Selection of adequate solvent for preparing packing slurry was made based in two criteria, suspension of the particles and low polymer swelling. Suspension was evaluated by weighting a fixed amount of polymer coated particles (100 mg), followed by addition of tested media and sonication for 20 min. Vials containing formed suspensions were maintain in repose for 1 h and stability was assessed based in visual sedimentation profiles. Images in Figure 3.6 show the vials utilized for suspension experiments for silica particles coated with poly (hydroxymethyl

acrylamide) (PHMAA) after 1 h of repose. Surprisingly, alcoholic mixtures and dimethyl sulfoxide (DMSO) displayed more stable suspensions compared with pure water.

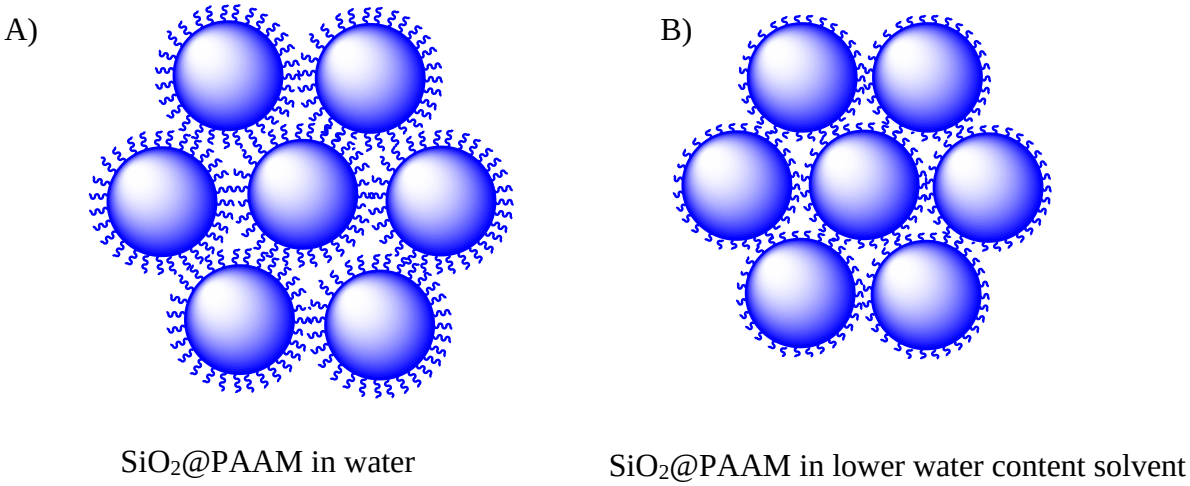

Figure 3.5. Depiction of polyacrylamide-grafted particles in water-rich and water-restricted solvents. A) In a water-rich solvent, polymer on surface swells and extends into the solvent. B) In a solvent with lower water content, polymer is collapsed on surface.

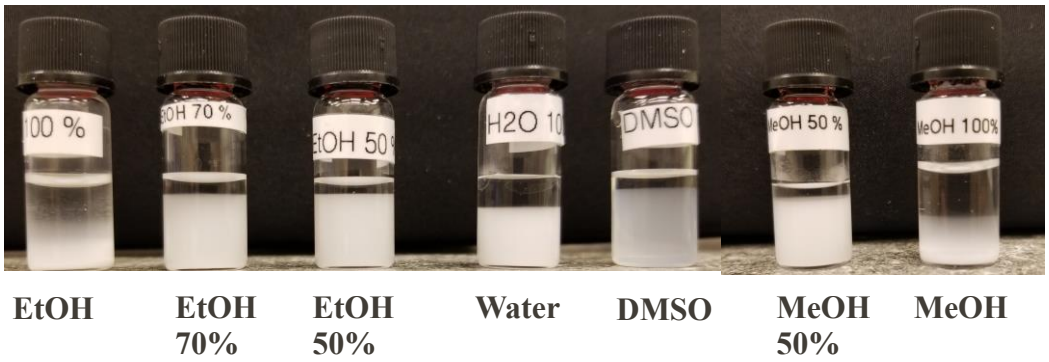

Figure 3.6. Vials used for testing suspension of SiO_2@PHMAA particles in different solvent mixtures after 1 h of repose.

In order to compare the swelling of polymer layers in selected solvents, dynamic light scattering (DLS) was employed. Since DLS indirectly measures hydrodynamic diameter of the particles, Z-average variation of the same sample of particles in different solvents can be used as an indication of the hydration layer formed around the particles, and therefore, swelling of the polymer layer in this case. Based on Z-average measurements listed in Table 3.1, ethanol 50 % was selected as solvent for preparing slurries for packing, since suspension is stable and polymer swelling is diminished.

Table 3.1. Dynamic Light Scattering (DLS) measurements in different solvent mixtures. PDI: polydispersity index

Particles	**Solvent**	**Z-average (d. nm)**	**PDI**
1.5 µm SiO_2 (rehydroxylated)	Water	1435	0.111
1.5 µm SiO_2@PHMAA	Water	1987	0.094
1.5 µm SiO_2@PHMAA	DMSO	1724	0.130
1.5 µm SiO_2@PHMAA	Ethanol 50 % vol.	1442	0.065
1.5 µm SiO_2@PHMAA	Methanol 50 % vol.	1548	0.086

An additional improvement to the packing procedure includes changing solvents during packing, just before placing the top frit to the column. Ideally, particles would be suspended in a non-aqueous solvent to minimize polymer swelling, but suspension experiments with organic solvents such as acetonitrile or IPA failed to produce stable slurries. So, the idea behind the proposed protocol is to utilize 50 % ethanol to form the slurry and place the particles inside the column and switch the solvent to a non-aqueous solvent to dry out the water and shrink the particles while a higher flow rate compacts the less swollen particles. Scheme in Figure 3.7 describes the optimized packing protocol. Slurry in 50 % ethanol is placed into the reservoir column attached to the column (not showed) and packing is accomplished until volume of collected solvent is at least twice the reservoir capacity (around 5 mL). Once the pump has depressurized, the solvent bottle in the pump is replaced with acetonitrile (ACN) and packing continues.

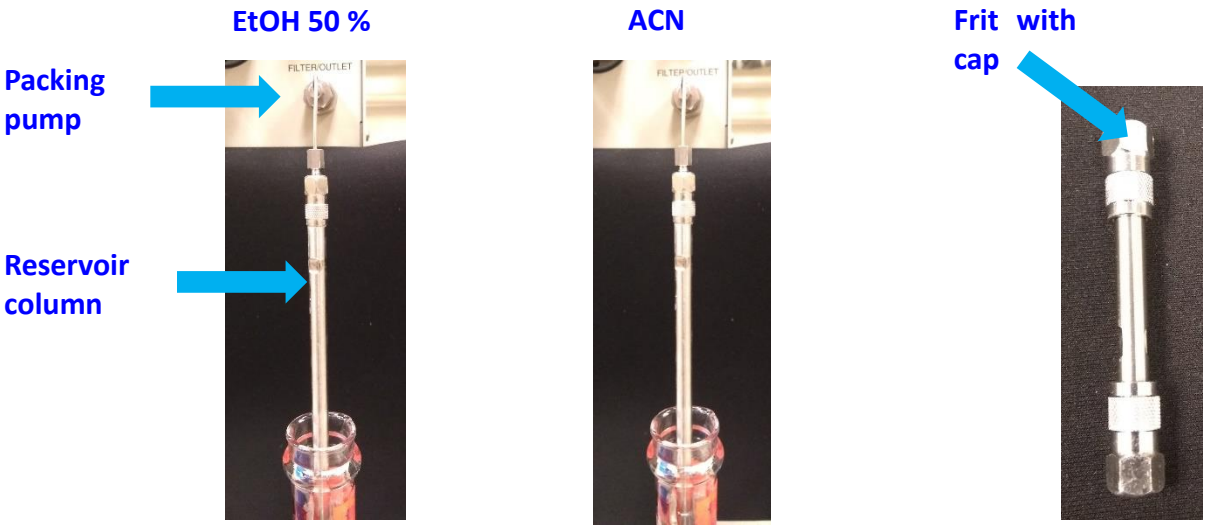

Stage 1: Suspend in 50 %EtOH and pack.

Stage 2: Replace solvent for ACN and finish packing.

Stage 3: Place top frit on the column.

Figure 3.7. Packing protocol for polyacrylamides-grafted silica particles.

3.4.2 Preliminary selection of different acrylamides as HILIC bonded phases

Polyacrylamide (PAAM) was used previously as HILIC bonded phases for separation of intact glycoproteins,[12, 19] showing excellent performance. In this section, similar monomers were evaluated as stationary phases for separation of Ribonuclease B as a model protein.

3.4.2.1 Polyacrylamide

1.5 µm silica particles were grafted in 30 % ethanol using AAM at a final concentration of 1.5 M during 60 min (3.3.5). Particles were suspended in 50 % ethanol and packed in a 50 mm x 2.1 mm column as described in section 3.3.9. Ribonuclease B was used to assess HILIC performance of obtained column. In previous works, it was identified that PAAM columns undergo degradation over time. Separation of Ribonuclease B is remarkable in PAAM columns as displayed in Figure 3.8A, however, as can be seen in Figure 3.8B, lower resolution is appreciable after 45 days of polymerization, even with few runs between that period (less than 20). This finding becomes the main problem for using PAAM as an HPLC bonded phase and motivated the present work.

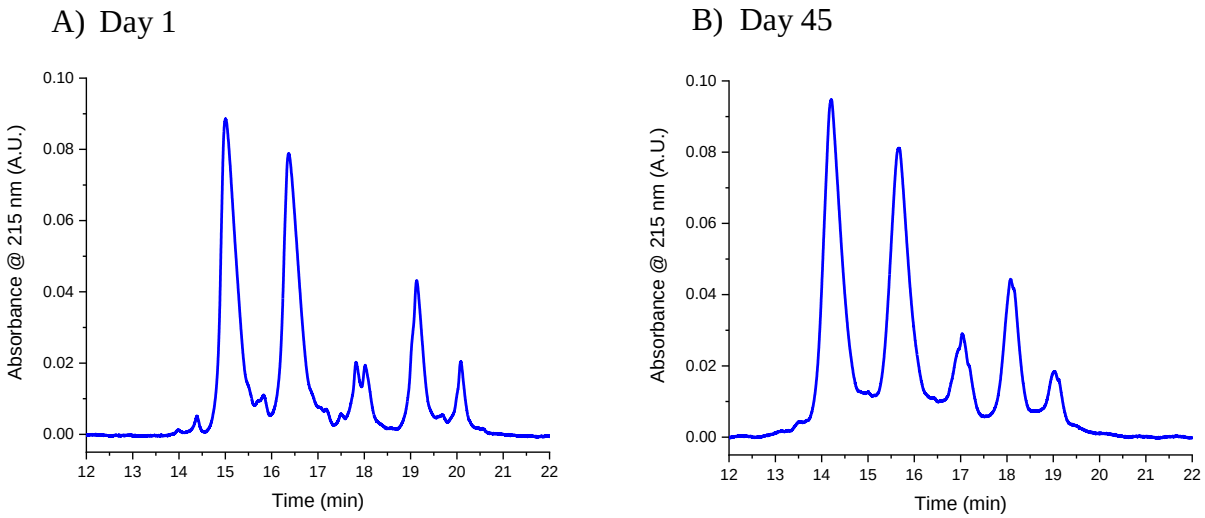

Figure 3.8. Chromatograms of Ribonuclease B analyzed using 1.5 µm SiO_2@PAAM column (50 x 2.1 mm). A) Run made the first day. B) Run made 45 days after the first run. Sample: Ribonuclease B 2 µg in 75 % ACN and 0.2 % TFA, flow rate: 100 µL/min, gradient: 75 % B to 65 % B in 20 min, temperature: 30 °C.

Initially, it was necessary to identify the origin of PAAM columns' loss of resolution over time. In previous research, it was established that PAAM can be hydrolyzed in aqueous solvents[23], producing acrylic acid units (Figure 3.9). Those acrylic acid units can cause subsequent polymer chains loss and exhibit other interactions with proteins (electrostatic, hydrogen bonding), which could explain the broader peaks in Figure 3.8B.

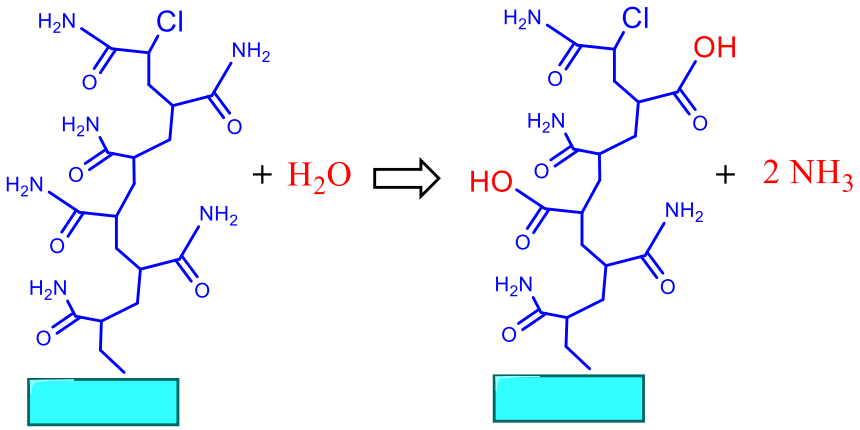

Figure 3.9. Scheme of polyacrylamide brushes hydrolyzing to produce units of acrylic acid.

Experiments were carried out using FTIR, to assess extent of PAAM hydrolysis. Silica particles grafted with PAAM were placed in a solution containing water: acetonitrile (40:60, 0.1 % TFA) to emulate HPLC running conditions. The temperature was maintained at 50 °C to speed up the hydrolysis reaction. Particles were sampled over several days and FTIR spectra were obtained. If polymer chains are not lost during the hydrolysis and only amide group is being replaced by hydroxyl group, the carbonyl group must be constant, so it was used to normalize FTIR data. In spectra displayed in Figure 3.10, the N-H stretch band (around 3300 $cm^{-1)}$ decreases with reaction time, which supports the hypothesis that HILIC conditions hydrolyzes PAAM layer. In HPLC, shear forces due to flow rate and high back pressure can generate additional polymer hydrolysis and chain loss.

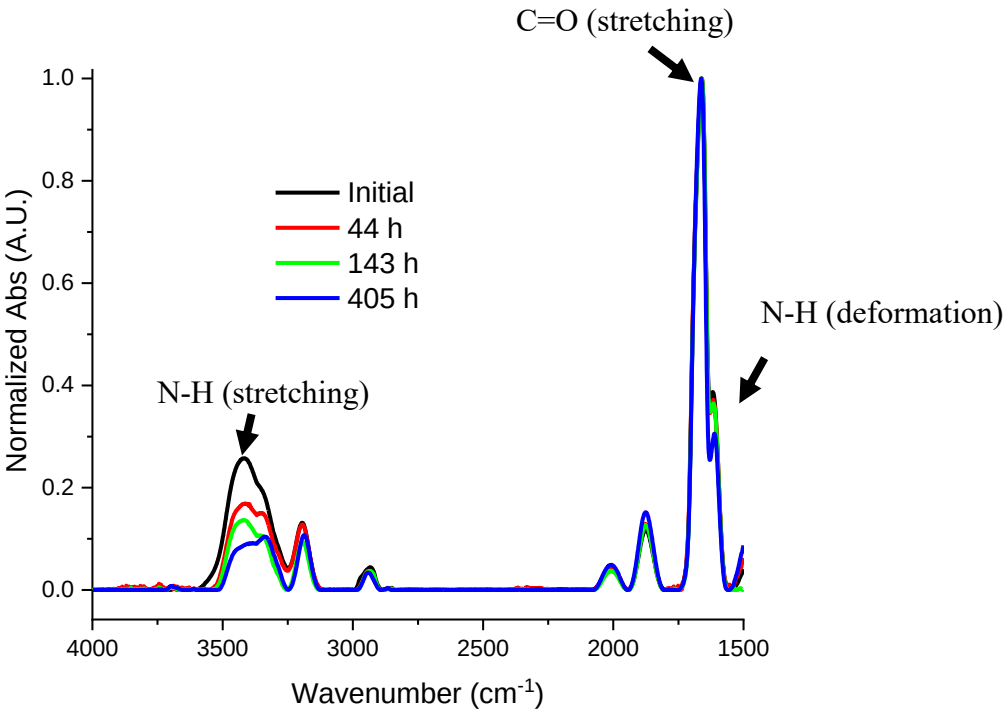

Figure 3.10. FTIR spectra of samples of 1.5 µm SiO_2@PAAM particles exposed to hydrolytic conditions. Solvent: water: acetonitrile (40:60), 0.1 % TFA, temperature: 50 °C. Carbonyl peak around 1700 cm^{-1} was used to normalize spectra.

3.4.2.2 Poly (N-hydroxyethyl acrylamide)

Selection of this monomer was based on its structural similarity with AAM (Figure 3.11), and its reported high hydrolysis stability, given by the hydroxyl group attached to the amide.[24] HEAA monomer is slightly more hydrophobic than AAM, and reaction rate was comparable. For AGET ATRP, 1.5 µm silica particles were grafted in 30 % ethanol using HEAA 1.5 M over 90 min, obtained particles are shown in Figure 3.2. Particles were suspended in 50 % ethanol and packed in a 50 mm x 2.1 mm column as described in section 3.3.9.

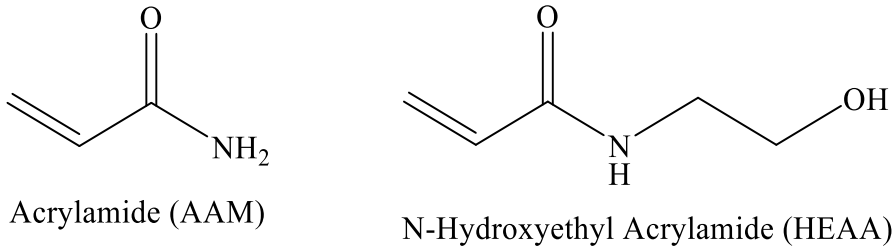

Figure 3.11. Chemical structures of acrylamide and N-hydroxyethyl acrylamide.

HILIC performance of the novel stationary phase was evaluated with Ribonuclease B. It was found that when starting at 75 % B, the most abundant glycoform peak (with 5 mannose units) elutes sooner (around 4 min, Figure 3.12A) and resolution was compromised, compared with gradient starting at 78 % B as presented in Figure 3.12B. This study shows that retention of PHEAA columns is lower compared with PAAM columns, as predicted based on higher hydrophobic character of PHEAA given the extra ethyl group.

Higher thermal resistance of PHEAA compared to PAAM allowed an increase in column temperature without instability showed by PAAM columns.[14] Figure 3.13 presents enhanced resolution produced by PHEAA at higher temperature. Despite the use of higher temperatures with PHEAA, Ribonuclease B glycoform resolution is still better with PAAM (Figure 3.8).

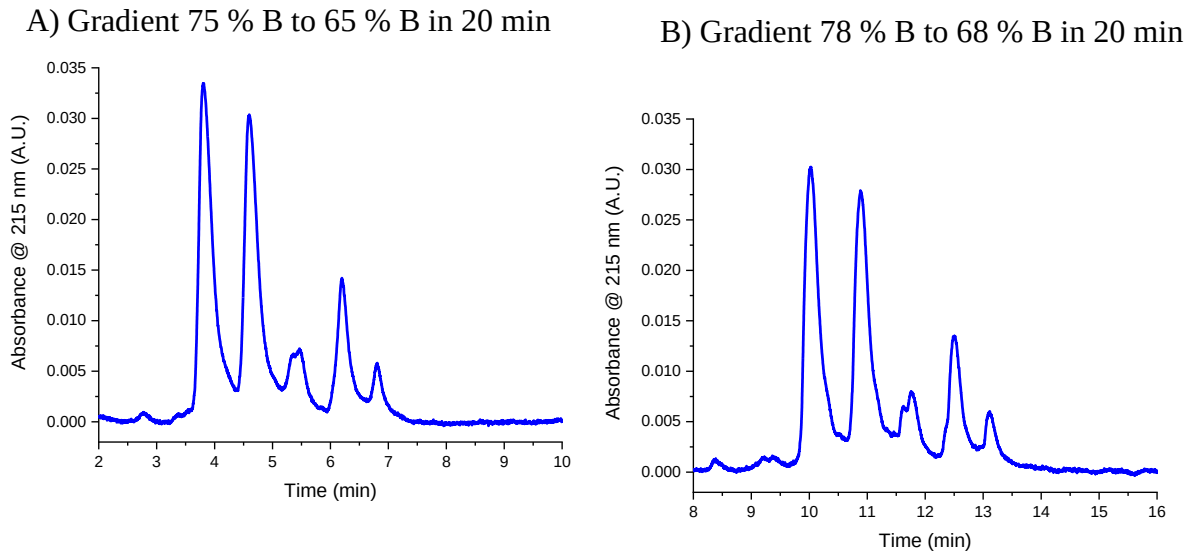

Figure 3.12. Chromatograms of Ribonuclease B analyzed using 1.5 µm SiO_2@PHEAA column (50 x 2.1 mm). A) Gradient 75 % B to 65 % B in 20 min. B) Gradient 78 % B to 68 % B in 20 min. Conditions: Ribonuclease B 0.5 µg in 75 % ACN and 0.2 % TFA, flow rate: 100 µL/min, temperature: 40 °C.

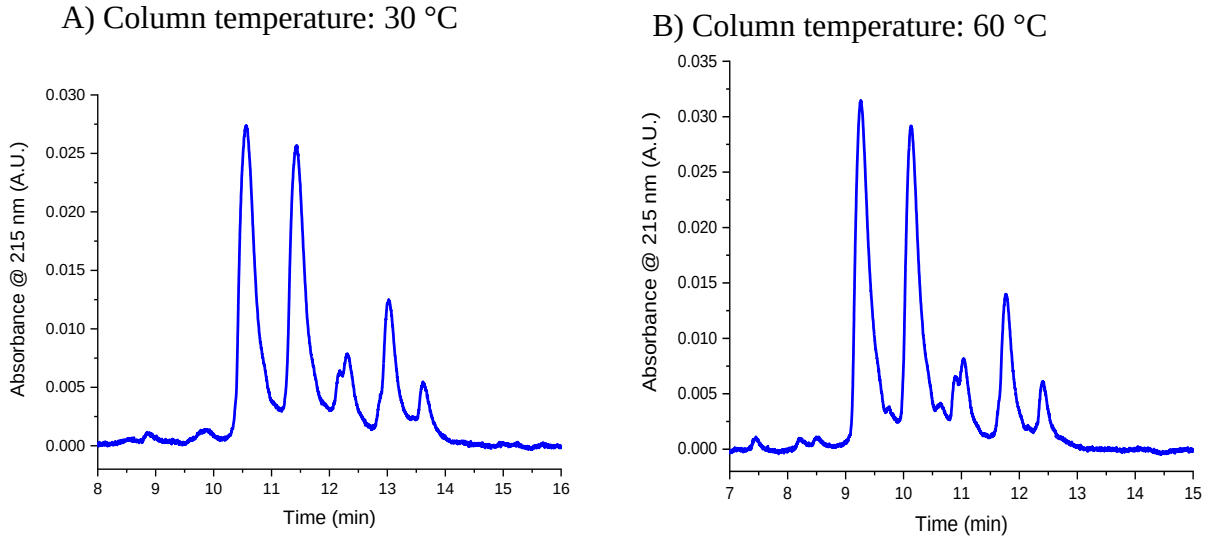

Figure 3.13. Chromatograms of Ribonuclease B analyzed using 1.5 µm SiO_2@PHEAA column (50 x 2.1 mm). A) Column temperature 30 °C. B) Column temperature 60 °C. Conditions: sample: Ribonuclease B 0.5 µg in 75 % ACN and 0.2 % TFA, flow rate: 100 µL/min, gradient: 78 % B to 68 % B in 20 min.

3.4.2.3 Poly N-[Tris(hydroxymethyl)methyl]acrylamide

Tris-AAM is a highly hydrophilic monomer due to its three hydroxy groups in addition to the amide group (Figure 3.14). This polymer was used previously as a bonded phase for HILIC separations, modifying silica particles.[17] Polymerization was especially challenging due to the high concentration of KCl (7 %) included with the monomer as a stabilizer. Chlorides act as common ions in the AGET ATRP reaction using $CuCl_2$ as catalyst, slowing the reaction.[25] Solvent used was 50 % methanol to speed up the reaction and monomer concentration was only 0.5 M (2.5 g), due to the high cost of the monomer. Reaction time had to be extended to 3 h to obtain a polymer layer thickness of 13 nm (Figure 3.15), but no copper precipitate was visible.

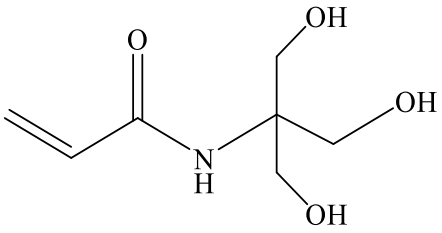

Figure 3.14. Chemical structure of N-[Tris(hydroxymethyl)methyl]acrylamide (Tris-AAM)

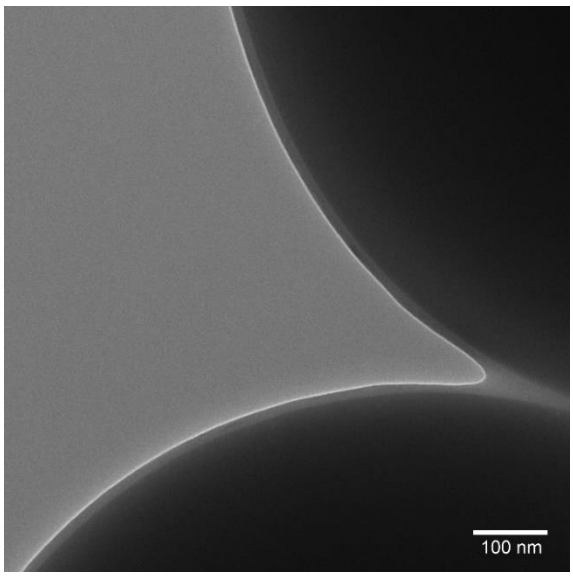

Figure 3.15. TEM micrograph of 1.5 µm SiO_2 grafted with poly (N-[Tris(hydroxymethyl)methyl]acrylamide) in 50 % methanol. Reaction conditions: [TrisAAM] 0.5 M, temperature: 35 °C, reaction time: 180 min. Polymer thickness: 14 nm.

HILIC performance was tested packing obtained particles in a 5 cm column (2.1 mm ID). As shown in Figure 3.16A, the resolution for Ribo B under HILIC conditions is not as good as for previously evaluated polymers. Even at optimized gradients (Figure 3.16B), peaks for glycoforms are not base line resolved. This could be explained by formation of strong hydrogen bonding interactions with the abundant hydroxyl groups and steric hindrance diminishes contact with amide groups.

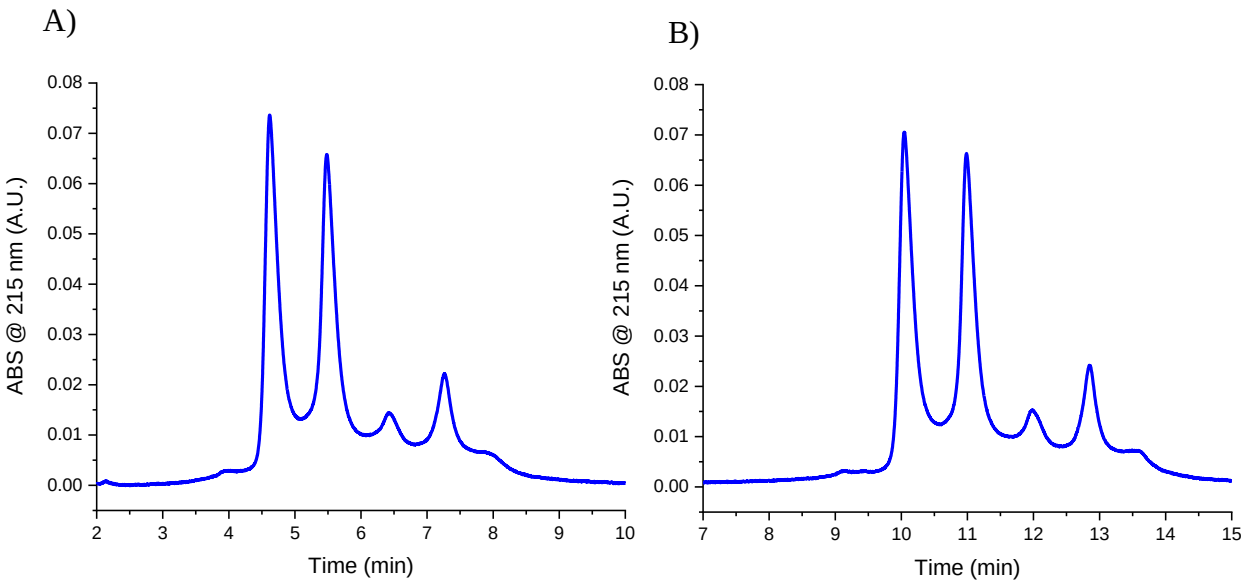

Figure 3.16. Chromatograms of Ribonuclease B analyzed using 1.5 µm SiO_2@PTrisAAM column (50 x 2.1 mm). A) Gradient 75 % B to 65 % B in 20 min. B) Gradient 78 % B to 68 % B in 20 min. Conditions: Ribonuclease B 0.5 µg in 75 % ACN and 0.2 % TFA, flow rate: 100 µL/min, temperature: 40 °C.

3.4.2.4 Copolymer of polyacrylamide and poly (N-hydroxyethyl) acrylamide

PAAM shows good resolution as bonded phases for HILIC, while PHEAA exhibits high hydrolysis resistance. Hence, it was considered if a copolymer of these two monomers could preserve advantages of both compounds. AGET ATRP polymerization was carried at using 0.75 M of each monomer in 30 % EtOH during 65 min to obtain a smooth 16 nm layer (Figure 3.17). Separation of Ribo B glycoforms is very good as seen in Figure 3.18A, with sharp peaks and almost baseline resolution. However, after 10 h running at 50 °C, mild bonded phase degradation

occurs, evident in loss of minor peak details shown in Figure 3.18B. It is concluded that there is an improvement is resistance, since PAAM alone degrades after 12 h of use even at 40 °C.[14]

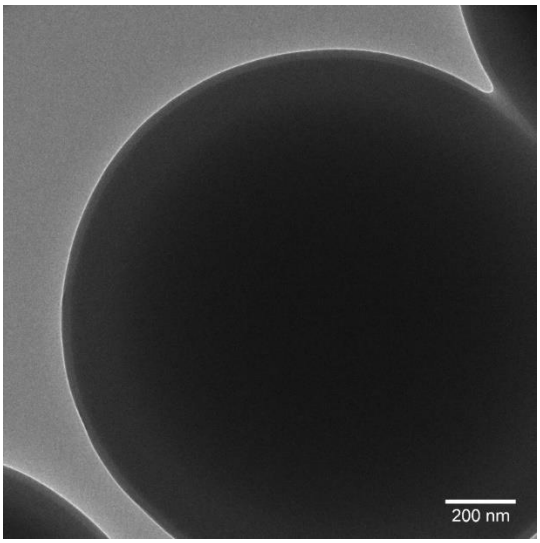

Figure 3.17. TEM micrograph of 1.5 µm SiO_2@PHEAA-co-PAAM. Reaction conditions: [AAM]=[PHEAA]= 0.75 M, EtOH 30 %, temperature: 35 °C, reaction time: 65 min. Polymer thickness: 16 nm.

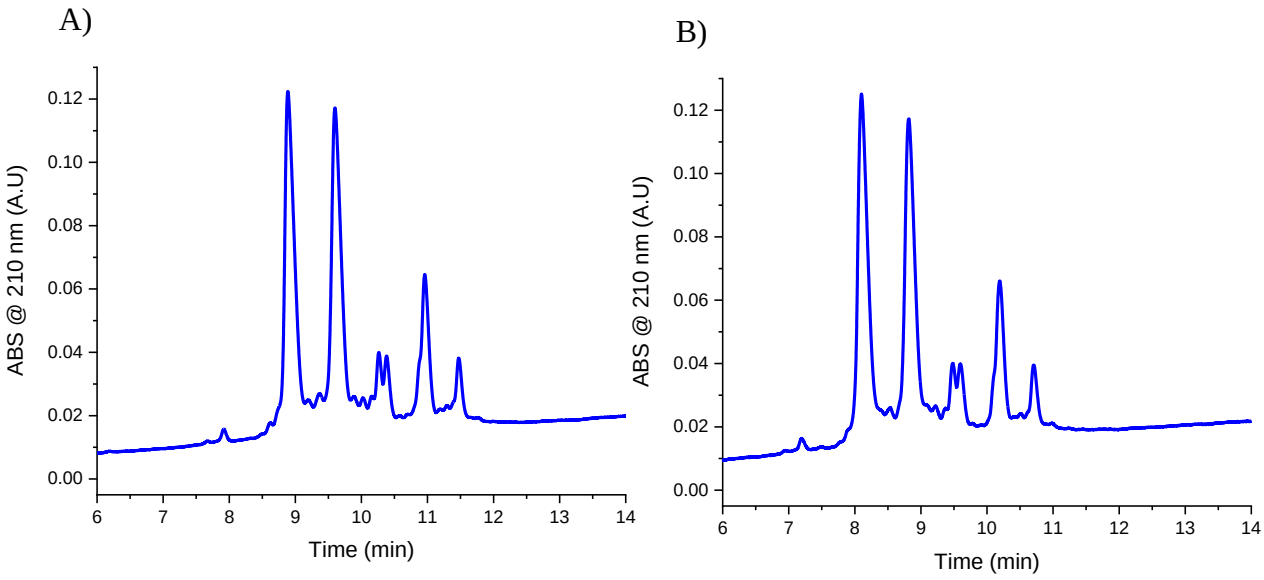

Figure 3.18. Chromatograms of Ribonuclease B using 1.5 µm SiO_2@PHEAA-co-PAAM column (50 x 2.1 mm). A) Initial run. B). Run after being ran at 50 °C during 10 h. Conditions: Ribonuclease B 0.5 µg in 75 % ACN and 0.2 % TFA, gradient 75 % B to 60 % B in 20 min, flow rate: 100 µL/min, temperature: 30 °C.

3.4.2.5 Poly (N-Hydroxymethyl acrylamide)

Considering that copolymer of PHEAA and PAAM showed excellent HILIC separation of Ribo B, based on a simple inspection of their chemical structures displayed in Figure 3.11, it was hypothesized that a polymer with an "intermediate" hydrophilicity could present good HILIC performance and hydrolysis resistance. N-hydroxymethyl acrylamide (HMAA) clearly presents similarities to those compounds as indicated in Figure 3.19. One less methyl group compared with PHEAA makes it less hydrophilic and steric hindrance also diminishes, allowing interaction with amide group. It is expected higher hydrolysis resistance compared with PAAM.

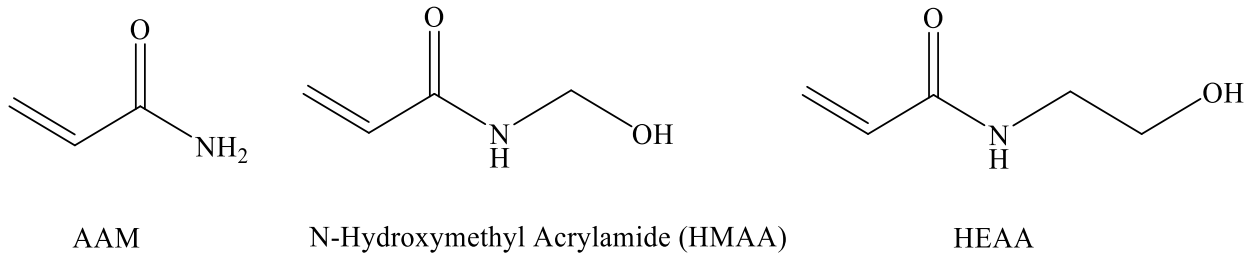

Figure 3.19. Comparison of chemical structures of N-hydroxymethyl acrylamide (HMAA) with AAM and HEAA.

AGET ATRP polymerization of 1.5 µm SI-silica particles with HMAA was carried out in 37.5 % ethanol, using a monomer concentration of 0.85 M over 100 min. As displayed in Figure 3.20, the polymer layer is smooth with a homogeneous thickness of 12 nm. Ribonuclease B was again used as a model glycoprotein to assess success of PHMAA coated silica particles for separation under HILIC conditions. Excellent separation was achieved with the packed column with 1.5 µm SiO_2@PHMAA particles as presented in Figure 3.21. Based on this preliminary evaluation, PHMAA underwent further characterization as a HILIC bonded phase, as presented in the next sections.

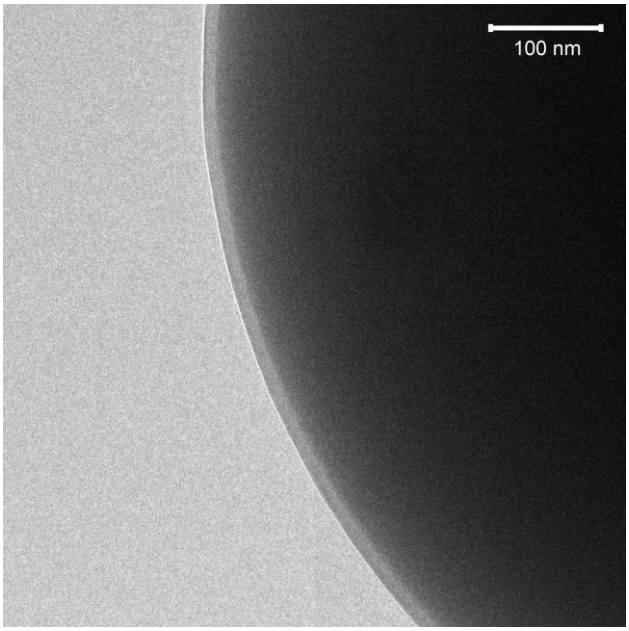

Figure 3.20. TEM micrograph of 1.5 µm SiO_2@PHMAA. Reaction conditions: [PHMAA]= 0.85 M, 37.5 % EtOH, temperature: 35 °C, reaction time: 100 min. Polymer thickness: 12 nm.

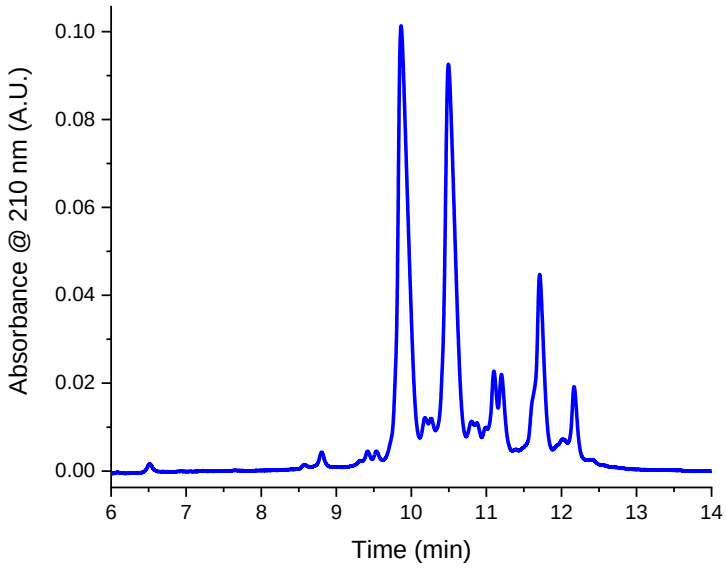

Figure 3.21. Chromatogram of Ribonuclease B using 1.5 µm SiO_2@PHMAA column (50 x 2.1 mm). Conditions: Ribonuclease B 0.5 µg in 75 % ACN and 0.2 % TFA, gradient 75 % B to 60 % B in 20 min, flow rate: 100 µL/min, temperature: 30 °C.

3.5 Characterization of poly N-hydroxymethyl acrylamide as bonded phase for intact glycoproteins analysis by Hydrophilic Interaction Liquid Chromatography

3.5.1 Hydrolysis resistance evaluation

As with PAAM, assessment of the extent of PHMAA hydrolysis was made via FTIR. Silica particles grafted with PHMAA were placed in a solution containing water: acetonitrile (40:60, 0.1 % TFA) and the temperature was kept at 50 °C. Sample during different days were removed and FTIR spectra obtained. Relative to the carbonyl band at 1700 cm^{-1}, the N-H stretch band is changing between experimental variation, and only decreasing slightly overtime as pictured in Figure 3.22.This indicates that PHMAA is more resistant than PAAM to hydrolysis, hence, PHMAA columns might last longer than PAAM under normal HILIC conditions.

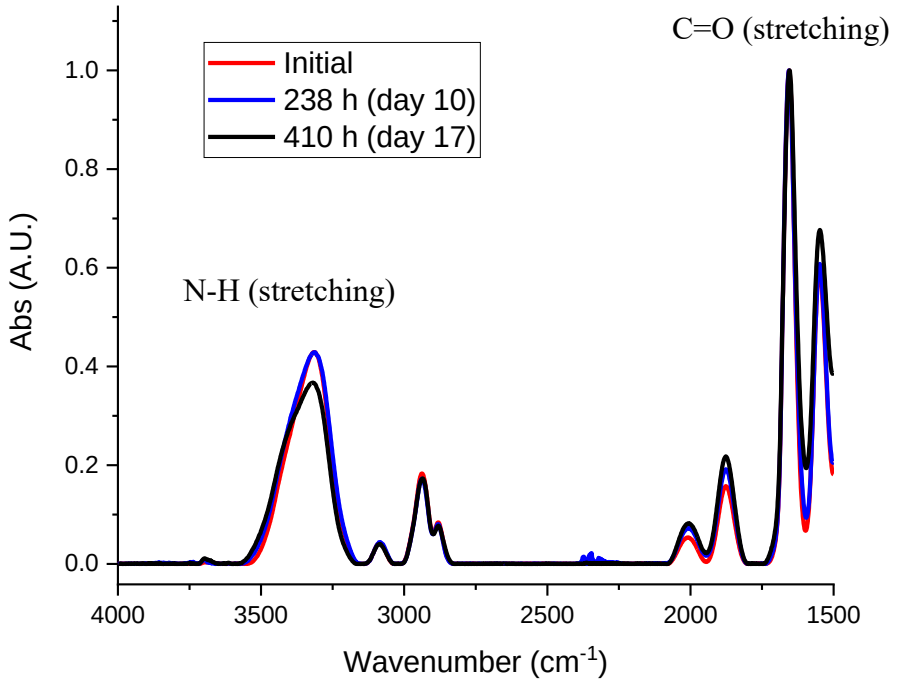

Figure 3.22. FTIR spectra of samples of 1.5 µm SiO_2@PHMAA particles exposed to hydrolytic conditions. Solvent: water : acetonitrile (40:60), 0.1 % TFA, temperature: 50 °C. Carbonyl peak around 1700 cm^{-1} was used to normalize spectra.

3.5.2 Optimization of AGET ATRP polymerization

Experimental conditions were adjusted based on preliminary data collected during monomer selection. Monomer concentration was set to 0.8 M and solvent was 37.5 % ethanol, maintaining other conditions as previously described (catalyst, ligand, reducing agent, and temperature). These changes produced very smooth surfaces with even thicknesses. To study AGET ATRP kinetics, samples were removed over time and TEM images were taken (Figure 3.23).

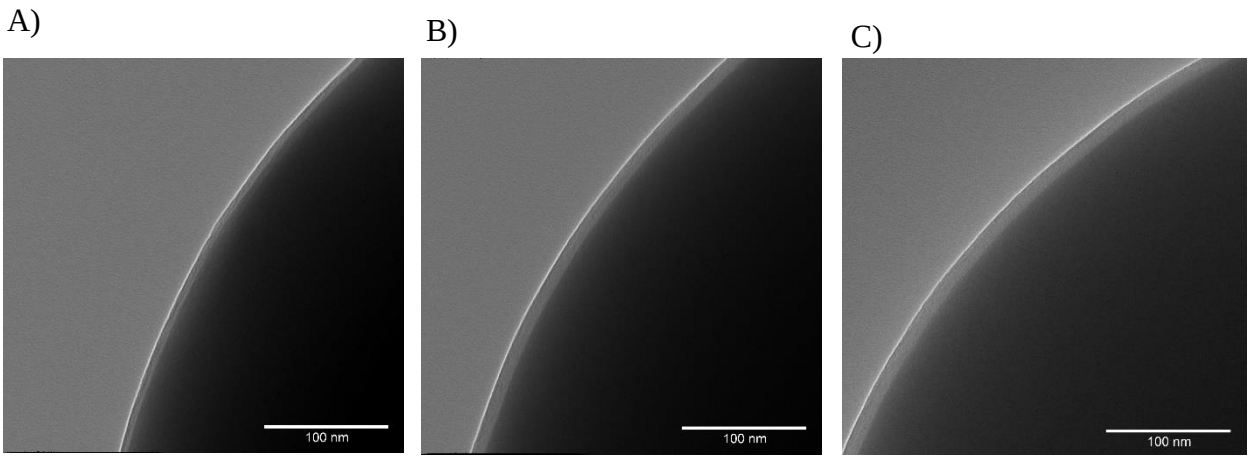

Figure 3.23 TEM micrographs of 1.5 µm SiO_2@PHMAA for reaction kinetics study. A) Reaction time 20 min. B) Reaction time 60 min. C) Reaction time 120 min. Reaction conditions: [PHMAA]= 0.80 M, 37.5 % EtOH, temperature: 35 °C.

According to data plotted in Figure 3.24, the first 20 minute's reaction rate is fast and after that slows down. This outcome can be explained considering that initially the faster initiator on the surface produces many radicals, coating the surface before extending polymer chains. It can be noticed that polydispersity (error bars in Figure 3.24) is small during that initial stage. Reaction rate decrement is related to two components. First, the propagation step uses the polymer end chains for forming new radicals; these new "initiators" are less stable and slower to react with a monomer compared with the benzyl chloride initiators on the surface. Second, as the reaction advances, some termination occurs, truncating some polymer layers and increasing polydispersity as seen for particles obtained after 120 min of reaction (error bars).

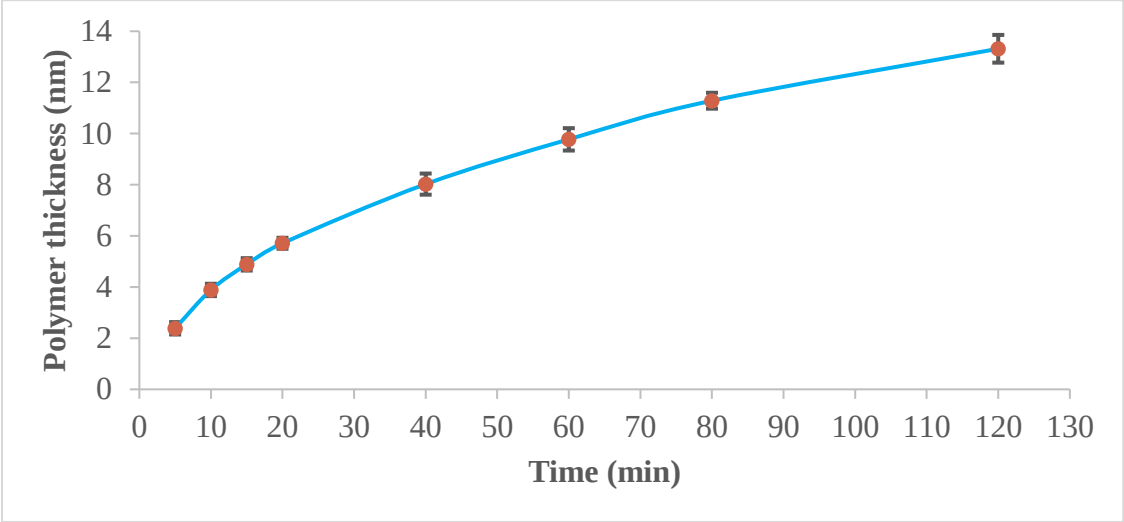

Figure 3.24. Polymer thickness measured by TEM as function of reaction time for AGET ATRP polymerization of SI 1.5 µm SiO_2. Reaction conditions as specified in caption of Figure 3.23.

As presented in Figure 3.25, optimized grafting produces extremely smooth and even surfaces, with a very good separation of Ribo B glycorforms.

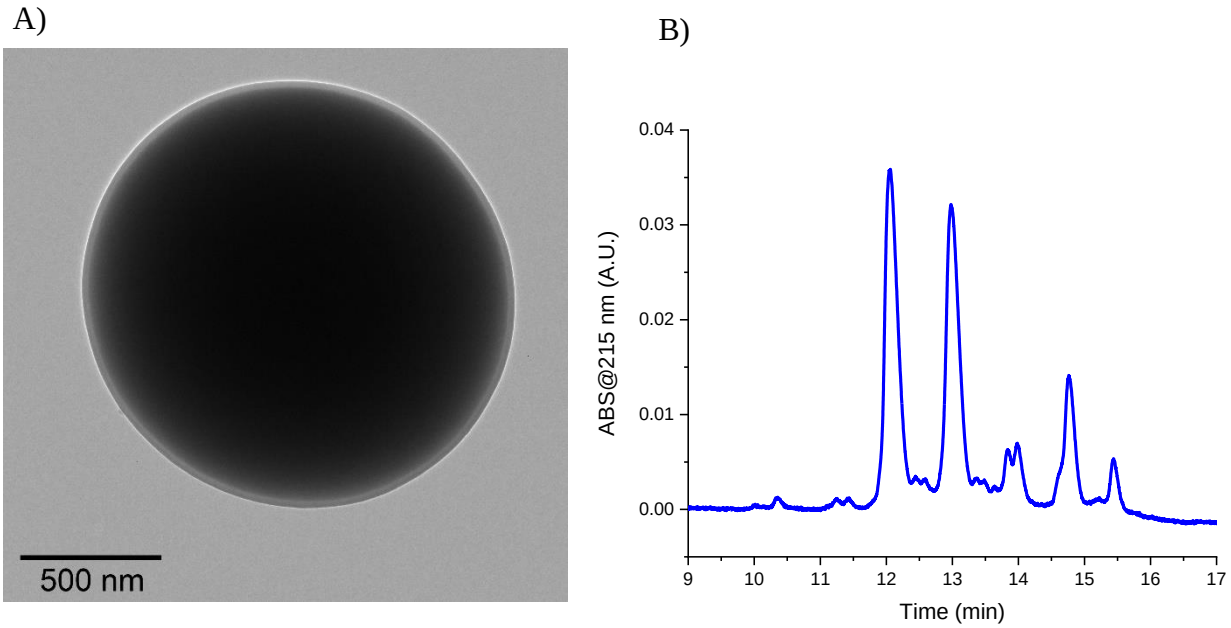

Figure 3.25. SiO_2@PHMAA Particles obtained by the optimized AGET ATRP polymerization. A) TEM micrograph. B) Chromatogram of Ribonuclease B obtained with a 5 cm column. Conditions: Ribonuclease B 0.3 µg in 75 % ACN and 0.2 % TFA, gradient 75 % B to 65 % B in 20 min, flow rate: 100 µL/min, temperature: 30 °C

3.5.3 Polymer thickness influence in separation of intact Ribonuclease B

Polymer brush length and density are vital parameters to obtain effective surface coverage. A high graft density provides steric hindrance to avoid direct interaction of molecules with the surface. Long polymer brushes minimize electrostatic interactions caused by free silanols in silica-based bonded phases. Given the importance of polymer brush length, the performance of PHMAA at different polymer thicknesses was evaluated as part of bonded phase optimization.

As displayed in Figure 3.26A, even a 7 nm polymer thickness successfully creates an adequate hindrance water layer to provide a good HILIC separation. As polymer thickness increases, resolution of the two most abundant peaks increases, and smaller peaks between them emerge. Furthermore, as polymer layer increases, so does retention time. Peaks are sharper, and intensity is enhanced when polymer is more than 11 nm thick. This reveals than polymer layers higher than 11 nm provide an effective silanol isolation and efficient retention.

One of the main concerns when using polymeric materials as stationary phases is the difficulty of packing a slurry of the swollen particles.[13] Also, thicker polymer layers reduce porosity of packing bed, increasing back pressure that limits maximum flow rate. Therefore, polymer thickness must be maintained in a range where separation is efficient, and the back pressure is minimized. Figure 3.26B shows back pressure evolution during chromatographic runs. For 11 nm and 13 nm the pressure is kept lower than 4000 psi, a value around 30 % of UPLC maximum allowed pressure (14000 psi).

Based on the obtained results, the optimal range to obtain good separation and minimal back pressure is between 11 nm and 13 nm.

3.5.4 HILIC mode evaluation

Ribonuclease B separation has already probed that PHMAA is an excellent HILIC bonded phase for resolution of glycoforms. Some studies made for new HILIC stationary phases include the evaluation of separation performance of nucleosides as adenosine and guanosine.[26] These hydrophilic analytes (Figure 3.27) are used to assess how retention changes with variation of solvent composition. In HILIC mode, retention factor decreases with an augment in eluent water content over organic phase (ACN). On the other hand, in RPLC mode, retention factor increases with higher aqueous solvents.

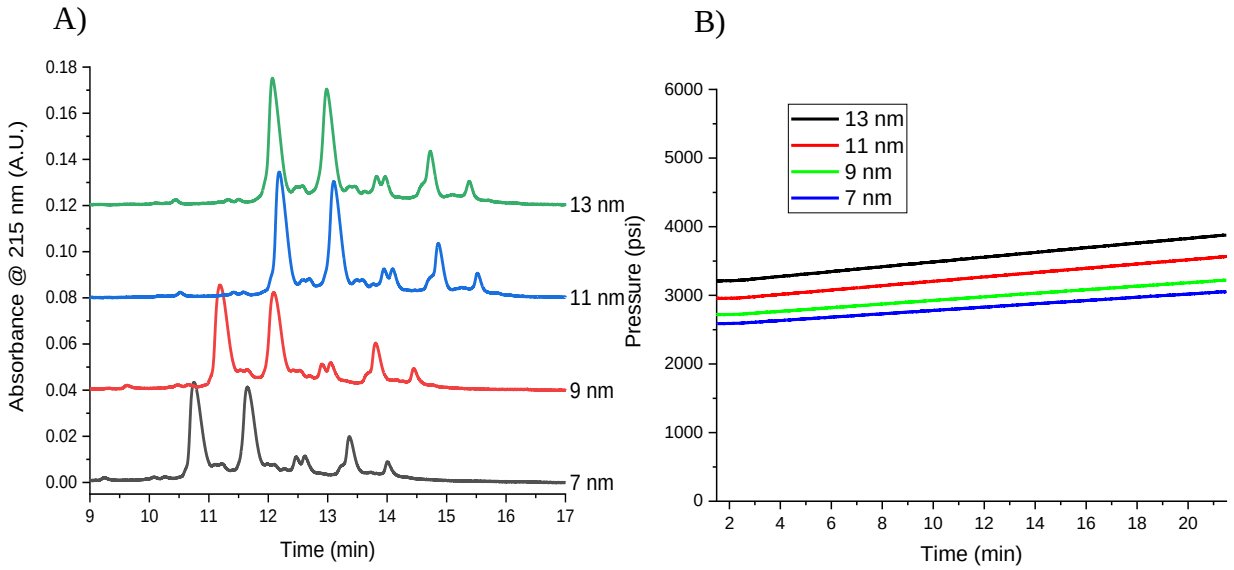

Figure 3.26. Chromatographic performance of SiO_2@PHMAA (50 x 2.1 mm, 1.5 µm) at different polymer thickness. A) Ribonuclease B chromatograms. B) Backpressure changes during runs. Conditions: sample: Ribo B 0.3 µg, gradient: 0 – 1 min: 75 % B, 1 – 21 min: 75 % to 65 % B. Flow rate: 100 µL/min. Temperature: 30 °C.

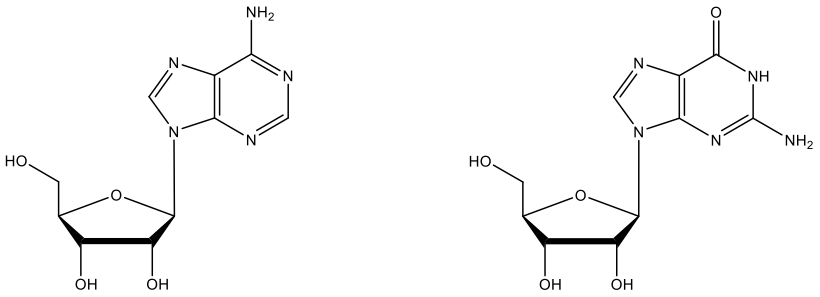

Adenosine Guanosine

Figure 3.27. Chemical structures of analytes used to evaluate HILIC mode separation

In Figure 3.28 and Figure 3.29 are presented chromatograms from different runs at various acetonitrile contents for adenosine and guanosine, respectively. As expected, both analytes elute sooner at lower ACN content (more water) of the eluent. Also, it is visible that the more hydrophilic guanosine is more retained than adenosine under the same composition for the mobile phase.

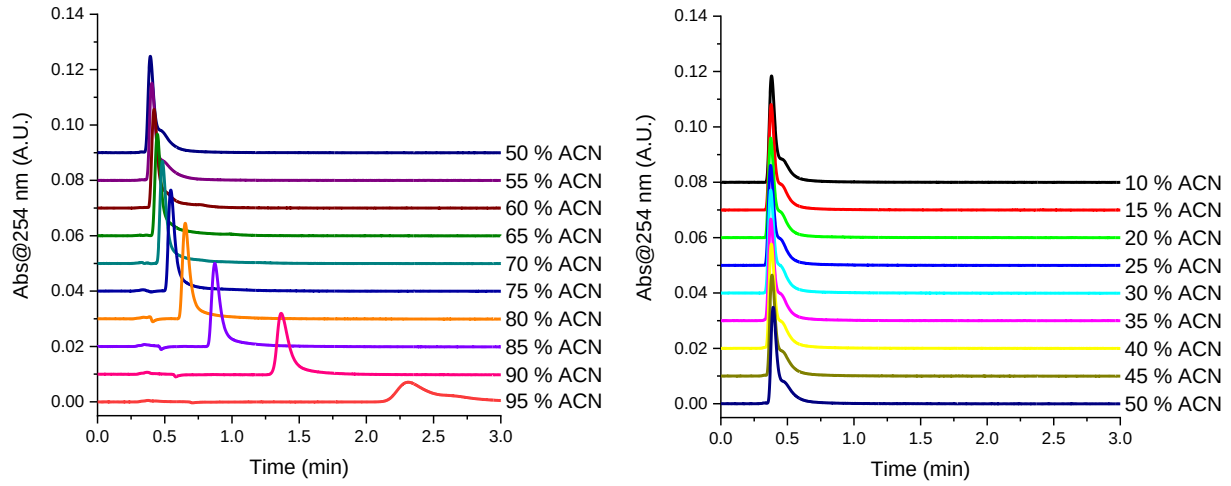

Figure 3.28. Chromatograms for adenosine from isocratic runs at different acetonitrile content (volume/volume). Conditions: solvent A: ACN (0.1 % TFA), solvent B: H_2O (0.1 % TFA), flow rate: 100 µL/min, column temperature: 30 °C

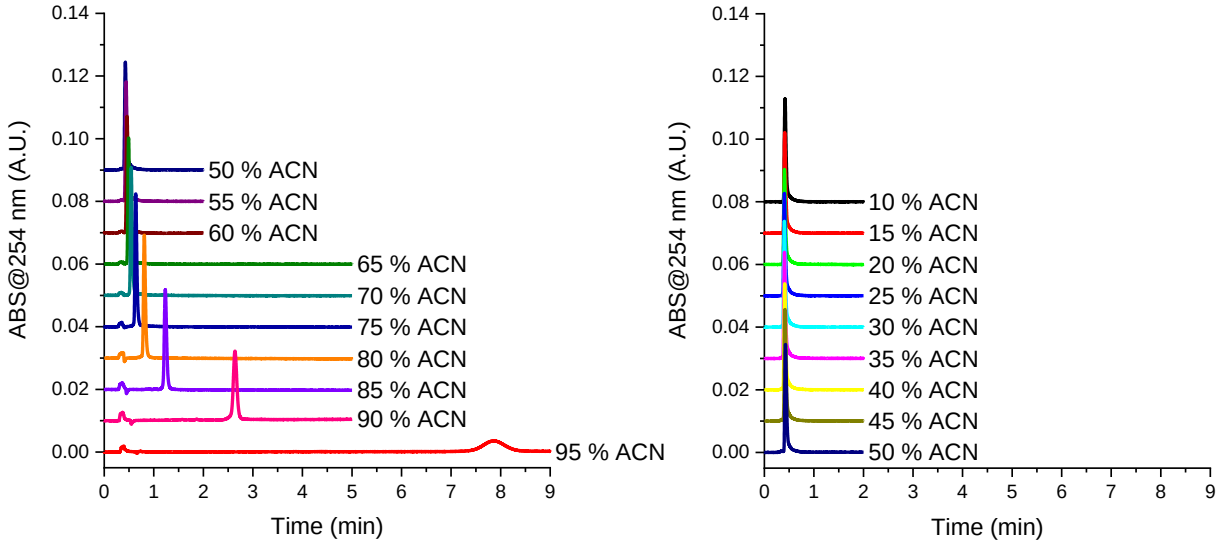

Figure 3.29. Chromatograms for guanosine from isocratic runs at different acetonitrile content (volume/volume). Conditions: solvent A: ACN (0.1 % TFA), solvent B: H_2O (0.1 % TFA), flow rate: 100 µL/min, column temperature: 30 °C

In Figure 3.30, the retention factor of both nucleosides decreased while the content of ACN reduced from 95 to 30 %. This is the characteristic HILIC behavior expected for the high hydrophilic character of PHMAA as the stationary phase. However, when ACN content reduces

to lower than 30 % (vol), retention factor increases as appreciated in the insert of Figure 3.30, generating the distinctive "U-shape" trend, revealing a small HILIC/RPLC mixed mode. This phenomenon indicates the presence of a hydrophobic interaction of methyl groups in the polymer with analytes once surface has been saturated with water. This effect has been previously reported for hydrophilic polymers containing hydrophobic groups.[27, 28]

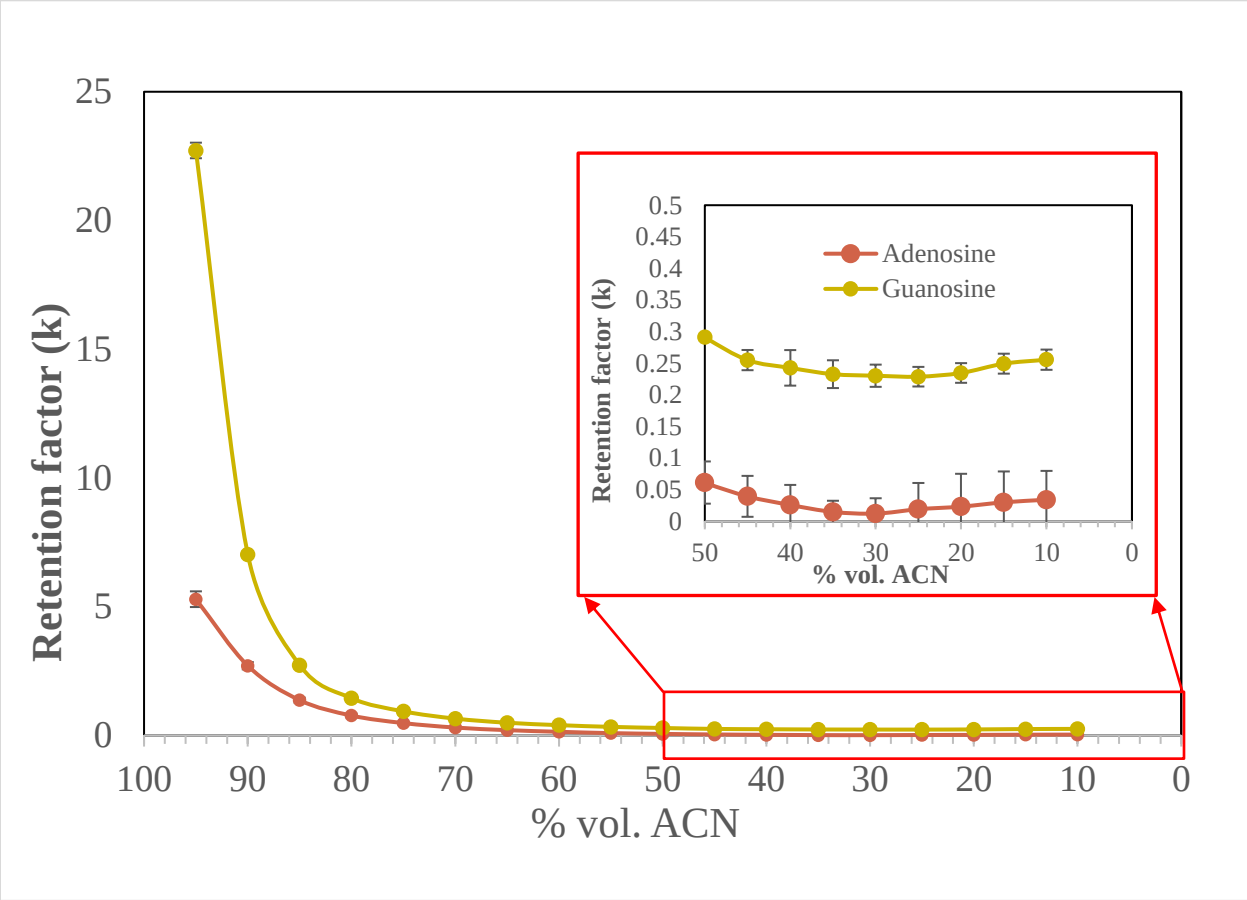

Figure 3.30. Effect of acetonitrile content in the mobile phase on retention factor of adenosine and guanosine. Conditions as described in Figure 3.29.

Multiple approaches have been used to study the retention mechanisms in chromatographic separations. The most studied mechanism involves partitioning of analyte between mobile phase and stationary phase. In the case of HILIC, such partitioning takes place between organic rich solvent and water layer formed on stationary phase. Mathematical model for partitioning mechanism is given in Equation 3.2:[29]

$$\text{Log k} = \text{Log k}_w\text{-S}\,\varphi \qquad \text{Equation 3.2}$$

where φ is the volume fraction of strong solvent (water for HILIC), and k_w is theoretical retention factor when φ = 0. S is the slope of the linear fit of Log k vs φ. This model was used to fit data obtained from varying mobile phase composition for HILIC of adenosine and guanosine, results are displayed in Figure 3.31. It is evident that this model fits data for adenosine in the "HILIC range" (95 % - 30 % ACN), while for guanosine the behavior is clearly non-linear, showing that other types of interactions undergo in HILIC separation of this more hydrophilic molecule. Obtained data allows to calculate k_w = 6.06, a rational value considering the k value for 5 % (5.29). Also, it is important to point out that large error bars obtained for last data of Log k values for adenosine, are mainly due to the low retention time values of those runs, very close to retention time for an unretained compound (t_0). Moreover, a linear trend with opposite slope is seen in the "RPLC mode" (25 - 10 % ACN), consistent with the same partitioning model in which the strong solvent is acetonitrile and not water.

Another studied mechanism in normal phase chromatographic system is surface adsorption, in which the relationship between the retention and molar fraction of the strong solvent (x_B) is given by Equation 3.3:[29]

$$\text{Log k} = \text{Log k}_B\text{-}\frac{A_S}{n_B}\text{Log x}_B \qquad \text{Equation 3.3}$$

where k_B is the solute retention factor when pure strong solvent is used (x_B = 1), A_s and n_B are the cross-sectional area occupied by the solute and number of B molecules, respectively. A linear-fit plot of Log k vs Log x_B reveals if adsorption is dominant. The absorption model was used to fit data obtained from varying mobile phase composition for HILIC of adenosine and guanosine, results are displayed in Figure 3.32. Based in the linear behavior in the HILIC mode range (95 - 40 % ACN), it is possible to conclude that for guanosine prevails absorption on the surface of PHMAA particles. On the other hand, this model does not fit data for adenosine, in agreement with previous results that concluded partitioning predominance. Based on Equation 3.3 and intercept from linear fit in Figure 3.32, the calculated retention factor for guanosine when eluent is pure water (k_B) is 0.075, a reasonable value compared with the retention factor for 60 % (v/v) H_2O of 0.23.

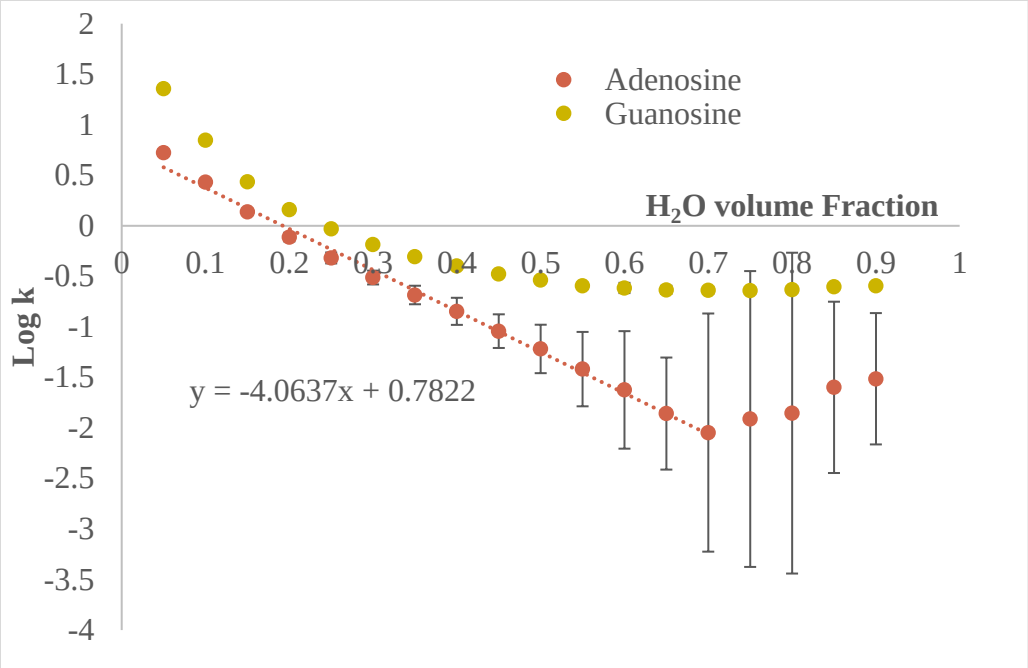

Figure 3.31. Partitioning mathematical model applied to HILIC separation of adenosine and guanosine.

3.5.5 Evaluation of different mechanisms involved in HILIC selectivity

Multiple interactions have been studied as responsible for analyte separation in HILIC.[29] Ibrahim et at.[30], developed a "simplified graphical representation of selectivity in HILIC" to compare retention mechanism in different bonded phases used for hydrophilic analytes. This work was inspired by previous approaches utilized to characterize RPLC stationary phases.[31] In their methodology, evaluated aspects included cation exchange, hydrophilic/hydrophobic and hydrogen bonding. For this purpose, model analytes exhibiting one predominant interaction were selected, their molecular structures and character evaluated are presented in Figure 3.33.

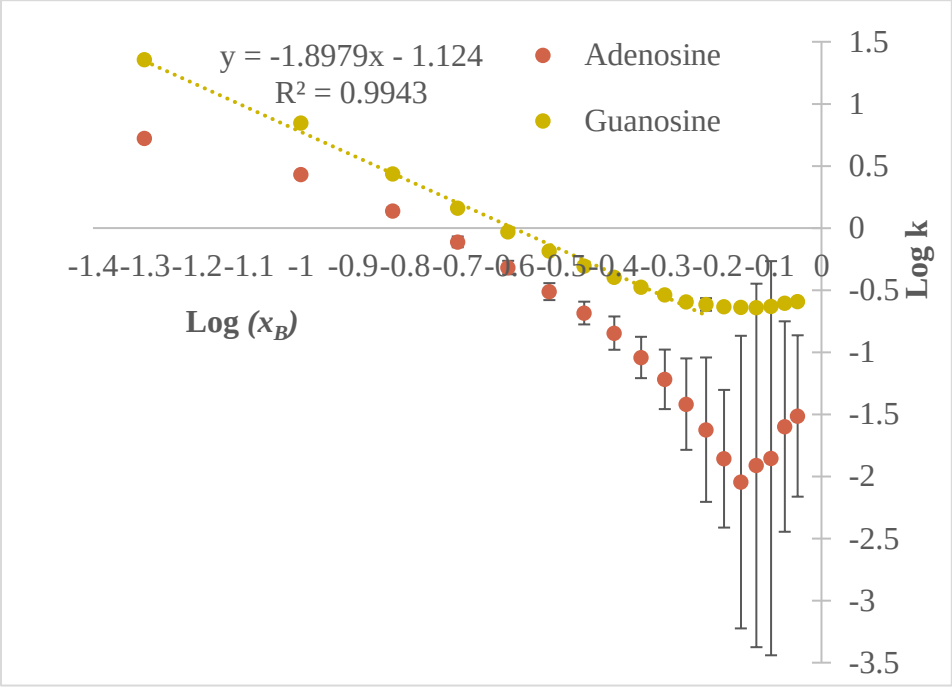

Figure 3.32. Absorption mathematical model applied to HILIC separation of adenosine and guanosine.

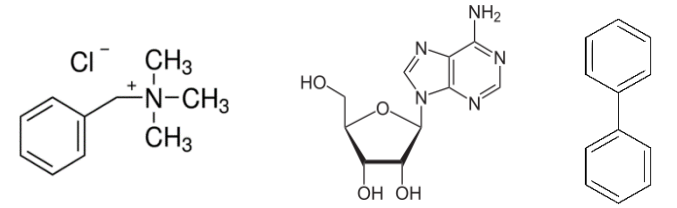

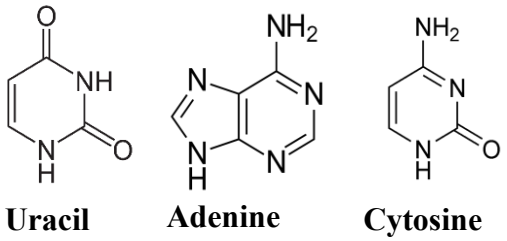

Retention ratio (k_1/k_2)	Character evaluated
BTMA/Cytosine	Cation exchange
Cytosine/Uracil	Hydrophilic/hydrophobic
Adenosine/Adenine	Hydrogen bonding

Figure 3.33. Analytes used to assess selectivity in HILIC. BTMA: Benzyltrimethylammonium chloride.

Cytosine/Uracil are hydrophilic analytes, cytosine being slightly more hydrophilic, hence, a higher retention ratio (Cytosine/Uracil) reveals a more hydrophilic stationary phase. BTMA is a quaternary amine, so it is positively charged despite of the eluent pH and can participate in cation exchange. Hence, BTMA/Cytosine retention ratio exposes ion exchanges of the stationary phase, since both compounds undergo all other interactions. Higher (BTMA/Cytosine) retention ratio shows stronger cation exchange character, while a lower (BTMA/Cytosine) retention ratio implies stronger ion exchange character. Adenosine has a higher capacity to take part in hydrogen bonding than adenine, as a result of its ribose unit. In this way, a higher (Adenosine/Adenine) retention ratio indicates the ability of the bonded phase to participate in H-bonding. Different from the cited reference, biphenyl was used as the unretained compound, due to its high hydrophobicity and strong UV absorption.

For these experiments, eluent consisted of a mixture of ACN/H_2O (80:20) containing 5 mM of ammonium acetate adjusted to pH 6.8 with HCl. This mobile phase guarantees neutrality and mild salt concentration in order to create a balance between studied mechanisms. Analyte concentrations were adjusted to obtain adequate absorbance and avoid overloading of the column. HILIC runs for the model analytes were performed using a 1.5 µm SiO_2@PHMAA (50 x 2.1 cm column), with a flow rate of 50 µL/min. For comparison, a commercial column (Acquity UPLC Glycoprotein Amide 300A 1.7 µm 2.1 x 100 mm, Waters) was also tested, using a flow rate of 100 µL/min. Figure 3.34 displays chromatographic runs of the described analytes in both columns. Retention ratios are summarized in Table 3.2.

Figure 3.35A compares ion exchange capability and hydrophilicity of the bonded phases. Stationary phases located in the left side of the plot are hydrophilic, while those to the right are more hydrophilic. The bonded phase reported in this work shows a hydrophilicity located between zwitterionic and silica-based phases, which was expected due to the hydrophilic amide and hydroxyl groups, but the presence of the methyl group introduces a hydrophobic unit. The Amide Waters column is extremely hydrophilic compared with evaluated columns by Ibrahim et at.[30], even though cytosine is more retained in PHMAA column, The Waters column retained less uracil, making the retention ratio higher. This implies a higher influence of hydrophilicity of the analytes in HILIC selectivity for Waters column compared with PHMAA column. Vertical axis of Figure 3.35A reflects ion-exchange ability of the stationary phase. As can be seen, PHMAA phase has low ion exchange, while Waters column behaves like zwitterionic phases, but exhibits less cation

exchange than silica phases. The fact than SiO_2@PHMAA presents low cation exchange compared with silica phases, demonstrates that polymer brushes are highly dense and long enough to avoid silanol interaction with the analytes.

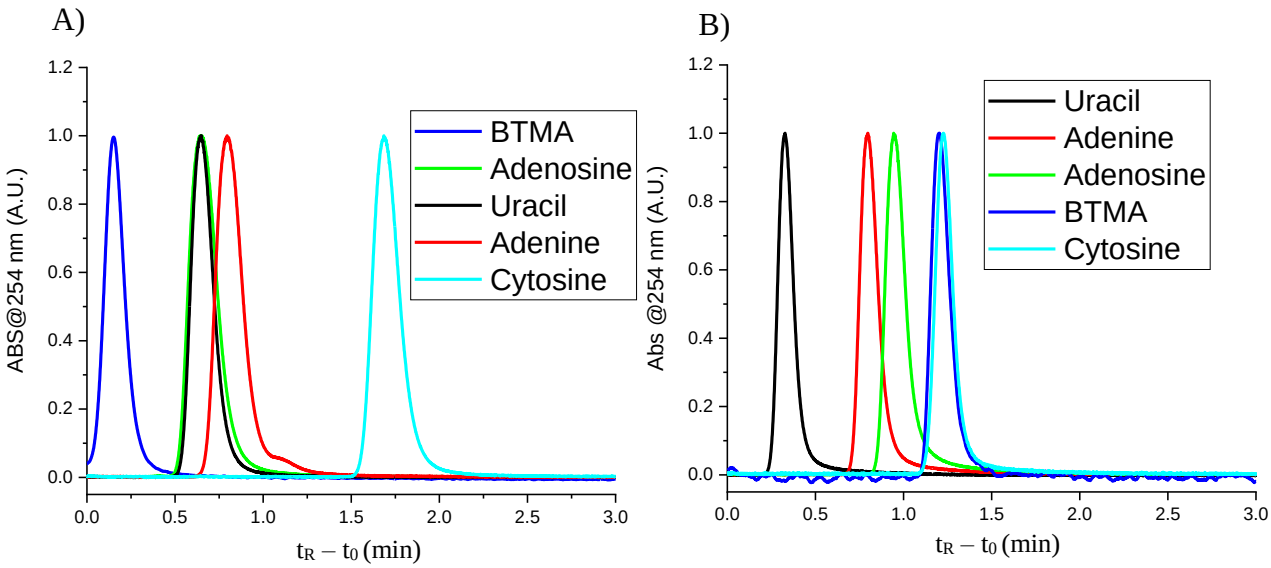

Figure 3.34. Chromatograms for analytes used for evaluating HILIC selectivity. A) 1.5 µm SiO2@PHMAA column (50 x 2.1 mm), 50 µL/min. B) Waters Glycoprotein column (100 x 2.1 mm), 100 µL/min. Conditions: mobile phase: ACN/H_2O (80:20) with 5 mM of ammonium acetate (pH 6.8), temperature: 30 °C. Absorbance at 254 nm normalized.

Table 3.2. Retention ratios of the selected analytes in tested columns for evaluation of HILIC selectivity.

Compounds	**SiO_2@PHMAA**	**Waters Glycoprotein®**
BTMA/Cytosine	0.09	0.98
Cytosine/Uracil	2.61	3.76
Adenosine/Adenine	0.81	1.19

Figure 3.35B represents a selectivity plot of stationary phases, comparing ion exchange with H-bonding capability. Phases to the right side of this plot are more likely to form hydrogen bonds with analytes than the ones located to the left side. PHMAA stationary phase reveals a similar H-bonding capability than silica phases, probably due to hydroxyl groups in the polymer layer. Waters column shows higher H-bonding formation even compared with zwitterionic phases.

A) B)

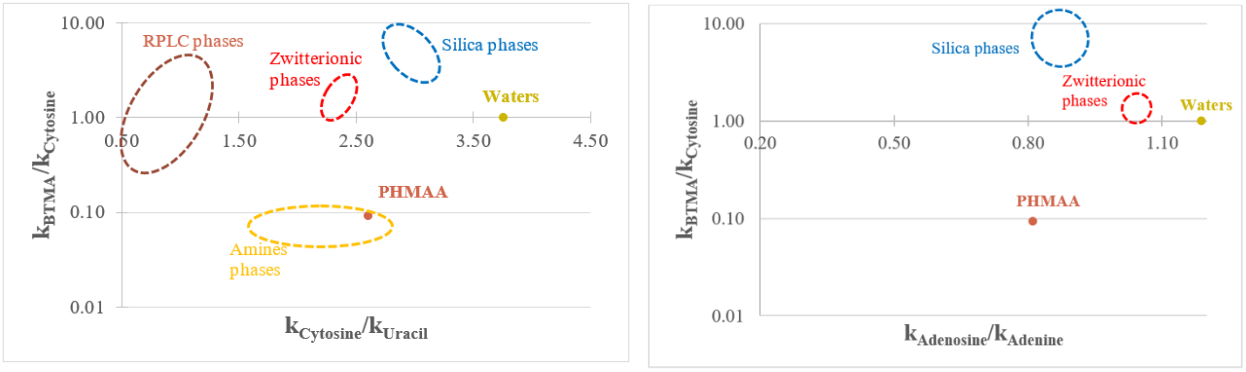

Figure 3.35. Selectivity plots for HILIC stationary phases. A) Ion exchange vs Hydrophilicity plot. B) Ion exchange vs H-bond formation capability. Dashed ellipses represent groups for different columns obtained in reference [30].

3.5.6 Efficiency in separation of Ribonuclease B Glycoforms

Separation in HILIC mode is based on interaction of hydrophilic portions of the sample with the bonded phase. In the case of glycoprotein analysis by HILIC, glycoforms with higher content of sugar units are more retained than those with lower sugar content, hence, last eluted peaks contain longer or more hydrophilic glycan chains. For Ribonuclease B, five main glycoforms have been identified, with mannose from 5 to 9 units.[12]

Since the only difference between Ribonuclease A and Ribonuclease B is the glycosylation (Ribonuclease A lacks glycosylation), a sample containing both proteins can be used to assess selectivity based on glycans in HILIC. As presented in Figure 3.36, resolution is very good between Ribo B with 5 mannose units (peak 2) and non-glycosylated form (Ribo A, peak 1), with narrow peaks and small full width at half maximum (FWHM). For the other peaks, even though separation is only one mannose unit, PHMAA column exhibits good separation. One interesting feature is the splitting of peak 4, likely due to isomers of the 7 mannose unit glycan (Figure 3.26). This demonstrates separation is based on glycan sequence, more than other interactions such as hydrophobicity of the protein.

An important factor affecting column efficiency is amount of injected sample with respect to peak width. It is necessary to consider that intact glycoproteins analysis implies an additional challenge for the size of the analyte, due to the effect that analyte size has on column capacity. Figure 3.37 shows results from isocratic runs to assess the effect of injected sample mass on peak

width. As can be seen in Figure 3.37A, separation is very good in isocratic elution as well with very small FWHM values. In Figure 3.37B narrow peak widths are obtained up to 1.0 µg of sample; however, it is evident that peak overlap is more accentuated at higher injections (0.7 µg and 1.0 µg). These outcomes were considered for all runs made in this work, so injections were used in the range of 0.1 µg to 0.3 µg to minimize overloading and to improve signal to noise ratio.

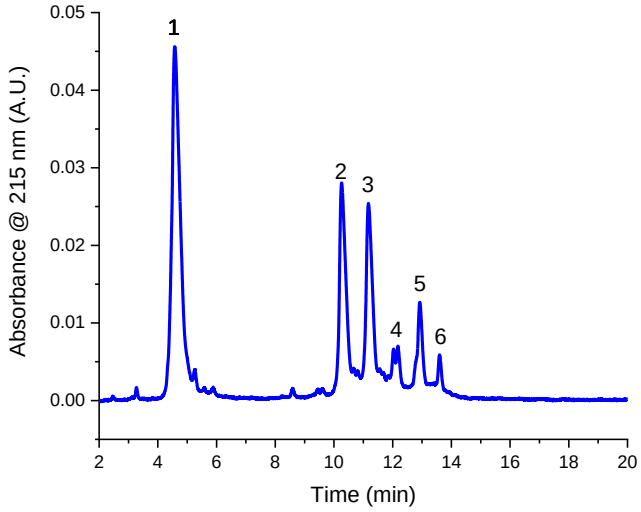

Peak	Species	Tr (min)	FWHM (min)	Rs
1	Ribo A	4.58	0.306	
2	Ribo B+MAN 5	10.26	0.244	12.20
3	Ribo B+MAN 6	11.17	0.244	2.21
4	Ribo B+MAN 7	12.18	0.319	2.11
5	Ribo B+MAN 8	12.93	0.186	1.74
6	Ribo B+MAN 9	13.60	0.149	2.37

Figure 3.36. Resolution of HILIC separation of Ribonuclease glycoform in SiO_2@PHMAA (30 x 2.1 mm, 1.5 µm) column. Conditions: sample: Ribo A 0.3 µg, Ribo B 0.3 µg, gradient: 0 – 1 min: 75 % B, 1 – 21 min: 75 % to 65 % B. Flow rate: 100 µL/min. Temperature: 30 °C.

Mass spectrometry coupled to LC (LCMS) is an important tool for the analysis of glycoproteins. To establish whether LCMS is possible with the PHMAA column, chromatographic detection was simultaneously performed using MS and UV detection, as shown in Figure 3.38. It is remarkable than even using TFA, a known ionization suppressor, signal intensity is strong enough for an appropriate detection as seen in Figure 3.38B, yet with a small amount injected (0.12 µg). Isomers of peak 3 (Figure 3.38A) reveal a single peak in chromatogram obtained with MS detection, demonstrating than PHMAA can separate compounds with small structural difference in the glycans. Figure 3.39A presents the clear mass spectrum for the main glycoform obtained with PHMAA column, giving the correct molecular weight (14.89 kDa) of this species. In Figure 3.39 (B to E), the increasing changes in the mass of the other glycoforms are shown, deconvoluted

in molecular masses in agreement with mannose increments. These results demonstrate the feasibility of LCMS coupling with PHMAA columns.

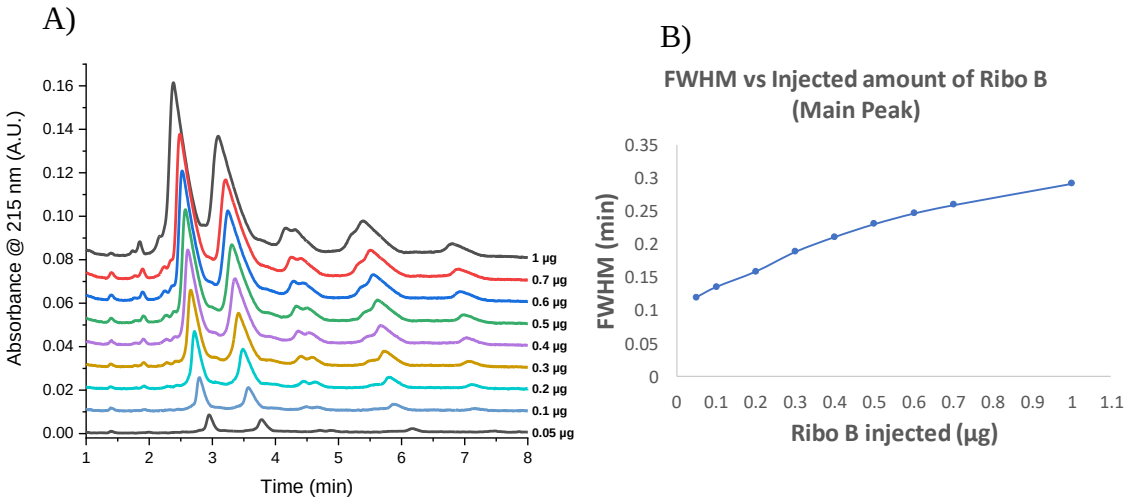

Figure 3.37. Effect of amount of Ribo B injected in FWHM for SiO_2@PHMAA (30 x 2.1 mm, 1.5 µm) column. A) Chromatographic runs under isocratic conditions. B) FWHW vs injected amount. Conditions: 100 µL/min of 71 % ACN (0.1 % TFA). Temperature: 30 °C

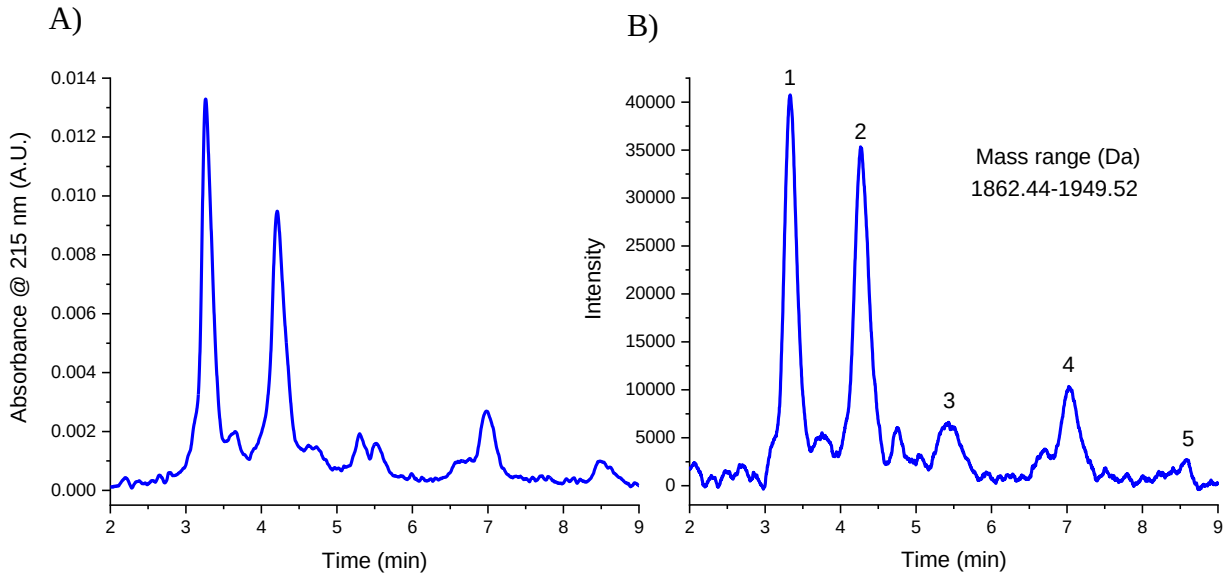

Figure 3.38. Isocratic elution of Ribonuclease B in SiO_2@PHMAA (30 x 2.1 mm, 1.5 µm) column. A) Chromatogram with UV detection. B) Chromatogram with MS detection, mass range 1862.44 Da to 1949.52 Da. Conditions: sample: Ribo B 0.12 µg, 71 % ACN (0.1 % TFA), 100 µL/min, temperature: 30 °C.

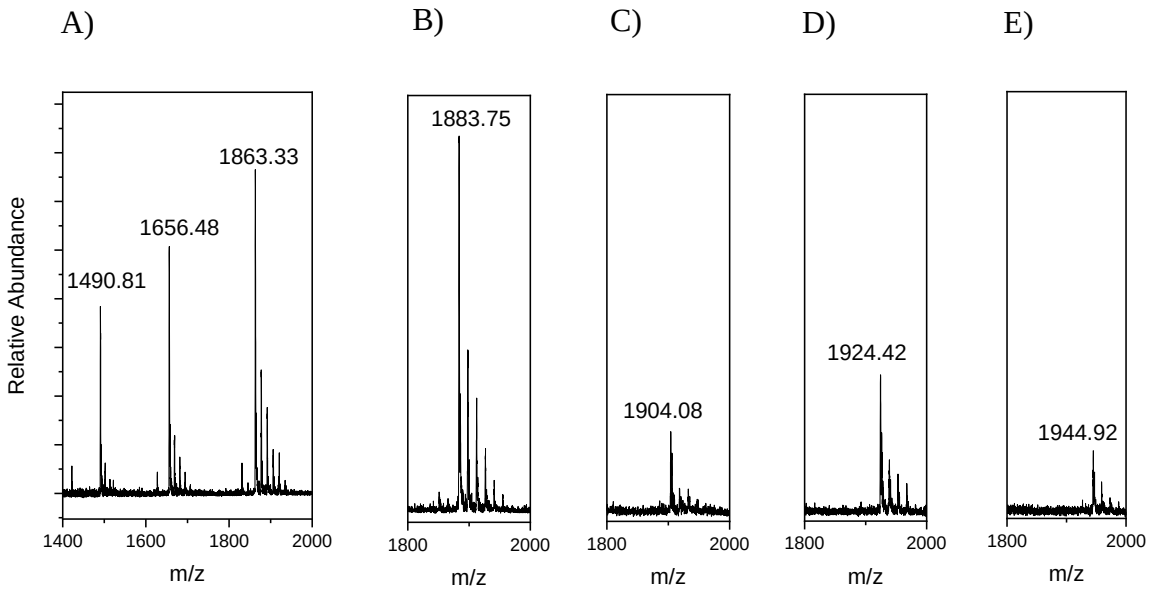

Figure 3.39. Mass spectra of Ribonuclease glycoforms from chromatogram in Figure 3.38B. A) MS of peak 1, corresponding to a mass of 14.89 kDa. B) MS of peak 2, corresponding to a mass of 15.06 kDa. C) MS of peak 3, corresponding to a mass of 15.22 kDa. D) MS of peak 4, corresponding to a mass of 15.38 kDa. E) MS of peak 5, corresponding to a mass of 15.55 kDa.

3.5.7 Chromatographic Repeatability

One of the main concerns with the use of polyacrylamides as stationary phase is the possibility of degradation, affecting separation over time and/or for extended use. It was already demonstrated than PHMAA shows enhanced hydrolysis resistance compared with PAAM (section 3.5.1). Nevertheless, those experiments were carried out under static conditions without the influence of flow and high backpressure that are present during HPLC. With the purpose of evaluating column stability, a single packed column was run over the course of two months, doing intermittent runs (100) in that period of time.

Polymer chains loss or breakage would produce a variation in backpressure due to an increment in column porosity. Hence, as an indicator of polymer degradation, back pressure change was monitored between runs as presented in Figure 3.40A. It is showed that during initial 20 runs backpressure decreases rapidly and then less fast until been almost invariable after around 40 runs. This decrement in pressure can be attributed to a polymer layer shrinking as an effect of the high back pressure during runs, which augments porosity of the column.

Regarding to chromatographic separation, it was observed that PHAA columns need a conditioning period of around 5 runs, during that period, resolution improves, and retention time stabilizes. After that initial stabilization, retention time remains almost invariant as evident in Figure 3.40B. Despite the pressure decrement, chromatographic performance is highly repeatable, demonstrating that PHMAA is stable enough for being used as HPLC stationary phase.

Conditioning is needed in commercial columns, reason why manufactures advise to make conditioning runs with the analyte when using a column for the first time or after an extended storage period. This also allows to saturate possible binding sites with analyte, so they will not cause strong interactions in subsequent analyses.

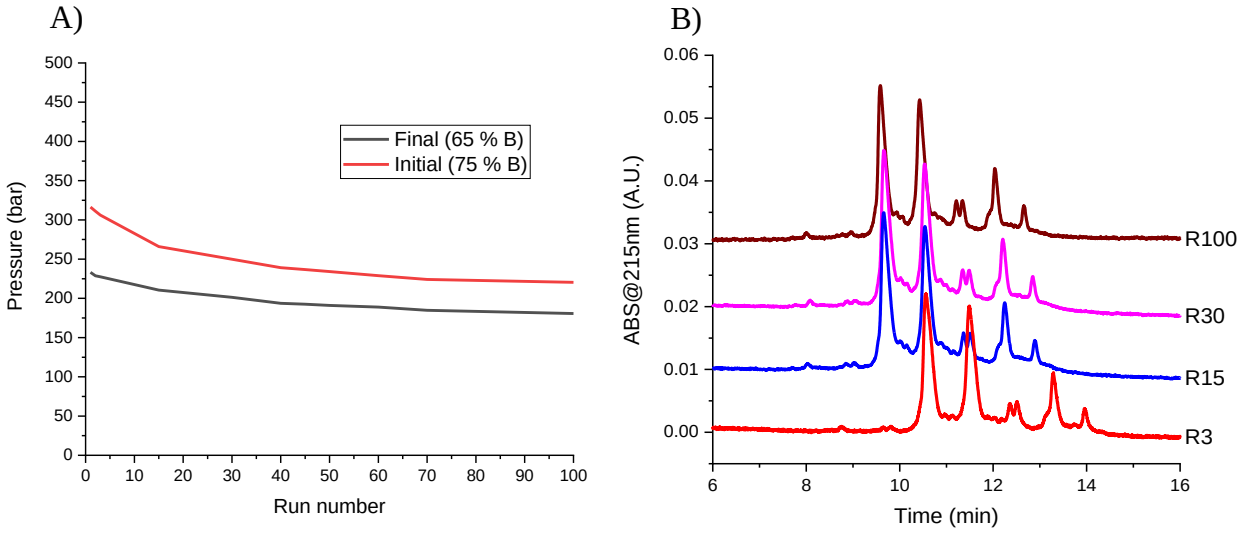

Figure 3.40. Chromatographic repeatability for SiO_2@PHMAA (30 x 2.1 mm, 1.5 µm) column. A) Back pressure change between first and last run. B) Chromatograms of selected runs. Conditions were the same as in Figure 3.26.

3.6 Conclusion

Various polyacrylamides grafted from 1.5 µm silica particles were tested as potential bonded phases for separation of intact glycoproteins. Poly N-Hydroxylmethyl acrylamide (PHMAA) provided higher resistance to hydrolysis and superior resolution among evaluated polymers. Transmission electron microscopy (TEM) was used to optimize PHMAA polymerization, allowing for synthesis of very smooth polymer layers with low polydispersity. An improved packing procedure permitted obtention of columns with adequate packed beds and low operational

back pressures. Higher retention of glycoproteins compared with nonglycosylated proteins demonstrated that separation is based on glycans' interactions with the hydrophilic PHMAA stationary phase, confirming HILIC separation mechanisms. Selectivity of the new stationary phase was evaluated with model analytes, demonstrating that PHMAA participates in hydrophilic interactions and H-bonding, but negligible ion exchange. LC coupled with mass spectrometry was used to resolve the five glycoforms of Ribonuclease B, in agreement with differences in mannose units. Chromatographic repeatability indicated PHMAA is stable during multiple runs and over time.

3.7 References

1. Varki, A., Biological roles of glycans. *Glycobiology* **2017,** *27* (1), 3-49.

2. Apweiler, R.; Hermjakob, H.; Sharon, N., On the frequency of protein glycosylation, as deduced from analysis of the SWISS-PROT database. *Biochimica et biophysica acta* **1999,** *1473* (1), 4.

3. Jaeken, J.; Peanne, R., What is new in CDG?(Report). *Journal of Inherited Metabolic Disease* **2017,** *40* (4), 569.

4. Freeze, H. H.; Eklund, E. A.; Ng, B. G.; Patterson, M. C., Neurological Aspects of Human Glycosylation Disorders. *Annu. Rev. Neurosci.* **2015,** *38* (1), 105-125.

5. Reis, C. A.; Osorio, H.; Silva, L.; Gomes, C.; David, L., Alterations in glycosylation as biomarkers for cancer detection. *Journal of Clinical Pathology* **2010,** *63* (4), 322.

6. Kirwan, A.; Utratna, M.; O'dwyer, M. E.; Joshi, L.; Kilcoyne, M., Glycosylation-based serum biomarkers for cancer diagnostics and prognostics. **2015,** *2015*.

7. Šagi, D.; Kienz, P.; Denecke, J.; Marquardt, T.; Peter-Katalinić, J., Glycoproteomics of N -glycosylation by in-gel deglycosylation and matrix-assisted laser desorption/ionisation-time of flight mass spectrometry mapping: Application to congenital disorders of glycosylation. *PROTEOMICS* **2005,** *5* (10), 2689-2701.

8. Guignard, C.; Jouve, L.; Bogéat-Triboulot, M. B.; Dreyer, E.; Hausman, J.-F.; Hoffmann, L., Analysis of carbohydrates in plants by high-performance anion-exchange chromatography coupled with electrospray mass spectrometry. *Journal of Chromatography A* **2005,** *1085* (1), 137-142.

9. Periat, A.; Fekete, S.; Cusumano, A.; Veuthey, J.-L.; Beck, A.; Lauber, M.; Guillarme, D., Potential of hydrophilic interaction chromatography for the analytical characterization of protein biopharmaceuticals. *Journal of Chromatography A* **2016,** *1448*, 81-92.

10. Tengattini, S.; Domínguez-Vega, E.; Temporini, C.; Bavaro, T.; Rinaldi, F.; Piubelli, L.; Pollegioni, L.; Massolini, G.; Somsen, G. W., Hydrophilic interaction liquid chromatography-mass spectrometry as a new tool for the characterization of intact semi-synthetic glycoproteins. *Analytica Chimica Acta* **2017,** *981*, 94-105.

11. Rinaldi, F.; Tengattini, S.; Calleri, E.; Bavaro, T.; Piubelli, L.; Pollegioni, L.; Massolini, G.; Temporini, C., Application of a rapid HILIC-UV method for synthesis optimization and stability studies of immunogenic neo-glycoconjugates. *Journal of Pharmaceutical and Biomedical Analysis* **2017,** *144*, 252-262.

12. Zhang, Z. a. W. Z. a. W. M. J., Polyacrylamide brush layer for hydrophilic interaction liquid chromatography of intact glycoproteins. *Journal of Chromatography A* **2013,** *1301*, 156--161.

13. Huckabee, A. G.; Yerneni, C.; Jacobson, R. E.; Alzate, E. J.; Chen, T. H.; Wirth, M. J., In-column bonded phase polymerization for improved packing uniformity. *Journal of Separation Science* **2017,** *40* (10), 2170-2177.

14. Jacobson, R. E. HILIC-MS analysis of protein glycosylation using nonporous silica. Purdue University, West Lafayette, IN, 2018.

15. Dai, X.; He, Y.; Wei, Y.; Gong, B., Preparation of hydrophilic polymer-grafted polystyrene beads for hydrophilic interaction chromatography via surface-initiated atom transfer radical polymerization. *Journal of Separation Science* **2011,** *34* (22), 3115-3122.

16. Ma, H.; Jiang, L.; Hajizadeh, S.; Gong, H.; Lu, B.; Ye, L., Nanoparticle-supported polymer brushes for temperature-regulated glycoprotein separation: investigation of structurefunction relationship. *J. Mater. Chem. B* **2018,** *6* (22), 3770-3781.

17. Bui, N. T. H.; Jiang, W.; Sparrman, T.; Irgum, K., Synthesis of poly(N -[tris(hydroxymethyl)methyl]acrylamide) functionalized porous silica for application in hydrophilic interaction chromatography. *Journal of Separation Science* **2012,** *35* (23), 3257-3269.

18. Chen, Y.; Shu, Y.; Yang, Z.; Lv, X.; Tan, W.; Chen, Y.; Ma, M.; Chen, B., The preparation of a poly (pentaerythritol tetraglycidyl ether-co-poly ethylene imine) organic monolithic capillary column and its application in hydrophilic interaction chromatography for polar molecules. *Analytica Chimica Acta* **2017,** *988*, 104-113.

19. Huckabee, A. G., *In-column polymer modifications: Advancing polymer bonded phases*. Ann Arbor : ProQuest Dissertations & Theses: 2016.

20. Zhang, Q. a. W. P. a. L. Z. a. M. R. a. G. J. a. A. A. a. W. C. a. H. D. M., Aqueous copper-mediated living polymerization: Exploiting rapid disproportionation of CuBr with Me6TREN. *Journal of the American Chemical Society* **2013,** *135* (19), 7355--7363.

21. Rickwood, D., Preparative centrifugation: a practical approach. In *Preparative centrifugation: a practical approach*, Oxford ; New York: IRL Press at Oxford University Press: Oxford New York, 1992.

22. Lide, D. R., *CRC handbook of chemistry and physics*. 82nd ed., 2001-2001.. ed.; Boca Raton : CRC Press: Boca Raton, 2001.

23. Caulfield, M. J. a. H. X. a. Q. G. G. a. S. D. H., Degradation on polyacrylamides. Part I. Linear polyacrylamide. *Polymer* **2003,** *44* (5), 1331--1337.

24. Zhao, C.; Zheng, J., Synthesis and characterization of poly(N-hydroxyethylacrylamide) for long-term antifouling ability. *Biomacromolecules* **2011,** *12* (11), 4071.

25. Tang, W.; Kwak, Y.; Braunecker, W.; Tsarevsky, N. V.; Coote, M. L.; Matyjaszewski, K., Understanding atom transfer radical polymerization: effect of ligand and initiator structures on the equilibrium constants. *Journal of the American Chemical Society* **2008,** *130* (32), 10702.

26. Chu, Z. a. Z. L. a. Z. W., Preparation and evaluation of maltose modified polymer-silica composite based on cross-linked poly glycidyl methacrylate as high performance liquid chromatography stationary phase. *Analytica Chimica Acta* **2018,** *1036*, 179--186.

27. Xu, L.; Peng, R.; Guan, X.; Tang, W.; Liu, X.; Zhang, H., Preparation, characterization, and application of a new stationary phase containing different kinds of amine groups. *Analytical and Bioanalytical Chemistry* **2013,** *405* (25), 8311-8318.

28. Zimmermann, A.; Horak, J.; Sánchez-Muñoz, O. L.; Lämmerhofer, M., Surface charge fine tuning of reversed-phase/weak anion-exchange type mixed-mode stationary phases for milder elution conditions. *Journal of Chromatography A* **2015,** *1409*, 189-200.

29. Hemström, P.; Irgum, K., Hydrophilic interaction chromatography. *Journal of Separation Science* **2006,** *29* (12), 1784-1821.

30. Ibrahim, M. E. A.; Liu, Y.; Lucy, C. A., A simple graphical representation of selectivity in hydrophilic interaction liquid chromatography. *Journal of Chromatography A* **2012,** *1260*, 126-131.

31. Neue, U. D., Stationary phase characterization and method development. *Journal of Separation Science* **2007,** *30* (11), 1611-1627.

CHAPTER 4. FUTURE DIRECTIONS

4.1 Magnetic retention for direct release in capillary columns

One of the most attractive features of magnetic particles is their capability of being fast and completely removed from solution using an appropriate external magnetic field. In the case of magnetic extraction beads, this capability makes them uniquely suitable for automation, reducing transfer stages, which minimizes sample loss.[1-3] In biological samples usually target analytes are in low concentrations, and even with preconcentration reached in immunoprecipitation by means of capture beads, eluted concentrations can be still below the detection limit of the analytical method.

In the particular cases of immunoprecipitation of BSA and PDE2 capture studied in this work, elution volume was minimized to improve the detection limit. However, the minimum practical volume that could be utilized during those experiments was 60 µL. Main limitations for a smaller volumes were the size of the vial to perform such elution with respect to the volume occupied by the particles themselves and the inevitable residual volume of elution solution adsorbed to the beads. Another experimental limitation is the injection volume of the chromatographic systems, which usually utilize injection loops filled with up to three times the actual injected volume, wasting sample. A possible method to overcome these difficulties is to perform direct elution inside of the chromatographic column, avoiding additional transfer steps and using a smaller volume of eluent.

As a proof of concept, fluorescent label BSA was captured with anti BSA antibody bound to epoxide beads and immobilized using the experimental set up shown in Figure 4.1A. In this assembly, a solution containing beads with analyte bound is suctioned with the syringe through the capillary, using an adequate low flow rate the magnetic particles are trapped by the magnetic field inside of the capillary as described in Figure 4.1B and C. The shape of the magnet used in this experiment was selected to geometrically enhance the magnetic field.[4] Once the particles are restrained inside, the small capillary tubing could be coupled with a capillary column for a subsequent elution. For this preliminary experiment, the elution was made using 80 % ACN (0.1 % DFA) as eluent without a chromatographic column at the edge of the capillary (Figure 4.2A). Elution profile displayed in Figure 4.2B is an evidence of the plausible success of this proposed

method. Despite the results, this approach needs to be further optimized and more realistic applications need to be evaluated.

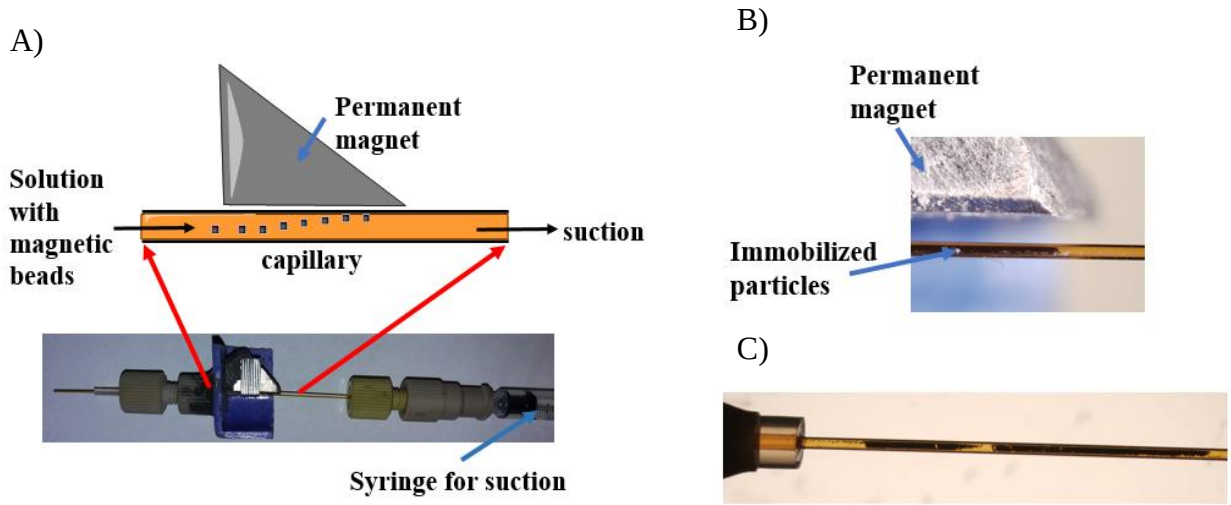

Figure 4.1 Immobilization of magnetic particles with analyte bound to the surface. A) Scheme of experimental set up. B) Close up of magnetic retained particles. C) Capillary after magnetic immobilization.

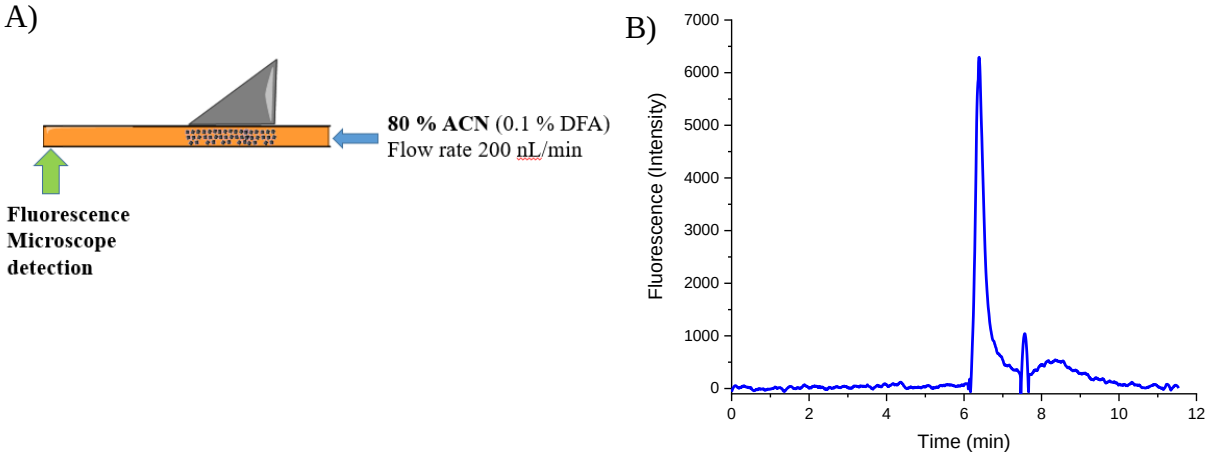

Figure 4.2. Release of fluorescence label BSA from trapped magnetic particles. A) Scheme of experimental conditions. B) Fluorescence measured during release as function of time.

4.2 Alternative epoxide monomers for improved hydrophilicity

As described previously, GMA is a versatile monomer extensively used to produce epoxide containing polymer brushes. However, the presence of the methyl group makes it hydrophobic, being necessary to blend it with hydrophilic monomers to diminish non-specific absorption.[5-7]

Regardless of good non-specific binding reached with the block copolymer of PHEAA and PGMA, hydrophilicity of the polymer brushes could be enhanced if a less hydrophobic epoxide containing monomers is used instead.

In Figure 4.3 are presented chemical structures of most common utilized epoxide monomers with their respective water solubilities,[8] as a way to contrast their hydrophilicities. Among considered compounds, glycidyl acrylate (GA) could be considered a great candidate to replace GMA, because its higher water solubility and possibility of ATRP. However, GA is expensive compared with GMA and to the date of finalization of the present work, it was not in stock until unknown date. Allyl glycidyl ether (AGE) is a cheaper and more hydrophilic monomer, but it is not ATRP polymerizable by itself due to formation of an unstable radical. On the other hand, it has been reported that AGE can be ATRP copolymerizable with methyl acrylate (MA), because the more stable vinyl radical from MA can initiate AGE chains.[9] Preliminary attempts to copolymerize AGE and HEAA were only possible when replacing the ligand Me6TREN by N, N, N',N'', N'' - pentamethyldiethylenetriamine (PMDETA) and directly on the surface initiated silica, not using SiO_2@PHEAA as initiator for a block copolymer. Despite of successful results in binding experiments of the SiO_2@PHEAA-co-PAGE surface, the polymer thickness was not enough to guaranty low non-specific binding (Figure 4.4), therefore more research needs to be done to accomplish an appropriated surface based on PAGE as epoxy source.

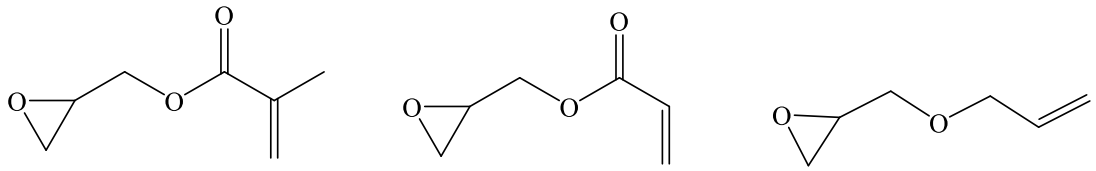

Glycidyl Methacrylate (GMA) | **Glycidyl Acrylate (GA)** | **Allyl glycidyl ether (AGE)**

10 mg/mL | 50 mg/mL | 140 mg/mL

Figure 4.3. Chemical structures of epoxide containing monomers with water solubilities.

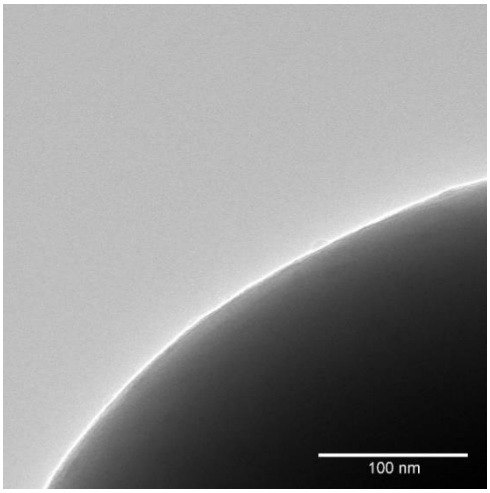

Figure 4.4. TEM micrograph of 1 µm SiO_2@PHEAA-co-PAGE. Polymer thickness around 2 nm.

4.3 Application of magnetic beads in click chemistry

In chapter 1 were discussed some of the main approaches to covalently bind molecules to surfaces, being epoxide one of the most used and versatile. Even with their high reactivity, reactions with amines are sometimes advised to be performed overnight when low temperatures are required for protein stability. Click chemistry has emerged as an important tool for the manipulation and synthesis of molecules in diverse fields.[10] Click reactions are usually carried out with derivatives from alkenes and alkynes, providing highly energetic and fast reactions. The copper catalyzed reaction between azides and terminal alkynes for the obtention of triazoles, as described in

Figure 4.5, is the most typical click reaction.[11] Applications of this type of reactions in drug discovery have been growing in last decade, being of special interest, in high-throughput screening.[12]

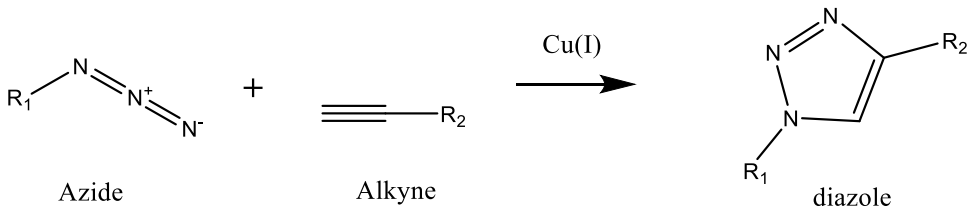

Figure 4.5. Click chemistry reaction between azides and alkynes to form diazoles.

Considering the drug evaluation made in this work, it would be very attractive to obtain azide functionalized magnetic beads for application in the pharmaceutical industry, allowing automation of process such as high-throughput screening. Feasibility of that gold seems pretty straight forward, since epoxide groups can be converted into azide under mild conditions, as previously reported for ATRP polymers.[13-14] Figure 4.6 describes the proposed approach to obtain azide magnetic beads. Applications of such particles would involve attachment of drug compounds with terminal alkynes functionalities with the reactive azide on the beads, a faster reaction compared with epoxide – amines.

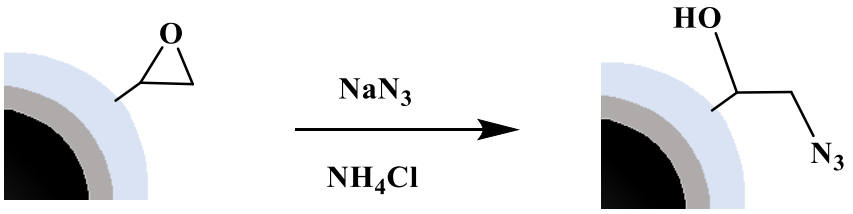

Figure 4.6. Azide transformation of epoxide group on polymer grafted silica coated magnetic particle.

4.4 Block copolymer with a hydrophobic first layer for diminishing silanol interaction for HILIC bonded phase

In order to improve silanol isolation in silica based stationary phase, polymer brushes need to have a high grafting density and proper length.[15] For chromatographic applications, a thick polymer layer usually enhances separation and avoids the need for an acidic modifier as difluoro or trifluoro acetic acids.[16] However, hydrophilic polymer layers undergo swelling in aqueous solvents, diminishing porosity of packed material, increasing backpressure. Therefore, a controlled polymer thickness provides an equilibrium between good separation and adequate operational pressure.

An alternative to reduce the necessity for a very thick hydrophilic layer is to include a not water swollen polymer as first layer and create a block copolymer with the HILIC polymer. As a proof of the possibility of such polymerization and the effect in HILIC, the hydrophobic poly N-tert-butyl acrylamide (PTBAA) was used as first layer over silica particles for a subsequent PHMAA layer (Figure 4.7A). As seen in Figure 4.7B, total polymer layer is only 6 nm and obtained surface is smooth and with low polydispersity.

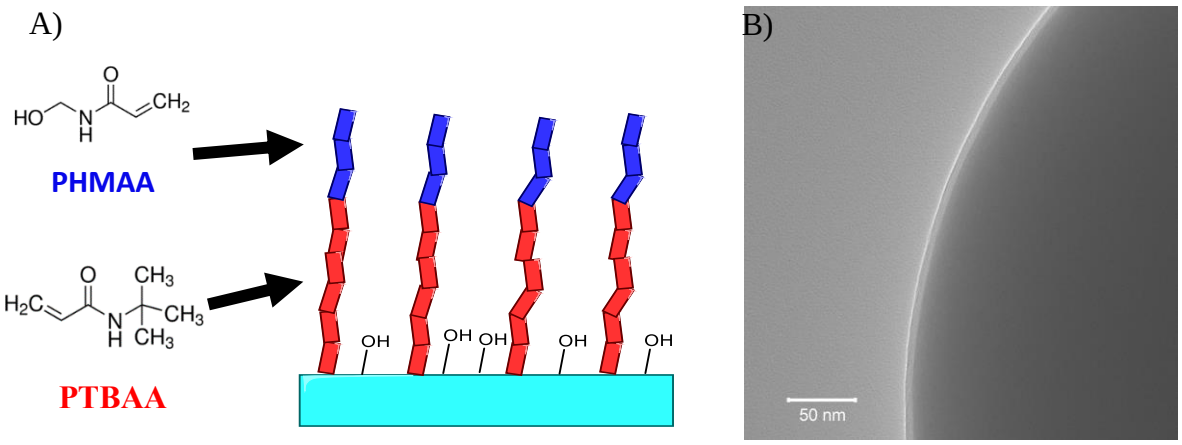

Figure 4.7. Block copolymer of PHMAA and PTBAA. A) Scheme of polymer bushes isolating silanols. B) TEM micrograph of 1 µm SiO_2@PTBAA-b-PHMAA. Thickness: 3 nm each layer for a total of 6 nm.

HILIC performance of the SiO_2@PTBAA-b-PHMAA was tested using 1 µm silica particles. As seen in Figure 4.8A, separation of Ribo B glycoforms has very good resolution and isomers of the 7 mannose units is improved. The backpressure is not extremely high compared with the obtained for 1.5 µm particles (Figure 4.8B), considering that tested particles were smaller (1 µm). In spite of these promising results, block copolymerization is challenging, since TBAA is very hydrophobic for being used with aqueous mixtures necessary for AGET ATRP when sodium ascorbate is the reducing agent. This limits the monomer concentration due to low solubility, making the reaction very slow and obtaining copper precipitates when polymerizations were allowed for more than 5 h to grow longer polymer brushes. Some other hydrophilic polymers such as methyl acrylate were tested, but second polymer layer was uneven and rough. Consequently, a more research needs to be done to optimize the proposed approach of a first hydrophobic later.

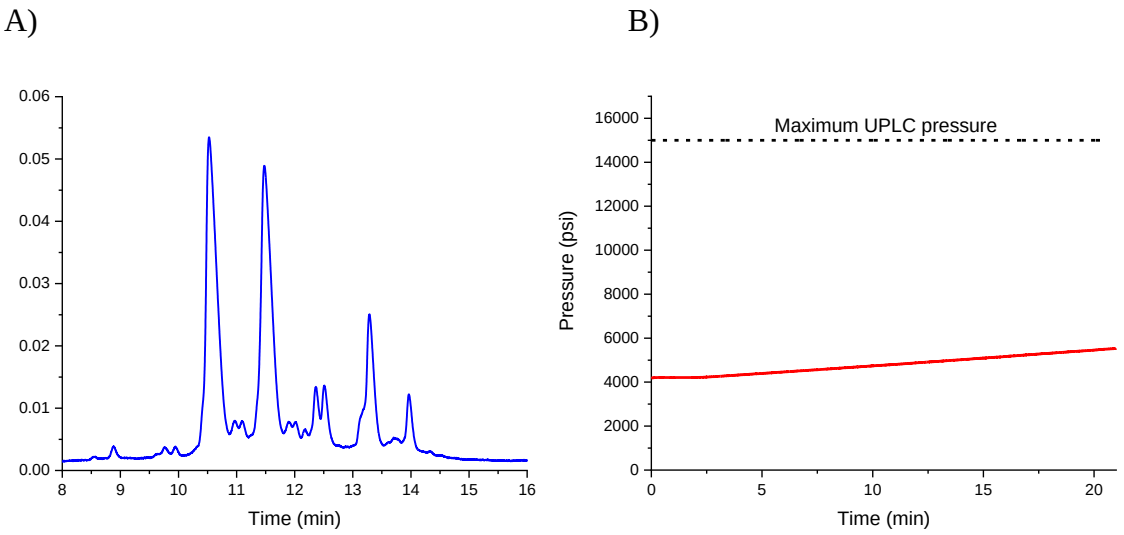

Figure 4.8 HILIC separation of Ribonuclease B in SiO_2@PTBAA-b-PHMAA column (30 x 2.1 mm, 1 µm). A) Chromatogram. B) Backpressure during run. Conditions: sample: Ribo B 0.3 µg, gradient: 0 – 1 min: 75 % B, 1 – 21 min: 75 % to 65 % B. Flow rate: 100 µL/min. Temperature: 30 °C.

4.5 Self-crosslinking of poly N-Hydroxymethyl acrylamide for better stability in HILIC

Another way to improve silanols isolation is with crosslinking of the polymer brushes. [16] Bisacrylamide (N,N'- methylenebisacrylamide)) is a common hydrophilic crosslinking agent used in ATRP.[17] Unfortunately, the use of bisacrylamide as crosslinking agent of acrylamides did not show good results for SI-silica particles, forming aggregation and gels, due to interparticle crosslinking. A plausible alternative is to take advantage of the reactivity of the hydroxy alkyl groups present in PHMAA. Cui and Du[18], and Moritani[19] demonstrated copolymerizations with PHMAA for a subsequent self-crosslinking using the hydroxyl groups, under acidic and/or heat treatment conditions, proposed mechanism is described in Figure 4.9. This proposed method could enhance hydrolysis resistance and separation performance, but the influence of the synthesis process on the polymer brushes and its hydrophilicity as a consequence of the water loss, need to be evaluated.

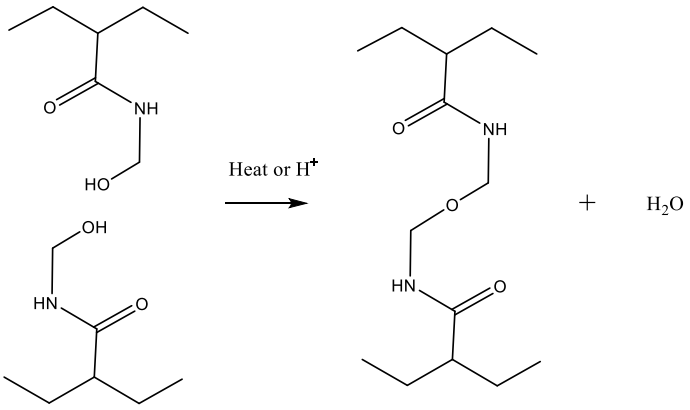

Figure 4.9. Scheme of proposed mechanism for self-crosslinking of PHMAA.

4.6 References

1. Calderilla, C.; Maya, F.; Leal, L. O.; Cerdà, V., Recent advances in flow-based automated solid-phase extraction. Trends in Analytical Chemistry 2018, 108, 370-380.

2. Kallupurackal, V.; Kausel, T.; Sulzer, A.; Voegeli, P.; Kratzer, A., Automating PrepFiler® forensic DNA extraction kit: Optimization and validation on Freedom EVO® 150. Forensic Science International: Genetics Supplement Series 2015, 5 (C), e101-e103.

3. Witt, S.; Neumann, J.; Zierdt, H.; Gébel, G.; Röscheisen, C., Establishing a novel automated magnetic bead-based method for the extraction of DNA from a variety of forensic samples. Forensic Science International: Genetics 2012, 6 (5), 539-547.

4. Hejazian, M.; Li, W.; Nguyen, N.-T., Lab on a chip for continuous-flow magnetic cell separation. Lab Chip 2015, 15 (4), 959-970.

5. Hu, W. a. L. Y. a. L. Z. a. L. C. M., Poly oligo(ethylene glycol) methacrylate-co-glycidyl methacrylate Brush Substrate for Sensitive Surface Plasmon Resonance Imaging Protein Arrays. Advanced Functional Materials 2010, 20 (20), 3497--3503.

6. Ren, T.; Mao, Z.; Moya, S. E.; Gao, C., Immobilization of Enzymes on 2-Hydroxyethyl Methacrylate and Glycidyl Methacrylate Copolymer Brushes. Chemistry – An Asian Journal 2014, 9 (8), 2132-2139.

7. Takasu, K.; Kushiro, K.; Hayashi, K.; Iwasaki, Y.; Inoue, S.; Tamechika, E.; Takai, M., Polymer brush biointerfaces for highly sensitive biosensors that preserve the structure and function of immobilized proteins. Sens. Actuator B-Chem. 2015, 216, 428-433.

8. NIH PubChem Database. https://pubchem.ncbi.nlm.nih.gov (accessed January 28th, 2019).

9. Yu, Q.; Zhang, M.; Li, X.; Bai, R., Living free-radical copolymerization of allyl glycidyl ether with methyl acrylate. Selected Publications from Chinese Universities 2007, 2 (4), 414-418.

10. Moses, J. E.; Moorhouse, A. D., The growing applications of click chemistry. Chemical Society Reviews 2007, 36 (8), 1249-1262.

11. Kolb, H. C.; Finn, M. G.; Sharpless, K. B., Click Chemistry: Diverse Chemical Function from a Few Good Reactions. Weinheim, 2001; Vol. 40, pp 2004-2021.

12. Thirumurugan, P.; Matosiuk, D.; Jozwiak, K., Click Chemistry for Drug Development and Diverse Chemical-Biology Applications. Chem. Rev. 2013, 113 (7), 4905-4979.

13. Tsarevsky, N. V.; Bencherif, S. A.; Matyjaszewski, K., Graft copolymers by a combination of ATRP and two different consecutive click reactions. Macromolecules 2007, 40 (13), 4439-4445.

14. Moni, L. a. C. A. a. D. A. I. a. D. A. a. G. F. a. M. A., Synthesis of sugar-based silica gels by copper-catalysed azide-alkyne cycloaddition via a single-step azido-activated silica intermediate and the use of the gels in hydrophilic interaction chromatography. Chemistry - A European Journal 2010, 16 (19), 5712--5722.

15. Yoshikawa, C. a. Q. J. a. H. C. F. a. S. Y. a. S. J. a. v. d. B. E., Non-biofouling property of well-defined concentrated polymer brushes. Colloids and Surfaces B: Biointerfaces 2015, 127, 213--220.

16. Chu, Z. a. Z. L. a. Z. W., Preparation and evaluation of maltose modified polymer-silica composite based on cross-linked poly glycidyl methacrylate as high performance liquid chromatography stationary phase. Analytica Chimica Acta 2018, 1036, 179--186.

17. Zhang, J.; Xiao, S.; Shen, M.; Sun, L.; Chen, F.; Fan, P.; Zhong, M.; Yang, J., Aqueous lubrication of poly(N -hydroxyethyl acrylamide) brushes: a strategy for their enhanced load bearing capacity and wear resistance. RSC Adv. 2016, 6 (26), 21961-21968.

18. Cui, H.-W.; Du, G.-B., Development of Novel Polymers prepared by vinyl acetate and N-hydroxymethyl acrylamide. Journal of Thermoplastic Composite Materials 2013, 26 (6), 762-776.

19. Moritani, T.; Okaya, T., Functional modification of poly(vinyl alcohol) by copolymerization: IV. Self-crosslinkable poly(vinyl alcohol)s. Polymer 1998, 39 (4), 923-931.

PUBLICATION

(to be submitted for publication)

High Magnetization Acid Stable Ferrimagnetic Particles for Immunoprecipitation

Edwin J. Alzate Rodriguez[a,b], Nicholas J. Sortedahl[a], Uthpala Seneviratne[c], Christopher am Ende[d], Thomas McLellan[d], Graham West[d], Bhagyashree Khunte[d], and Mary J. Wirth[a]

[a]Department of Chemistry, Purdue University, West Lafayette, Indiana , U.S.
[b]Escuela de química, Universidad Tecnológica de Pereira, Pereira, Colombia
[c]Pfizer Worldwide Research and Development, Portland Street, Cambridge, Massachusetts, U.S
[d]Pfizer Worldwide Research and Development, Eastern Point Road, Groton, Connecticut, U.S

Abstract

Magnetic particles have been extensively used for immunoprecipitation because of the feasibility of fast extraction and biocompatibility. Commonly used magnetic beads have an iron core embedded in a polymer with a reactive group such NHS ester or epoxide to allow binding of antibodies. The purpose of the present work is to obtain ultrastable magnetic Fe_3O_4 particles with high magnetization and improved binding capabilities. First, commercially available magnetic nanoparticles were coated with silica by modified Stöber process. It was established that calcination at 600 °C under vacuum produces an impermeable shell, resistant to concentrated HCl exposure. TEM analysis revealed a 50 nm thick silica layer, smothered after heat treatment. Fe_3O_4@SiO_2 particles were aggregated into 1 µm sized agglomerates during coating process because of residual magnetism of starting material. Silica surface was grafted using aqueous AGET-ATRP with a two layers block copolymer of polyhydroxyethyl acrylamide, to reduce protein adsorption, and polyglycidyl methacrylate, to covalent binding of antibodies. Resulting polymer coated particles exhibited excellent dispersion in aqueous solution. Magnetization measurements determined that reported particles are almost three times more magnetic that commercial Dynabeads. Immunoprecipitation of fluorescent labeled BSA showed a 2-fold binding capacity compared to Dynabeads, with similar non-specific binding.

1. Introduction

Magnetic nanoparticles (MNPs) are widely used in multiple fields, including magnetic inmunoprecipitations,[1] protein purification,[2] ferrofluids,[3] drug delivery[4] and biosensors.[5] Application for bio-separations are based in their magnetic properties that allow for a facile recovery of biomolecules from complex matrices. Naked Fe_3O_4 particles are highly reactive and can be easily oxidized in air, losing their magnetic properties. Consequently, magnetic particles are commonly coated to improve chemical resistance. These approaches include grafting of or coating of the surface with a broad type of compounds, such as biomolecules, surfactants, and polymers, or using an inorganic layer such as silica, metal oxides or sulfides.[6] Surface coating not only produces more stable iron oxide particles, but also allows subsequent funcionalization.[7]

Modified Stöber process is the most commonly used method to obtain silica-coated Fe_3O_4 particles.[8] However, the addition of nonmagnetic silica to the surface frequently produces a reduction in saturation magnetization of small magnetic particles.[9] To overcome this situation, preserving extraction efficiency, research efforts have been focused in coating larger ferrimagnetic particles.[10-11] Furthermore, silica coating obtained by Stöber method is not completely impermeable and shows microporous,[12-13] so iron core is not entirely protected against oxidation.

Since Fe_3O_4 cores are susceptible to acid corrosion, hydrochloric acid exposure can be used to evaluate stability and quality of silica-coated magnetic particles. Approaches to obtain acid-resistant silica-coated MNPs include addition of an intermediate hydrophobic silica layer (using dimethyldiethoxysilane)[14] and silane post-modification with (3-aminopropyl)triethoxysilane,[15] but these methods produce particles that can only resist HCl concentrations up to 1 M.

Silanes are extensively used as surface modifiers for silica. Noncorrosive ethoxy silanes are preferred because they preserve silica coating, although, do not provide a dense surface coverage.[17] In contrast, chlorosilanes afford much dense surface functionalization, feature that makes them very useful in fields like chromatography where highly coated surfaces are essential.[16] Attachment of chlorosilanes requires more aggressive reaction conditions, thus, an appropriate silica coating is necessary, restricting their use to pure silica or extremely well coated surfaces.

When applying MNPs as capture agents, binding specificity and efficacy are provided by modification of the surface with active groups. Such groups can interact with target molecules directly by electrostatic forces and/or hydrogen bonds, like in the case of amino-modified surfaces.[17] Also, more specialized capture can be afforded by covalent attachment of specific entities like antibodies for a particular antigen extraction.[18] Functional groups that facilitate immobilization of bioactive molecules on surfaces throughout formation of covalent bonds with amine groups include N-hydroxysuccinimide (NHS) ester,[19] and epoxide.[20] NHS esters are not stable in aqueous conditions and suffer from hydrolysis, compromising their binding capacity over time.[21] On the other hand, epoxy groups are stable in aqueous media and are very reactive to not only amines but also to sulfhydryl groups.[22]

Epoxides can be introduced to silica coated magnetic nanoparticles by grafting epoxide-containing polymers such polyglycidyl methacrylate (PGMA).[23] However, PGMA is hydrophobic enough to exhibit non-specific absorption of undesirable molecules.[24] Hydrophilic polymers such as polyacrylates and polyacrylamides have been used to obtain antifouling [25] and low protein adsorption surfaces.[26] Consequently, a copolymer of PGMA with a hydrophilic low adsorption polymer can be used to improve anti-biofouling functionality, obtaining a material with high reactivity for amines with low non-specific binding.

In this work, commercial iron particles were silica-coated and thermally treated under vacuum to obtain an impermeable surface, tolerating HCl concentration up to 11 M. Enhanced resistance, permits surface functionalization with nitric acid under reflux and aggressive chlorosilanes. Using "grafting from" approach with AGET ATRP,[27-28] a uniform low biofouling block copolymer with PGMA and polyhydroxyethyl acrylamide (PHEAA), was synthetized. Copolymer surface binding performance was evaluated using immunoprecipitation of Bovine Serum Albumin., showing enhanced specific to non-specific binding ratio compared with commercial magnetic extraction beads.

2. Experimental

2.1. Materials

Deionized water was obtained using a Milli-Q Gradient equipment to a final conductivity of 0.055 mS. Fe_3O_4 nanoparticles (50 nm – 100 nm) were obtained from Nanostructured & Amorphous Materials, Inc. Ethanol (200 proof) was acquired from Decon Laboratories. Tetraethyl orthosilicate (TEOS, 97%), branched polyethylenimine (PEI, Mw ~ 25,000 Mn 10,000), N-hydroxyethyl acrylamide (HEAA, 97%), glycidyl methacrylate (GMA, 97%), $CuCl_2$ (99.995%),

phosphate buffered saline (PBS, tablet), 2-Amino-2-(hydroxymethyl)-1,3-propanediol (TRIS, 99.9%), ammonium hydroxide solution (28 %), and sodium dodecyl sulfate (SDS, 98.5 were purchased from Sigma Aldrich. Protein free T-20 blocking buffer, hydrochloric acid (37 %), Dynabeads M-270 epoxide and toluene (99.5%) were distributed by Thermo Fisher Scientific. Sodium L-Ascorbate (98 %) were obtained from TCI chemicals. Tris(2-dimethylaminoethyl) amine (Me6Tren, 97%) was a product of Alfa Aesar. Chloromethyl phenylethyl dimethylchlorosilane (98 %) was procured from Gelest. 1 µm silica particles were obtained from Superior Silica. Fluorescent Bovine Serum Albumin (BSA, Alexa Fluor® 555 or 488 conjugate) and BSA antibody (Anti-BSA, 70-BC67) were purchased from Fitzgerald.

2.2. Silica coating

2 g of Fe_3O_4 was dispersed in 400 mL ethanol with sonication (Branson 3800) for 3 h. Next, the particles were magnetically separated, and dried under vacuum at 60 ˚C for 2 h. 1 g of the dried solid was suspended into a solution of 200 mL of water and 2 g of PEI. This dispersion was sonicated and overhead stirred (Chemglass) for 8 h, followed by separation via centrifugation. 500 mg of the PEI treated Fe_3O_4 was transfer to 500 mL of water and sonicated with overhead stirring for 15 min. Then, 200 mL of ethanol were added and sonicated/stirred for extra 5 min. The stirrer was removed, and sonication only was allowed for 5 min. Then, 10 mL of TEOS were added, and sonication was extended for 1 h. Fe_3O_4 particles were magnetically extracted, rinsed three times with ethanol and dried under vacuum at 60 °C for 2 h. 250 mg of the silica coated particles were sonicated and stirred for 15 min in a mixture of 800 mL of ethanol and 160 mL of water. Stirring was stopped and 16.6 mL of NH_4OH and 2 mL of TEOS were added. Sonication only was continued for 1 h. Finally, the silica coated magnetic particles were magnetically extracted and dried at 60 °C under vacuum for 2 h.

2.3. Thermal treatment

500 mg of dry silica coated material was transferred to a quartz boat and placed inside a tube oven (MTI corporation, model OTF-1200 X). The tube was sealed and purged with nitrogen for 3 min and vacuumed for 2 min, four more purge/vacuum cycles were performed leaving the tube under active vacuum before starting the heat treatment.

2.4. HCl resistance evaluation

After thermal treatment, weighted particles were placed in a tared glass 20 mL Scintillation vial and initial mass was measured. 10 mL of 37 % HCl were added and the vial was capped and sonicated for 1 h at room temperature. Afterwards, supernatant was removed using a magnet to retain the particles. Vial was rinsed with DI water until neutral pH. Container was dried at 60 °C under vacuum until constant weight. Mass loss percentage was calculated as in Equation 1.

$$\% \, mass \, loss = \frac{m_s - (m_{tf} - m_v)}{m_s} \, x \, 100 \qquad \text{(Equation 1)}$$

where: m_s: mass of sample before acid, g
m_{tf}: mass of vial and sample dried, g
m_v: mass of the empty vial, g

2.5. AGET ATRP surface initiation

500 mg of heat treated Fe_3O_4@SiO_2 was added to 10 mL of 37 % HCl and sonicated for 1 h. Then, material was washed with deionized water until a neutral pH was reached. Next, 250 mL of 1.5 M HNO_3 was added and heated under reflux during 24 h. Particles were washed five times with deionized water and once with ethanol, followed by drying at 60 °C under vacuum for 2 h. In a dried round bottom flask, 500 mg of particles were dispersed in 100 mL of dried toluene under a nitrogen atmosphere. 2 mL of chloromethyl phenylethyl dimethylchlorosilane and 100 µL of butylamine were incorporated. The mixture was refluxed for 3 h. After reaction completion, the particles were washed twice with toluene and twice with acetonitrile and dried at 60 ˚C.

2.6. Polymer grafting

Water and ethanol were purged with nitrogen under sonication for 15 min to remove dissolved oxygen. In a 50 mL two necked round bottom flask equipped with a homemade sealed overhead stirrer, 200 mg of surface-initiated particles and 15 mL of ethanol were sonicated until dispersion. Then, a mixture of 6.3 g of HEAA (53 mmol) with 14 mL of water was added to the flask and sonication with nitrogen sparging was applied for 10 min. A solution of 40 mg of $CuCl_2$ (0.295 mmol), 80 µL of Me6Tren (0.298 mmol) in 2.5 mL of water was incorporated. The reaction was started by addition of 2.5 mL of water containing 27 mg of sodium ascorbate (0.136 mmol). The reaction flask was transfer to a water bath kept at 35 °C, nitrogen flow was suspended, and polymerization was allowed for 75 min under hermetic conditions. Upon completion, PHEAA coated particles were magnetically extracted, washed thrice with water, and once with ethanol.

For the second copolymer layer, in a 25 mL two necked round bottom flask equipped with a homemade sealed overhead stirred, 100 mg of PHEAA coated particles were suspended in 18 mL of ethanol, 13 mL of water and 0.9 g of HEAA and sonicated with nitrogen purging for 10 min. A prepared solution of 15 mg of $CuCl_2$ (0.1104 mmol), 29 µL of Me6Tren (0.1079 mmol) in 3 mL of water was transfer to the reaction flask. After homogenization, 1.05 mL of glycidyl methacrylate (3.73 mmol) were added. With addition of 10 mg of sodium ascorbate (0.0505 mmol) dissolved in 2 mL of water, the reaction was run at room temperature for 20 min under nitrogen (no flowing) and stirring. Epoxy containing magnetic particles were rinsed once with acetonitrile, twice with ethanol followed by two water rinses. Particles were completely dried under vacuum at room temperature.

2.7. Transmission Electron Microscope Analysis

1 µg of material was suspended in 500 µL of solvent (ethanol for silica coatings and water for polymer coatings). 5 µL of the slurry was transferred to a F/C 300 mesh Cu grid (TED PELLA Inc.). TEM micrographs were acquired in a FEI Tecnai G2 20 Transmission Electron Microscope.

2.8. Infrared Analysis

Samples were grinded with dried KBr, in an agate mortar to get a 0.2 % homogeneous fine powder. 50 mg of the mixture were hydraulically compressed to form a pellet. IR spectra were measured using a FT-IR spectrometer (Tensor 37, Bruker)

2.9. Magnetic Characterization

A sample of 5 mg was introduced into a SQUID straw, and a four-quadrant scan was done using an MPMS-3 magnetometer at 300 K. For correcting the residual magnetic moment of the equipment at zero magnetic field, an identical scan using a gadolinium gallium garnet was performed.

2.10. Fluorescence Analysis

Fluorescence measurements were performed in a Edinburgh Instruments FLS980 Steady State Fluorescence Spectrometer.

2.11. Antibody binding Capacity

5 mg of epoxide coated beads were suspended in 1 mL of PBS 1X containing 0.1 mg of Anti-BSA, incubation for 3 h was performed on a horizontal shaker at 750 rpm. After binding, 50 µL of supernatant were transferred to a new vial containing 500 µL of T-20 blocking buffer, reaction was allowed for 1 h. Magnetic extracted beads were washed three times with PBS 1X and then incubated for 1 h in 1 mL of fluorescent BSA (0.1 g/L in PBS 1X). Particles were rinsed 3 times with TRIS buffer (20 mM, pH 8.2). Elution was performed for 30 min with 20 µL of 2 % SDS. 10 µL of final supernatant were diluted with PBS 1X to 2 mL for fluorescence quantitation.

2.12. Non-specific Binding

3 mg of epoxide magnetic beads were incubated in 600 µL of T-20 blocking buffer for 1 h. Particles were magnetically extracted and rinsed 3 times with PBS 1X and 100 µL of fluorescent BSA (40 mg/mL in PBS 1X), allowing binding for 1 h. Particles were washed 6 times with TRIS buffer (20 mM, pH 8.2). Elution was performed as for antibody capacity.

3. Results and Discussion

3.1. Coating of magnetic particles

Commercial iron particles were first coated with a silica layer and after surface initiation, grafted using AGET ATRP, with epoxide containing block polymer as depicted in Figure 1. Individual stages are discussed in this section.

3.1.1. Silica Coating

Initially, iron particles are coated with PEI, to produce a positive zeta potential, enhancing suspension, and allowing subsequent silica deposition. Silica coating is obtained using a modified two steps Stöber procedure.[29] At this point, silica layer is not completely hermetic and shows a

rough topography (Figure 1A), if treated with 37 % HCl under sonication, the iron core is dissolved (Figure 1B).

It is known that thermal treatment, seals silica cracks and condenses the siloxane groups creating an impermeable and denser shell. [30-32] However, if iron oxide is heated under oxygen atmosphere, it oxidizes, losing its magnetic properties.[33] So, material needs to be heat treated under free oxygen environment. This is achieved by using a tube furnace, purging with nitrogen before heating and maintaining the high vacuum along the cycle. Common heat treatment includes annealing in a wide range of temperatures (800 °C – 1200 °C) and calcination (400 °C – 600 °C). [30-32] With this in mind, an optimization for the thermal cycle (Figure 3) was performed, using mass loss in HCl after every tested program to evaluate silica stability. Initially, annealing at 1050 °C without calcination was evaluated during 10 min and 30 min (Table 1, programs 1 and 2), but obtained particles were almost entirely dissolved in HCl. Calcination at 600 °C was added to annealing (program 3), showing a slightly improvement over only annealing, though only around 20 % of the material survived the acid. Decrement in annealing temperature to 800 °C (programs 4 and 5), exhibited lower mass loss in acid. Despite this, it was appreciated that longer calcination at 600 °C had an enhanced effect over silica quality. Hence, only calcination was finally used, given the lowest mass loss after 3 h (program 6). These results could be explained considering that calcination is efficient in removing excess reagents from Stöber process (ethanol, water, ammonia), making silica denser and sealing pores. Annealing temperatures, on the other hand, can make silica softer, allowing subtle deformation, that for a thin layer (about 50 nm) could yield to exposed iron cores, make them susceptible to acid attack. After effective heat treatment, silica layer is smoother and thinner (presumably denser) as appreciated in Figure 1C, preventing oxidation of Fe_3O_4 under strong acid conditions (Figure 1D).

3.1.2. Surface initiated AGET ATRP

Once calcinated, silica coated magnetic nanoparticles are robust enough to be re-hydroxylated under acidic conditions (1.5 M HNO_3 for 24 h) at strong reflux temperature as well as a following chlorosilane modification to include active groups for ATRP polymerization. As discussed previously, GMA is used as epoxide containing polymer, but its hydrophobicity hinders its use as homopolymer for a low biofouling surface. Polyacrylamides were considered to form a copolymer with GMA, due to their high hydrophilic character and biocompatibility. Polyacrylamide shows good non-specific absorption behavior,[25] but it undergoes hydrolysis under aqueous conditions, producing acrylic acid.[34] On the other hand, poly-N-Hydroxyethyl acrylamide (PHEAA) is higher resistant to degradation than normal polyacrylamide and demonstrates low biofouling.[35-37] Hence, a copolymer of PGMA and PHEAA was selected to develop a more hydrophilic surface with high binding capacity.

Since, obtention of silica coated magnetic particles is a time-consuming process, optimization of surface initiated AGET ATRP was made using 1 µm SiO_2 particles, with same silane functionalization. The goal of this optimization was to synthetize a dense and smooth polymer layer with a thickness of at least 10 nm,[38-39] to obtain a surface with non-specific absorption and high binding capacity. Initially, copolymerization of GMA and HEAA was carried out using 0.4 M of both monomers. As seen in Figure 4A, these conditions yielded to an uncontrollable polymerization, showing particle aggregation and even free polymer growing in solution after only

10 min of reaction. Lower monomer concentrations (0.1 M) were used, increasing reaction time to 20 min to obtain an appropriate polymer thickness. Formation of aggregates was lower, but surface was still irregular and polymer thickness was only 3 nm (Figure 4B)

Controlled ATRP reactions require proper selection of initiator.[40] Chlorine initiators provide slower reaction rates compared with commonly used bromide initiators.[41] Also, bromide initiators are less stable and need to be used in short time after functionalization. These factors were previously considered to select a benzyl chloride as initiator. So, using a bromide initiator would not help to improve reaction control. Monomer reactivity also plays a vital role in ATRP performance, being methacrylates more reactive than acrylamides.[42] So, the difference in reaction rates for GMA and HEAA is the main reason for this uncontrolled reaction. Living character of ATRP provides a way to not only obtain block copolymers, but also, to "change initiator", since halogens at end chains become initiators for next polymerization.[43-45] These principles, allowed to overcome the difficult PGMA-co-PHEAA polymerization. First, adjusted conditions allowed to grow an 8 nm homopolymer PHEAA (Figure 4), producing very hydrophilic particles with increased water dispersity. The PHEAA grafted particles were used for the copolymerization of PGMA and PHEAA. Using 0.2 M monomer concentrations the reaction was controlled during 20 min, with no appreciable aggregation, adding 5 nm of epoxy containing polymer (Figure 4D).Variation in molar ratio of monomers were subsequently evaluated with similar polymerization control in all tests and concluding that 1:1 molar ratio of monomers permits a balance between binding capacity and particle hydrophilicity (see supporting information).

The optimized method allowed to obtain a controlled polymerization over the silica coated magnetic particles. As revealed in Figure 5B, PHEAA layer is smooth and around 8 nm, in agreement with the polymerization on the 1 µm silica particles. The second polymerization increases the homogeneous polymer thickness to around 13 nm, as presented in Figure 5C. These TEM micrographs demonstrate that the block copolymerization approach was effective to obtain a controlled growing of PGMA-co-PHEAA.

3.2. Infrared Spectroscopy characterization

In Figure 6 are displayed the chemical structures for the components of coated material: iron core (magnetite), silica coating (SiO_2) and block copolymer (PGMA and PHEAA). Fourier-transform infrared spectroscopy confirms chemical composition of material along coating process. Figure 7, presents FT-IR spectra of material after main steps. Magnetite (Fe_3O_4) absorption band can be located around 800 cm^{-1} and 500 cm^{-1}. [46-47] Silica coating produces additional peaks at 1080 cm^{-1} due to Si-O-Si stretching and at 1050 cm^{-1} to 1250 cm^{-1} by Fe-O-Si stretching vibration. [48-49] PHEAA composition is verified by characteristic carbonyl vibration of at 1728 cm^{-1},[50] and amide absorption band at N-H stretching at 3300 cm^{-1} – 3500 cm^{-1}. One of the most important features of the surface is the presence of the epoxide ring at 908 cm^{-1}, [51] an intact oxirane group in the final material is vital for binding with amine groups in proteins.

3.3. Magnetic characterization

A faster magnetic extraction, compared with other separation techniques as centrifugation, makes very attractive the kind of material presented in this work. In order to reduce waiting time and maximize recovery, the material must have high magnetization in the presence of an external

magnetic field. Figure 8A, shows variation of magnetization during different coating stages. It is possible to appreciate a decrement in magnetic saturation, starting with more than 90 emu/g for Fe_3O_4, then after silica coverage is reduced to 56 emu/g and finally becomes 45 emu/g for polymer coated particles. This variation is mainly due to the addition of non-magnetic materials (silica and polymer) and possible minimal oxidation of iron during heat treatment. It is necessary to point out that plotted moment values are per mass unit, and since silica and polymer cause a net diminution in material density, a unit mass of coated material has less magnetic iron cores compared with pure Fe_3O_4.

Another evident feature displayed in Figure 8A, is the residual magnetic moment, intrinsic to starting material and almost constant during coating steps. This characteristic causes aggregation of particles during coating, hindering obtention of singly silica coated particles as pictured in TEM micrographs of Figure 2 and supporting material. Some efforts have been made to obtain individually silica coated magnetic particles;[10-11] however, such coating processes give very low yields and require several synthesis steps. Figure 8B compares magnetic hysteresis loops of the epoxy magnetic beads obtained in this work with two commercially available extraction beads: Dynabeads M-270 epoxy and BcMag. Particles developed here, have a higher magnetic saturation (45 emu/g) contrasted with Dynabeads (32 emu/g) and BcMag (19 emu/g). This feature permits to use smaller particle size for a higher surface area, keeping a fast removal from suspension.

3.4. Binding performance

As a basic test of binding capacity, common immunoprecipitation test was performed. BSA antibody was bound to the surface at different binding times, particles were blocked and incubated for 1 h with fluorescent BSA. Eluted BSA from beads was quantified via fluorescence measurements. Similar protocols were followed with commercial beads and results are pictured in Figure 9. Saturation of all studied particles is reached around 4 h, although silica coated magnetic nanoparticles exhibit higher binding capacity (1.83 µg BSA/mg) than Dynabeads and BcMAg (approximately 0.9 µg BSA/mg).

Despite this difference, it is important to point out that the comparison is made by mass of particles, and it could be unfair for noticeable differences in density and surface area. Therefore, it was investigated the non-specific binding of all the beads to contrast them with their specific binding, in order to obtain the signal to noise ratio as a fair comparison. As shown in Table 2, Fe_3O_4@SiO_2@copolymer particles have 1.85 times more SNR compared to Dynabeads and almost 16-fold contrasted against BcMag, despite the fact BcMag have higher surface area. This could be attributed to the obtained block copolymer, with high graft density and long chains (more than 10 nm), improving resistance to protein absorption.[52]

There are notable differences in structure of compared particles (see supporting information), Dynabeads and BcMag are similar in morphology. Dynabeads are 2.7 µm polystyrene spheres inserted with superparamagnetic iron nanoparticles. BcMag are silica coated magnetic particles, with smaller size and have only 1 nm of epoxide linker.[53] Lower non-specific binding of the magnetic particles reported by this work can be attributed to the longer dense polymer layer (13 nm), which avoids interaction of proteins with silanols present on silica surface.

4. Conclusions

Commercially available magnetic nanoparticles were coated with silica using a two steps Stober and heat treated to obtain a strong acid resistant surface. Large Fe_3O_4 particles have high magnetization and can be easily extracted with regular neodymium magnets. Impervious silica coating can be functionalized to obtain surface-initiated particles. A two steps AGET ATRP, permits control over the copolymerization of monomers with different reactivity to produce a hydrophilic layer preserving binding capacity of epoxide groups. Composition analysis and TEM showed a successful optimized stepwise coating process. Immunoprecipitation performance of the reported particles indicated higher binding capacity in short time and lower nonspecific binding compared with some commercial extraction beads.

5. References

1. Tang, D. a. Y. R. a. C. Y. a. A. H., Magnetic-core/porous-shell CoFe2O4/SiO2 composite nanoparticles as immobilized affinity supports for clinical immunoassays. *Advanced Functional Materials* **2007,** *17* (6), 976--982.

2. Lee, J. a. C. J., Facile and high-efficient immobilization of histidine-tagged multimeric protein G on magnetic nanoparticles. *Nanoscale Research Letters* **2014,** *9* (1), 664.

3. Philipse, A. P. a. B. M. P. B. V. a. P. C., Magnetic Silica Dispersions: Preparation and Stability of Surface-Modified Silica Particles with a Magnetic Core. *Langmuir* **1994,** *10* (17), 92--99.

4. Tokajuk, G.; Niemirowicz, K.; Deptuła, P.; Piktel, E.; Cieśluk, M.; Wilczewska, A. Z.; Dąbrowski, J. R.; Bucki, R., Use of magnetic nanoparticles as a drug delivery system to improve chlorhexidine antimicrobial activity. *International Journal of Nanomedicine* **2017,** *12*, 7833-7846.

5. Baniukevic, J. a., Magnetic gold nanoparticles in SERS-based sandwich immunoassay for antigen detection by well oriented antibodies. *Biosensors and Bioelectronics* **2013,** *43* (1), 281--288.

6. Wu, W.; He, Q.; Jiang, C., Magnetic Iron Oxide Nanoparticles: Synthesis and Surface Functionalization Strategies. *Nanoscale Research Letters* **2008,** *3* (11), 397-415.

7. Poole, C. F., New trends in solid-phase extraction. *Trends in Analytical Chemistry* **2003,** *22* (6), 362-373.

8. Stber, W. a. F. A. a. B. E., Controlled growth of monodisperse silica spheres in the micron size range. *Journal of Colloid and Interface Science* **1968,** *26* (1), 62--69.

9. Sun, Y. a. D. L. a. G. Z. a. D. Y. a. M. M. a. X. L. a. Z. Y. a. G. N., An improved way to prepare superparamagnetic magnetite-silica core-shell nanoparticles for possible biological application. *Journal of Magnetism and Magnetic Materials* **2005,** *285* (1-2), 65--70.

10. Marcelo, G. a. P. E. a. C. T. a. P. C., Stabilization in water of large hydrophobic uniform magnetite cubes by silica coating. *Journal of Physical Chemistry C* **2011,** *115* (51), 25247--25256.

11. Park, J. a. P. M. D. a. G. M. C., Silica encapsulation of ferrimagnetic zinc ferrite nanocubes enabled by layer-by-layer polyelectrolyte deposition. *Langmuir* **2015,** *31* (11), 3537--3545.

12. Parnell, S. R.; Washington, A. L.; Parnell, A. J.; Walsh, A.; Dalgliesh, R. M.; Li, F.; Hamilton, W. A.; Prevost, S.; Fairclough, J. P. A.; Pynn, R., Porosity of silica Stöber particles determined by spin-echo small angle neutron scattering. *Soft Matter* **2016,** *12* (21), 4709--4714.

13. Li, S.; Wan, Q.; Qin, Z.; Fu, Y.; Gu, Y., Unraveling the Mystery of Stöber Silica's Microporosity. *Langmuir* **2016,** *32* (36), 9180--9187.

14. Wang, D.; Guan, K.; Bai, Z.; Liu, F., Facile preparation of acid-resistant magnetite particles for removal of Sb(Ⅲ) from strong acidic solution. *Science and Technology of Advanced Materials* **2016,** *17* (1), 80-88.

15. Bai, Y.; Cui, Y.; Paoli, G. C.; Shi, C.; Wang, D.; Zhou, M.; Zhang, L.; Shi, X., Synthesis of amino-rich silica-coated magnetic nanoparticles for the efficient capture of DNA for PCR. *Colloids and Surfaces B: Biointerfaces* **2016,** *145*, 257-266.

16. Zhang, Z. a. W. Z. a. W. M. J., Polyacrylamide brush layer for hydrophilic interaction liquid chromatography of intact glycoproteins. *Journal of Chromatography A* **2013,** *1301*, 156--161.

17. Bai, Y.; Cui, Y.; Paoli, G.; Shi, C.; Wang, D.; Shi, X., Nanoparticles Affect PCR Primarily via Surface Interactions with PCR Components: Using Amino-Modified Silica-Coated Magnetic Nanoparticles as a Main Model. *ACS Appl. Mater. Interfaces* **2015,** *7* (24), 13142-13153.

18. Yang, C.-C.; Yang, S.-Y.; Ho, C.-S.; Chang, J.-F.; Liu, B.-H.; Huang, K.-W., Development of antibody functionalized magnetic nanoparticles for the immunoassay of carcinoembryonic antigen: a feasibility study for clinical use.(Report). *Journal of Nanobiotechnology* **2014,** *12* (1).

19. Pirani, P.; Patil, U.; Apsunde, T.; Trudell, M.; Cai, Y.; Tarr, M., Protein surface labeling reactivity of N -hydroxysuccinimide esters conjugated to Fe 3 O 4 @SiO 2 magnetic nanoparticles. *An Interdisciplinary Forum for Nanoscale Science and Technology* **2015,** *17* (9), 1-11.

20. Sung, D. a. P. S. a. J. S., Facile immobilization of biomolecules onto various surfaces using epoxide-containing antibiofouling polymers. *Langmuir* **2012,** *28* (9), 4507--4514.

21. Wong, S. Y.; Putnam, D., Overcoming limiting side reactions associated with an NHS-activated precursor of polymethacrylamide-based polymers. *Bioconjugate chemistry* **2007,** *18* (3), 970.

22. Thierry, B.; Jasieniak, M.; de Smet, L. C. P. M.; Vasilev, K.; Griesser, H. J., Reactive epoxy-functionalized thin films by a pulsed plasma polymerization process. *Langmuir : the ACS journal of surfaces and colloids* **2008,** *24* (18), 10187.

23. Krishnan, R. a. S. K. S. V., Controlled/"Living" Radical Polymerization of Glycidyl Methacrylate at Ambient Temperature. *Macromolecules* **2003,** *36* (6), 1769--1771.

24. Krishnan, S. a. W. C. J. a. O. C. K., Advances in polymers for anti-biofouling surfaces. *Journal of Materials Chemistry* **2008,** *18* (29), 3405--3413.

25. Zhao, C.; Zhao, J.; Li, X.; Wu, J.; Chen, S.; Chen, Q.; Wang, Q.; Gong, X.; Li, L.; Zheng, J., Probing structure-antifouling activity relationships of polyacrylamides and polyacrylates. *Biomaterials* **2013,** *34* (20), 4714.

26. Chen, H. a. Z. M. a. Y. J. a. Z. C. a. H. R. a. C. Q. a. C. Y. a. Z. J., Synthesis and characterization of antifouling poly(N - acryloylaminoethoxyethanol) with ultralow protein adsorption and cell attachment. *Langmuir* **2014,** *30* (34), 10398--10409.

27. Jiang, L. a. Z. X. a. W. G. a. L. X. a. W. W. a. Q. J., Preparation and characterization of poly(glycidyl methacrylate)-grafted magnetic nanoparticles: Effects of the precursor concentration on polyol synthesis of Fe 3 O 4 and PMDETA 0 CuBr 2 0 ratios on SI-AGET ATRP. *Applied Surface Science* **2015,** *357*, 1619--1624.

28. Sun, H.; Wang, T.; Zhou, Y.; Li, P.; Kong, Y., Synthesis of well-defined amphiphilic block copolymers via AGET ATRP used for hydrophilic modification of PVDF membrane. *Journal of Applied Polymer Science* **2015,** *132* (24), n/a-n/a.

29. Park, J.; Porter, M. D.; Granger, M. C., Silica Encapsulation of Ferrimagnetic Zinc Ferrite Nanocubes Enabled by Layer-by-Layer Polyelectrolyte Deposition. *Langmuir* **2015,** *31* (11), 3537-3545.

30. Gorsd, M. N. a. P. L. R. a. B. M. N., Synthesis and Characterization of Hollow Silica Spheres. *Procedia Materials Science* **2015,** *8*, 567--576.

31. Newby, J. J. a. L. M. A. a. R. B. a. W. M. J., Annealing of silica to reduce the concentration of isolated silanols and peak tailing in reverse phase liquid chromatography. *Journal of Chromatography A* **2011,** *1218* (31), 5131--5135.

32. Chabanov, A. A. a. J. Y. a. N. D. J., Elimination of cracks in self-assembled photonic band gap crystals. **2003,** *55455*, 18--21.

33. Kemp, S. J.; Ferguson, R. M.; Khandhar, A. P.; Krishnan, K. M., Monodisperse magnetite nanoparticles with nearly ideal saturation magnetization. *RSC Adv.* **2016,** *6* (81), 77452-77464.

34. Caulfield, M. J. a. H. X. a. Q. G. G. a. S. D. H., Degradation on polyacrylamides. Part I. Linear polyacrylamide. *Polymer* **2003,** *44* (5), 1331--1337.

35. Zhao, C. a. P. K. a. A. L. M. a. L. Z. a. H. R. a. C. H. a. L. X. a. L. L. a. Z. G. a. C. Y. a., Antifouling and biodegradable poly(N-hydroxyethyl acrylamide) (polyHEAA)-based nanogels. *RSC Advances* **2013,** *3* (43), 19991--20000.

36. Narumi, A. a. C. Y. a. S., Poly(N-hydroxyethylacrylamide) prepared by atom transfer radical polymewater-solublerization as a nonionic, water-soluble, and hydrolysis-resistant polymer and/or segment of block copolymer with a well-defined molecular weight. *Macromolecular Chemistry and Physics* **2009,** *210* (5), 349--358.

37. Zhao, C. a. Z. J., Synthesis and characterization of poly(N -hydroxyethylacrylamide) for long-term antifouling ability. *Biomacromolecules* **2011,** *12* (11), 4071--4079.

38. Higaki, Y. a. K. M. a. M. D. a. T. A., Anti-fouling behavior of polymer brush immobilized surfaces. *Polymer Journal* **2016,** *48* (4), 325--331.

39. Kostina, N. Y. a. R.-E. C. a. H. M. a. B. E. a. M. J., Non-fouling hydrogels of 2-hydroxyethyl methacrylate and zwitterionic carboxybetaine (meth)acrylamides. *Biomacromolecules* **2012,** *13* (12), 4164--4170.

40. Tang, W.; Kwak, Y.; Braunecker, W.; Tsarevsky, N. V.; Coote, M. L.; Matyjaszewski, K., Understanding atom transfer radical polymerization: effect of ligand and initiator structures on the equilibrium constants. *Journal of the American Chemical Society* **2008,** *130* (32), 10702.

41. Matyjaszewski, K.; Shipp, D. A.; Wang, J. L.; Grimaud, T.; Patten, T. E., Utilizing halide exchange to improve control of atom transfer radical polymerization. *Macromolecules* **1998,** *31* (20), 6836-6840.

42. Peng, C. H.; Kong, J.; Seeliger, F.; Matyjaszewski, K., Mechanism of halogen exchange in ATRP. *Macromolecules* **2011,** *44* (19), 7546-7557.

43. Li, X.; Wang, M.; Wang, L.; Shi, X.; Xu, Y.; Song, B.; Chen, H., Block copolymer modified surfaces for conjugation of biomacromolecules with control of quantity and activity. *Langmuir* **2013,** *29* (4), 1122-8.

44. Li, Y. a. A. S. P. a. J. X. a. Z. S., Direct synthesis of well-defined quaternized homopolymers and diblock copolymers via ATRP in protic media. *Macromolecules* **2003,** *36* (22), 8268--8275.

45. Kagawa, Y. a. M. H. a. O. M. a. Z. J., Preparation of block copolymer particles by two-step atom transfer radical polymerization in aqueous media and its unique morphology. *Polymer* **2005,** *46* (4 SPEC. ISS.), 1045--1049.

46. Roca, A. G. a. M. M. P. a. S. C. J., Synthesis of Monodispersed Magnetite Particles From Different Organometallic Precursors. *IEEE Transactions on Magnetics* **2006,** *42* (10), 3025--3029.

47. Cabrera, L. a. G. S. a. M. N. a. M. M. P. a. H. P., Magnetite nanoparticles: Electrochemical synthesis and characterization. *Electrochimica Acta* **2008,** *53* (8), 3436--3441.

48. Marcelo, G.; Perez, E.; Corrales, T.; Peinado, C., Stabilization in Water of Large Hydrophobic Uniform Magnetite Cubes by Silica Coating. *Journal of Physical Chemistry C* **2011,** *115* (51), 25247-25256.

49. Martinez, J. R. a. R. F. a. V. Y. V. a. P.-R. F. a. G.-H. J., Infrared spectroscopy analysis of the local atomic structure in silica prepared by sol-gel. *Journal of Chemical Physics* **1998,** *109* (17), 7511--7514.

50. Gunes, D. a., Poly(N-hydroxyethyl acrylamide)-b-polystyrene by combination of ATRP and aminolysis processes. 2013; Vol. 127, pp 2684--2689.

51. Edmondson, S. a. H. W. T. S., Controlled growth and subsequent chemical modification of poly(glycidyl methacrylate) brushes on silicon wafers. *Journal of Materials Chemistry* **2004,** *14*, 730.

52. Yoshikawa, C. a. H. S. a. H. T. a. H. C. F. a. K. H., Non-biofouling property of well-defined concentrated poly(2-hydroxyethyl methacrylate) brush. *Materials Letters* **2012,** *83*, 140--143.

53. Inc, B. BcMag DEAE Magnetic Beads. http://www.bioclone.us/DEAE-magnetic-beads-particle-resin-matrix.html (accessed 04/28/2019).

Table 1. Heat treatment optimization programs. T_C and T_A are calcinating and annealing temperatures at times t_C and t_A, respectively. Empty boxes indicate that the step was omitted.

Program	T_C [°C]	T_C [min]	T_A [°C]	T_A (min)	% Mass loss
1	---	---	1050	10	92 ± 3.5
2	---	---	1050	30	97 ± 2.8
3	600	20	1050	10	80 ± 5.6
4	600	20	800	40	48 ± 3.8
5	600	120	800	40	18 ± 2.5
6	600	180	---	---	12 ± 1.7

Table 2. Comparison of specific and non-specific binding of fluorescent BSA for silica coated magnetic particles and commercial beads. Signal to noise ratio (SNR) was calculated as the quotient of specific/non-specific. Binding time was 2 h for both specific and non-specific.

Beads	Specific binding (µg/mg)	nonspecific binding (µg/mg)	SNR	Surface area (m^2/g)
BcMag	0.91 ± 0.08	0.225 ± 0.005	4.05 ± 0.35	100
Dynabeads M-270	0.92 ± 0.11	0.026 ± 0.003	34.69 ± 5.7	2 to 5
Fe_3O_4@SiO_2@copolymer	1.83 ± 0.04	0.029 ± 0.004	64.21 ± 8.01	0.04

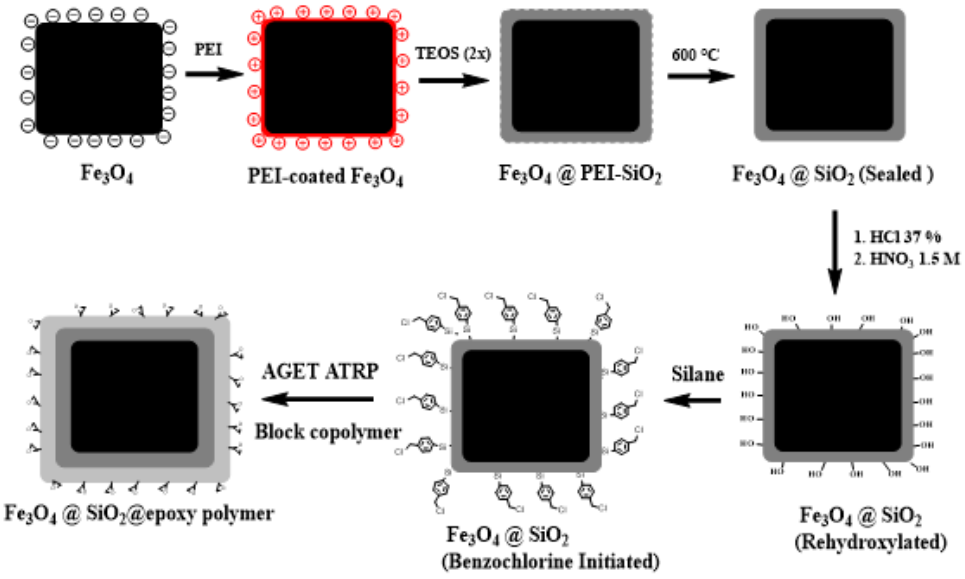

Figure 1. Scheme of coating process or magnetic particles: iron particles are coated initially with PEI and then with a silica layer. Surface silane initiation is performed after rehydroxylation, and finally a block copolymer through AGET ATRP yields to a low biofouling, high capacity surface.

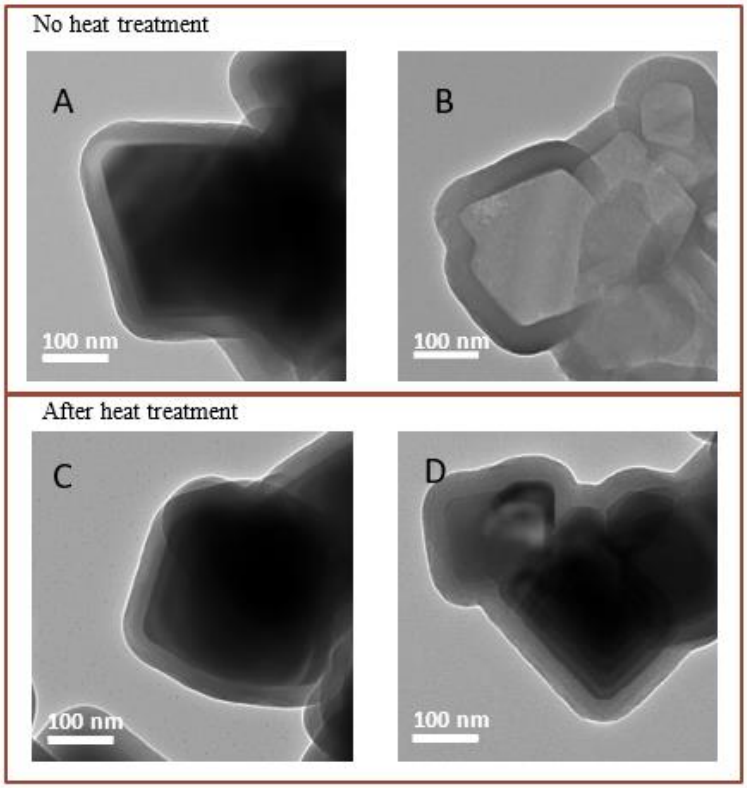

Figure 2. TEM micrographs of Fe_3O_4@SiO_2. (A) Before thermal treatment, synthetized surface is rough and porous. (B) After sonicating in 37 % HCl for 1 h, non-calcinated particles' magnetic core have been dissolved due to the porosity of silica coating. (C) Calcinating at 600 °C for 3 h produces a smother, thinner, non-porous silica surface that protects the iron core from acid attack. (D) Heat treated particles are not dissolved after sonication in 37 % HCl for 1 h.

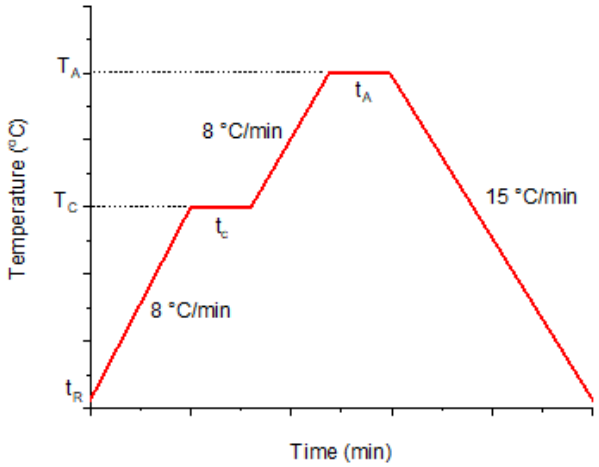

Figure 3. Evaluated heat treatment for Fe_3O_4@SiO_2 particles included two stages, calcination at T_C during t_C time and annealing at T_A during t_A time. Heating up and cooling down rates were kept constant between vacuum tube furnace specifications. Mass loss in HCl after every tested program was used to assess its effectiveness. Results are summarized in Table 1.

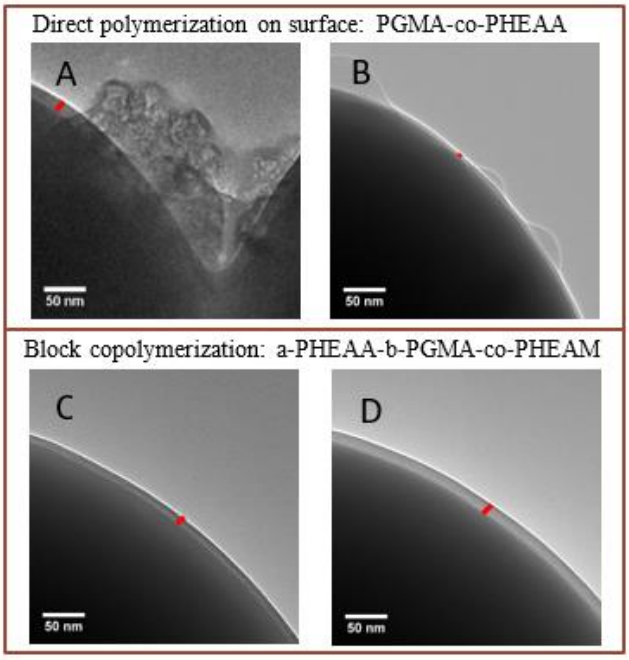

Figure 4. TEM micrographs of 1µm silica particles grafted with polymer A) SiO2@ PGMA-co-PHEAA ([monomers] = 0.4 M, 10 min reaction), direct polymerization onto chlorosilane initiated surface shows particle aggregation and irregular polymerization. B) SiO2@ PGMA-co-PHEAA ([monomers] = 0.1 M, 20 min reaction), lower monomer concentration reduces aggregation, but surface is still irregular, and thickness is only 3 nm. C) SiO2@ PHEAA (1.3 M, 60 min), first PHEAA layer (8 nm) is smooth and no aggregation was observed. D) SiO2@ PHEAA-b-PGMA-co-PHEAA (0.1 M, 20 min) second block copolymer grows evenly and controlled, adding 5 nm to total thickness.

19

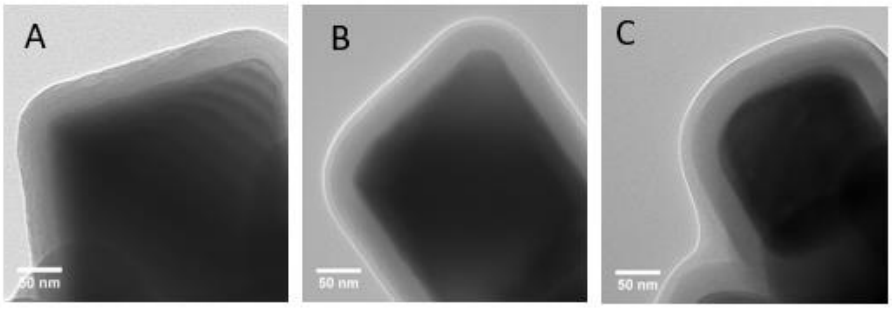

Figure 5. TEM micrographs of polymerization process of silica coated magnetic particles. A) Initial Fe_3O_4@SiO_2 chlorosilane initiated. B) Fe_3O_4@SiO_2@PHEAA after first AGET-ATRP polymerization. C) Fe_3O_4@SiO_2@PHEAA-b-PGMA-PHEAA, final block copolymer.

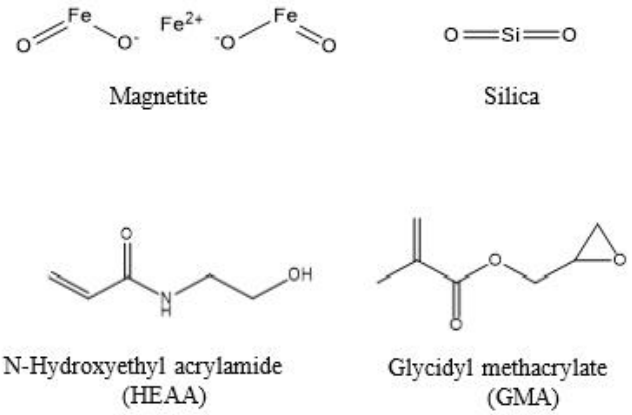

Figure 6. Chemical structures of components of epoxide coated magnetic beads.

20

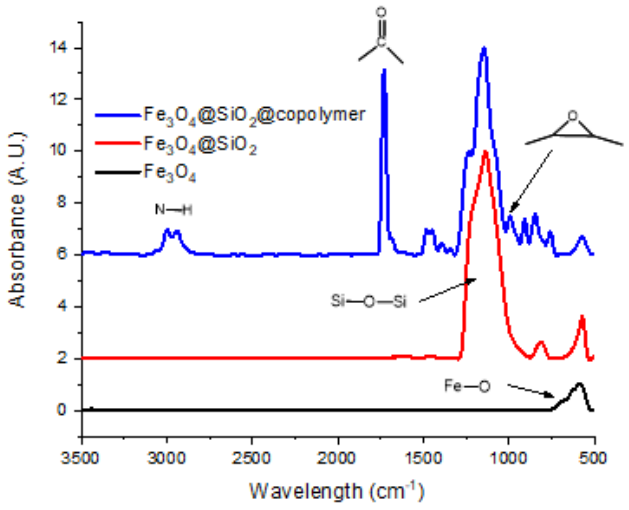

Figure 7. FT-IR spectra of iron oxide (Fe_3O_4), silica coated iron after calcination (Fe_3O_4@SiO_2), and after block copolymerization (Fe_3O_4@SiO_2@copolymer). Silica peak (1100 cm^{-1} – 1000 cm^{-1}) absorbance was used for normalization of spectra.

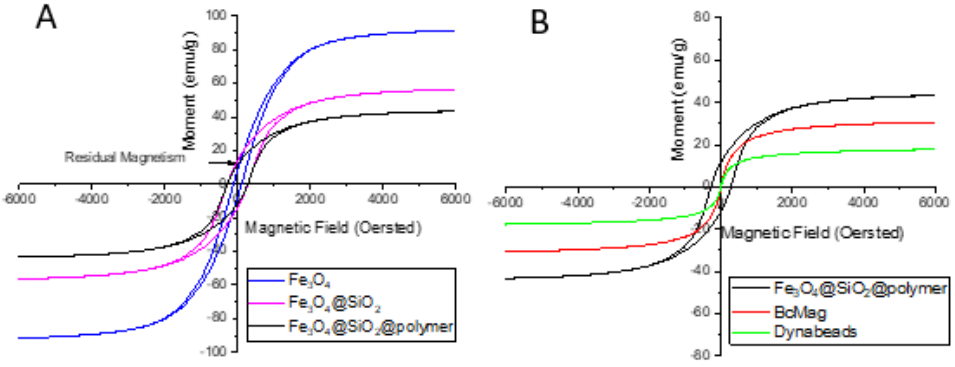

Figure 8. Magnetic hysteresis loops. A) Variation of magnetization during coating stages, reduction of magnetic saturation is mainly due to addition of layers of non-magnetic materials and changes in material density B) Comparison of epoxide magnetic beads (Fe_3O_4@SiO_2@polymer) and commercial beads.

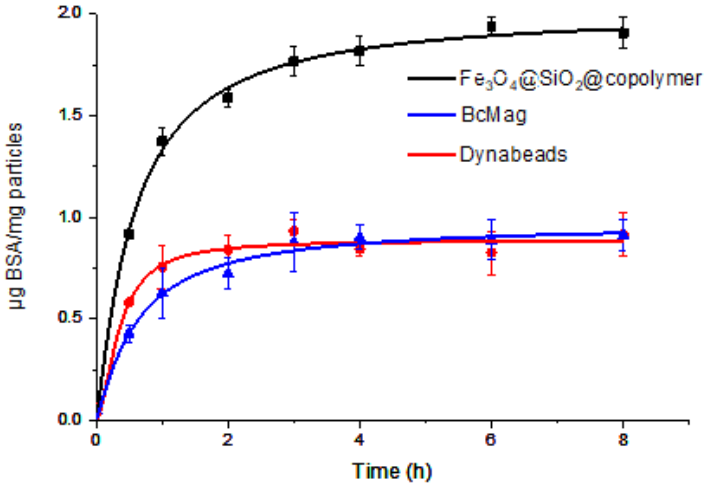

Figure 9. BSA antibody binding kinetics measured via eluted fluorescent BSA. All concentrations were 0.1 µg/µL.